GEOLOGICAL SURVEY OF CANADA
OPEN FILE 6978

Integrated analysis of vitrinite reflectance, Rock-Eval 6, gas chromatography, and gas chromatography-mass spectrometry data for the Mallik A-06, Parsons N-10 and Kugaluk N-02 wells, Beaufort-Mackenzie Basin, northern Canada

D.R. Issler, M. Obermajer, J. Reyes and M. Li

2012

Natural Resources Canada   Ressources naturelles Canada

Canada

GEOLOGICAL SURVEY OF CANADA
OPEN FILE 6978

Integrated analysis of vitrinite reflectance, Rock-Eval 6, gas chromatography, and gas chromatography-mass spectrometry data for the Mallik A-06, Parsons N-10 and Kugaluk N-02 wells, Beaufort-Mackenzie Basin, northern Canada

D.R. Issler, M. Obermajer, J. Reyes and M. Li

2012

©Her Majesty the Queen in Right of Canada 2012

doi:10.4095/289672

This publication is available from the Geological Survey of Canada Bookstore (http://gsc.nrcan.gc.ca/bookstore_e.php).
It can also be downloaded free of charge from GeoPub (http://geopub.nrcan.gc.ca/).

Recommended citation:
Issler, D.R., Obermajer, M., Reyes, J. and Li, M., 2012. Integrated analysis of vitrinite reflectance, Rock-Eval 6, gas chromatography, and gas chromatography-mass spectrometry data for the Mallik A-06, Parsons N-10 and Kugaluk N-02 wells, Beaufort-Mackenzie Basin, northern Canada; Geological Survey of Canada, Open File 6978, 78 p. doi:10.4095/289672

Publications in this series have not been edited; they are released as submitted by the author.

TABLE OF CONTENTS

LIST OF FIGURES

LIST OF TABLES

ABSTRACT

Core and cuttings samples were selected from the Mallik A-06 (Mackenzie Delta), Parsons N-10 (Tuktoyaktuk Peninsula) and Kugaluk N-02 (Anderson Plain) wells of the Northwest Territories for Rock-Eval/TOC and vitrinite reflectance analysis. Selected Rock-Eval samples were extracted and analysed using gas chromatography and gas chromatography-mass spectrometry. Rock-Eval parameters are strongly affected by sample contamination from drilling mud additives and migrated oil. For the Mallik A-06 well, most Rock-Eval pyrograms in the Iperk, Mackenzie Bay and Kugmallit sequences show evidence of drilling mud contamination. Approximately 50% of the pyrograms in the Richards and Taglu sequences are anomalous and GC-MS and GC-MS-MS analysis for selected extracts indicate extensive contamination by migrated and biodegraded Upper Cretaceous (Boundary Creek/Smoking Hills formations) derived oil. For the Parsons N-10 well, coal samples within the Iperk and Aklak sequences have anomalous pyrograms that are probably related to their low level of maturity. However, most pyrograms from the Cenozoic (Iperk and Aklak sequences) and Upper Cretaceous (Mason River, Smoking Hills and Boundary Creek sequences) successions show evidence of significant sample contamination. The upper part of the Albian Arctic Red formation shows similar contamination but there is an abrupt change below a depth of 2195 m where most pyrograms appear to be normal within the Lower Cretaceous-Upper Jurassic succession. For the Kugaluk N-02 well, all pyrograms have been disturbed by contamination from oil-based mud and yield low Tmax values as a result.

Tmax thermal maturity estimates for the least disturbed pyrograms show very good agreement with measured vitrinite reflectance values for the Mallik A-06 and Parsons N-10 wells. Measured mean random vitrinite reflectance varies from 0.23 (Iperk Sequence) to 0.65 $\%Ro_R$ (Taglu Sequence) for the Mallik A-06 well and 0.25 (Iperk Sequence) to 0.66 $\%Ro_R$ (Husky Formation) for the Parsons N-10 well. A number of vitrinite reflectance measurements for samples from the Richards and Taglu sequences in the Mallik A-06 well have been suppressed due to staining by migrated Cretaceous-derived oil. The Paleozoic succession in the Kugaluk N-02 well is overmature with measured vitrinite reflectance values ranging from 1.6 (Imperial Formation) to 2.0 $\%Ro_R$ (Landry Formation) over a 960 m depth interval. Extrapolated maturity is 2.7 $\%Ro_R$ in the Franklin Mountain Formation at the base of this well. There is qualitative agreement between the expected and observed degree of apatite fission track annealing for apatite fission track samples in all three wells and this provides independent support for the thermal maturity estimates. Exponential curves were fit to the $\%Ro_R$-depth data and extrapolated to an initial surface value of 0.2 $\%Ro_R$ to obtain estimates on the magnitude of erosion at each well location. For the Mallik A-06 and Parsons N-10 wells, the estimated thickness of strata eroded prior to the deposition of the Iperk Sequence is approximately 700 and 1300 m, respectively. For the Kugalik N-02 well, the modest maturity gradient implies that up to 8 km of strata may have been removed by erosion.

INTRODUCTION

The Geological Survey of Canada (GSC) is involved with a multi-disciplinary, industry-government funded study of petroleum systems of the Beaufort-Mackenzie Basin. This multi-year research project was initiated in December 2000 and work was done under the former GSC Project Approval System (PAS) (2001-2003), and the Earth Sciences Sector (ESS) Northern Resources Development (2003-2006) and Secure Canadian Energy Supply

(2006-2009) programs. Work is continuing under the ESS Geo-Mapping for Energy and Minerals (GEM) Program. As part of this research, thermal maturity (vitrinite reflectance, Rock-Eval Tmax) data are being acquired for key petroleum exploration wells across the basin to help constrain quantitative models of thermal history and petroleum generation.

Geological recycling of organic matter is a common problem in the Mackenzie Delta region and therefore samples may contain multiple populations of coal macerals with different thermal maturity. Also, because cuttings samples are used, there is the potential for drilling-related mixing of sample material from different depths (e.g. borehole caving, recirculation of cuttings through mud system) and contamination by organic mud additives. Migrated oil is another form of sample contamination. Some types of drilling-related contamination can be avoided by using core samples and this was done where possible. Petrographic analysis of samples was used to distinguish anomalous vitrinite reflectance values (due to caving, recycling and suppression by oil staining, for example) from primary *in situ* values. Sample contamination has a significant adverse effect on the quality of results from bulk analytical methods such as Rock-Eval pyrolysis. Rock-Eval pyrograms were used to identify contaminated samples and selected samples were extracted for organic geochemical analysis (gas chromatography and gas chromatography-mass spectrometry) to investigate the nature of the contamination.

To improve on the quality of data and interpretations, we use an integrated approach to thermal maturity evaluation by assessing complementary data sets. For example, the Rock-Eval Tmax and vitrinite reflectance data in this report provide independent measures of thermal maturity. Also, apatite fission track (AFT) thermochronological data are available for many of the key wells used in the Beaufort-Mackenzie petroleum systems study (to be published elsewhere). Fission tracks are linear regions of crystal damage that form continuously through geological time by the spontaneous fission decay of trace amounts of ^{238}U within apatite crystals (e.g. Wagner and Van den Haute, 1992; Gallagher *et al*., 1998; Gleadow *et al*., 2002). They form with the same initial length (approximately 16 μm) but undergo length reduction (thermal annealing) and corresponding AFT age reduction at elevated temperatures, producing a distribution of AFT lengths that depends on the thermal history of a sample. Any discordance between the degree of AFT annealing and the level of organic maturity for a sample indicates a problem in the data that requires further investigation. We have used this criterion to re-examine several wells with vitrinite reflectance data that have been reported by other groups and included with the National Energy Board (NEB) well history reports at the GSC in Calgary.

WELL LOCATIONS AND STRATIGRAPHY

Figure 1 shows the location of the three onshore study wells in the Mackenzie Delta region. The Mallik A-06 well is located near the northern coast of Richards Island close to the Mallik L-38 gas discovery well (Dixon *et al*., 1994; NEB, 1998) and the Mallik gas hydrate research wells (Dallimore *et al*., 1999, 2005). The Taglu gas field, which is one of the three anchor fields for the proposed Mackenzie Valley gas pipeline, is situated immediately to the west of Mallik A-06. The Parsons N-10 well is located at the southwest end of Tuktoyaktuk Peninsula within the Parsons Lake gas field, another anchor field for the proposed Mackenzie Valley pipeline (Figure 1). The Kugaluk N-02 well is situated south of Tuktoyaktuk Peninsula on the southeastern basin margin within the physiographic region known as the Anderson Plain.

Mesozoic-Cenozoic stratigraphy for the Beaufort-Mackenzie Basin is shown in Figure 2 and the generalized stratigraphy for the Anderson Plain region is shown in Figure 3. The Mallik A-06 well penetrated nearly 4 km of Cenozoic strata and terminated within the Eocene Taglu Sequence. To the southeast, the Parsons N-10 well encountered a thinner (approximately 1.5 km) and more deeply eroded Cenozoic succession and an underlying Jurassic-Cretaceous succession of similar thickness before terminating in Cambro-Ordovician dolomite of the Franklin Mountain Formation. Further to the southeast in the Anderson Plain region, the Kugaluk N-02 well penetrated a 2.4 km thick Paleozoic succession (Imperial to Franklin Mountain formations; Figure 3) capped by approximately 50 m of Quaternary sediments. Kugaluk N-02 is a stratigraphic test well with one inch diameter core collected over most of its length.

METHODS

Rock-Eval Pyrolysis

Rock-Eval pyrolysis is used extensively for characterizing the quality, quantity and thermal maturity of organic matter in sedimentary rocks, parameters that are essential for assessing the petroleum potential of sedimentary basins. Lafargue *et al*. (1998) and Behar *et al*. (2001) provide details on the Rock-Eval pyrolysis method using the newest version of the technology (Rock-Eval 6 apparatus) and these papers form the basis for the brief description below. Readers are referred to these two papers for a more comprehensive discussion of the technique.

Well core and cuttings samples were analysed at the GSC in Calgary following the *Basic Method* using a Turbo Rock-Eval 6 device as described by Behar *et al*. (2001). Normally well cuttings samples are washed in an attempt to remove any residual drilling mud. However, the wells in this study were drilled more than 30 years ago (Kugaluk N-02 – 1969; Mallik A-06 – 1972; Parsons N-10 – 1973) and the sample collections have been depleted. Therefore, given the small quantities of sample available for analysis, unwashed samples were used. Unwashed whole rock samples were crushed into a powder and sample aliquots (typically 70 mg) were placed in stainless steel crucibles, inserted into an oven and subject to non-isothermal, open system pyrolysis in a nitrogen atmosphere.

Figure 4 illustrates an idealized Rock-Eval pyrogram for a sample standard. Initially samples were heated at 300°C for 3 minutes to volatilize any free hydrocarbons (HC) and these are represented by the **S1** curve (Figure 4). Ideally, the area under the **S1** pyrolysis curve (mg HC/g of initial rock) represents hydrocarbons generated *in situ* over geologic time but sample impregnation by migrated hydrocarbons, expulsion and loss of hydrocarbons or organic drilling contaminants (e.g. oil-based drilling mud) can also affect the results. Following this isothermal heating step, samples were heated linearly from 300°C to 650°C at 25°C/minute, yielding an **S2** curve that represents thermal cracking of sedimentary organic matter (Figure 4). Under ideal conditions, the area under the **S2** curve (mg HC/g of initial rock) represents the remaining potential of the rock sample to generate petroleum from kerogen at increased thermal maturity levels but results can be affected by migrabitumen (migrated bitumen) and organic drilling contaminants. The temperature at peak generation on the **S2** pyrolysis curve (Tpeak; Figure 4) is converted to the relative temperature and accepted thermal maturity parameter, **Tmax** (in °C), which was established using the older Rock-Eval 2 technology.

The **S3** curve corresponds to the amount of CO_2 (mg CO_2/g of initial rock) generated from organic matter during the initial isothermal heating step and the programmed heating phase up to 400°C. CO_2 generated between 400°C and 650°C is from the thermal decomposition of carbonate minerals. The Rock-Eval 6 instrument also records the amount of CO generated during pyrolysis and attributes various proportions to organic carbon and mineral sources, depending on sample temperature (see Behar *et al*. (2001) for details). The amount of pyrolysable organic carbon (**PC**) is determined by combining the S1, S2, S3 and CO contributions according to a specific formula (Behar *et al*., 2001). Pyrolysis mineral carbon is determined from the high temperature portions of the CO and CO_2 pyrolysis curves. Following pyrolysis, samples were transferred to an oxidation oven where they were linearly heated from 300°C to 850°C to determine the amount of residual organic carbon (**RC**) and oxidation mineral carbon from CO and CO_2 generated during oxidation. The total organic carbon (**TOC** in weight %) is the sum of the pyrolysable and residual organic carbon. Similarly, mineral carbon (**MINC**) is the sum of the pyrolysis and oxidation mineral carbon.

Other key Rock-Eval parameters included in this report are production index (**PI** = S1/(S1 + S2)), hydrogen index (**HI** = (S2x100)/TOC in mg HC/g TOC) and oxygen index (**OI** = (S3x100)/TOC in mg CO_2/g TOC). **PI** can be used as a crude thermal maturity indicator because **S1** and therefore **PI** should increase within the mature zone for petroleum generation. However, petroleum migration and expulsion and drilling mud contamination can affect both **S1** and **S2** and therefore **PI** values. Plots of **HI** versus **OI** (Espitalié *et al*., 1977) can provide information on sample organic matter type and thermal maturity and such plots are included in this report. However, **HI** and **OI** values are also sensitive to sample contamination and therefore results must be interpreted carefully. **HI** versus **Tmax** plots (Espitalié *et al*., 1984) can also be used to examine organic maturation pathways in situations where **OI** values are anomalously high due to contributions from mineral carbon or other factors (Peters, 1986). These plots are also included in this report.

Peters (1986) discusses various factors that influence Rock-Eval parameters and presents guidelines for interpreting Rock-Eval data. For immature rocks, sample contamination (natural or drilling related) is indicated by multi-modal **S2** peaks and **PI** values > 0.2. For **TOC** values < 0.5 wt%, pyrolysate adsorption on the mineral matrix can affect **S1**, **S2** and **Tmax** values, an effect most significant for argillaceous rocks. Peters (1986) suggests that **Tmax** values are unreliable for **S2** values < 0.2 mg HC/g rock. However, this criterion is likely to vary depending on the type of organic matter and rock matrix. Obermajer *et al*. (2007) suggest a minimum **S2** value of 0.35 mg HC/g rock for interpreting Tmax values, based on data from the Arctic Islands, and Riediger *et al*. (2004) use a value of 0.5 mg HC/g rock in their study of Triassic rocks from north-eastern British Columbia. Using data from Espitalié *et al*. (1980), Dahl *et al*. (2004) investigated a “worst case” example for mineral matrix effects (Type II kerogen in illite) and showed that pyrolysate adsorption could affect Rock-Eval parameters for **S2** values < 3 mg HC/g rock.

Gas Chromatography and Gas Chromatography-Mass Spectrometry

A few grams of a hand-pulverized sample were used for extracting the solvent-soluble organic matter. The extraction was carried out for 24 hours in a Soxhlet apparatus using approximately 350 ml of an azeotropic mixture of 87% chloroform and 13% methanol. After the solvent was removed in a rotary evaporator (at 35º-40ºC), the extracts were dissolved in chloroform and treated with colloidal copper to remove elemental sulphur (considered to be an artefact of pyrite oxidation during sample handling). The mixture was filtered through glass fibre filter paper to remove the copper sulphide and excess copper, and then the filtrate was rotary-evaporated, dried and weighed until a constant weight was obtained. Total extracts were then dissolved in a minimal amount of chloroform, treated with pentane to precipitate asphaltenes, and then vacuum filtered to remove the precipitate. The asphaltenes were dissolved in chloroform, collected in a separate tared flask, rotary-evaporated and weighed to constant weight.

A mixture of 28-200 mesh Silica Gel (MCB) and 80-200 mesh alumina (ALCOA) (1/3:2/3 by weight respectively) was used as a support for the column. The support was activated by heating at 120º-150ºC for 12 hours. A glass wool plug was placed at the bottom of the column and covered with a 1 cm thick layer of sand. The support, weighed as 1 g of support/10 mg of deasphalted sample, was slowly settled in pentane and any air trapped was released by gentle tapping on the column. A deasphalted sample, dissolved in a minimal amount of previously measured pentane, was then added to the column. Saturates were recovered by eluting with pentane (3.5 ml/g support), aromatics with a 50:50 mixture of pentane and dichloromethane (4 ml/g support), resins with methanol (4 ml/g support) and any remaining asphaltenes with chloroform. The solvents were rotary-evaporated, then separate fractions were transferred to tared 1 dram vials, dried in a slow stream of nitrogen and weighed to constant weight.

Saturate fractions were analysed at the GSC in Calgary using gas chromatography (GC). A Varian 3800 FID gas chromatograph was used with 30m DB-1 column with helium as the carrier gas. The programmed temperature was 60ºC to 300ºC at a rate of 6ºC/min and then isothermal for 30 minutes. The eluting compounds were detected and determined quantitatively using a hydrogen flame ionization detector.

Gas chromatography-mass spectrometry (GC-MS) analyses of the saturate fraction for samples from the Mallik A-06 well were done at the GSC in Calgary using an Agilent 6890 GC coupled to a Waters Autospec Magnetic Sector Mass Spectrometer. Samples from the Parsons N-10 well were analyzed at the GSC on a Varian 3800 GC coupled to a Varian 1200L Triple Quadrupole Mass Spectrometer. Both gas chromatographs were fitted with a DB5ms, 30m x 0.25µm film thickness x 0.32mm id capillary column and a split/splitless injector operated in split mode (injector temperature 280°C) and used helium as the carrier gas. Temperature was initially held at 80°C for 3 minutes, then ramped to 180°C at a rate of 40°C/min , then programmed at a rate of 4°C/min to 320°C and held for 7 minutes. Mass spectrometers were operated in Selected Ion Monitoring mode and used a +ve ion electron impact source for ionization.

Vitrinite Reflectance

Vitrinite reflectance is a well established and widely used thermal maturity parameter for evaluating the petroleum potential of sedimentary basins. Basin thermal history models commonly incorporate temperature-dependent kinetic models for vitrinite reflectance (e.g. Sweeney and Burnham, 1990) and thus model thermal predictions can be calibrated using measured vitrinite reflectance.

Whole rock cuttings and conventional core samples were prepared for organic petrology and vitrinite reflectance analysis by incident light microscopy at the GSC in Calgary generally following standard procedures for coal petrology (Stach *et al*., 1982). After gentle crushing, 1 to 10 mm sample particulates were mounted in epoxy to form pellets that were ground using carborundum and diamond grit followed by polishing on cloth and silk in an alumina-water slurry. An incident light microscope with white and fluorescent light sources, and oil, air and water immersion objectives (up to 2500x magnification) was used for organic petrography. Random per cent reflectance in oil ($\%Ro_R$) was measured on various macerals using the Leitz MPV II and Zeiss UMP systems with plane polarized white light at 546 nm and the polarizer set at 45 degrees. Data were collected using a Zeiss UMSP microscope fitted with a UMP photometer and a Leitz MPM II microscope with a PC-controller system. Glass standards of known refractive index (0.299, 0.506 %Ro) were used for reflectance calibration.

For Mesozoic and Cenozoic samples, $\%Ro_R$ was measured on vitrinite macerals (eu-ulminite B and telovitrinite A were preferred where possible). For Paleozoic samples, measurements were also made on bitumen and isotropic pyrobitumen and values were converted to vitrinite-equivalent $\%Ro_R$ values using the relation of Jacob (1989). In general, vitrinite is abundant in Cenozoic and Mesozoic strata and the number of reflectance measurements varied from approximately 10 to 60. The Paleozoic samples have less organic matter and the number of reflectance measurements per sample ranges from 4 to 36. Primary, caved and recycled vitrinite could be distinguished using optical criteria and by the analysis of reflectance histograms.

RESULTS AND INTERPRETATIONS

Rock-Eval Pyrolysis

Tables 1 to 3 list Rock-Eval 6 results for the three study wells. Data are presented in the familiar Rock-Eval 2 format plus a column for mineral carbon. Sample depths were recorded originally in feet for the three study wells. Therefore, Rock-Eval sample depths are given in both feet and metres in the data tables and for the plots showing Rock-Eval parameters versus depth. All three wells contain samples with anomalous (disturbed) pyrograms that are most likely caused by contamination. Colour coding is used to distinguish between normal or minimally disturbed pyrograms (green) and anomalous pyrograms (purple and orange) (e.g. multi-modal, asymmetric, irregular, etc.) (Tables 1 to 3). Also, sample depths are highlighted in yellow where vitrinite reflectance data are available. Tmax values for the least disturbed pyrograms were averaged to obtain representative thermal maturity estimates for each rock formation or stratigraphic sequence. These estimates can be assessed by comparison with the thermal maturity estimates obtained from vitrinite reflectance measurements.

Mallik A-06

Table 1 contains Rock-Eval 6 results for the Mallik A-06 well and selected parameters are shown plotted as a function of depth in Figure 5. Problems with data quality are evident in Figure 5 and this is confirmed by the analysis of individual pyrograms that show anomalous features (abnormally low Tmax, multimodal S1 and S2 peaks, asymmetric S2 curves with left and right shoulders; see comments in Table 1) that commonly are associated with sample contamination from drilling mud additives and migrated oil or bitumen (Peters, 1986).

Significant contamination is likely due to the generally poor condition of these unwashed cuttings samples. Of the three study wells, cuttings from the Mallik well are the most heavily depleted due to intense sampling over the years. When first collected, the wet drill cuttings were placed in cloth bags to dry. Consequently, for many of the samples, a significant amount of the remaining unwashed material has adhered to the sides of the sample bags, possibly introducing cloth fibres into the samples. Unfortunately, the mud reports in the well history are not very detailed but additives are mentioned that could affect Rock-Eval pyrograms. These include Kelzan (a carbohydrate biopolymer used as a mud viscosifier) and Peltex (ferrochrome lignosulphonate used as a mud thinner). Lignosulphonates give low Tmax (330-380°C) and high TOC (16-30 wt %) values but normally are not a problem because they can be washed out of samples (Roberston Group, 1989). Furthermore, organic petrological observations indicate that woody material is present in cuttings samples throughout the well whereas it is not present in core samples. In general, organic mud additives tend to decrease Tmax and can increase S1, S2, HI, PI and TOC values, depending on their composition (Peters, 1986).

Samples from the Iperk Sequence have anomalously high S2 and TOC values and elevated PI and HI values relative to many of the deeper samples in underlying stratigraphic sequences (Figure 5; Table 1). This unit also has some anomalously low Tmax values (< 400°C). Approximately 90% of the pyrograms are anomalous; the least disturbed pyrograms yield an average Tmax of 425.7±0.6°C (Table 1). The Iperk Sequence is immature and contains recycled organic matter that gives Tmax values higher than expected for its true level of maturity.

The underlying Mackenzie Bay Sequence shows a trend of slightly decreasing Tmax with depth as well as having some anomalously low Tmax values (Figure 5). Approximately 75% of the pyrograms show significant disturbance; the least affected pyrograms give an average Tmax value of 423.2±2.2°C (Table 1). Included in this average are two samples from 1110 and 1140 feet (338.3 and 347.5 m) with TOC values of approximately 0.3 wt%, S2 values of 0.26 and 0.24 mg HC/g rock, and Tmax values of 426 and 427°C, respectively. Although these TOC values are less than the 0.5 wt % limit recommended by Peters (1986) for limiting mineral matrix effects, corresponding S2 values slightly exceed his 0.2 mg HC/g rock limit for obtaining reliable Tmax values. It is possible that pyrolysate adsorption has increased the Tmax values by several degrees for these samples but any errors are not large; omitting these samples decreases the average Tmax by one degree to 422.3±1.3°C.

Kugmallit Sequence samples also show evidence of significant contamination with 78% of pyrograms identified as anomalous although all sample pyrograms have some degree of disturbance (Table 1). In the upper part of the Kugmallit Sequence, there is a trend of increasing Tmax with depth down to 3360 feet (1024 m), with Tmax increasing by more than 10°C over 1240 feet (378 m) (Figure 5). It is unlikely that this is a true thermal maturity trend. The more reasonable explanation is that Tmax is showing progressively less disturbance with depth. Although many of the S2 curves are unimodal over this interval, they are broad and asymmetric in shape and it is probable that labile organic contaminants are contributing to the observed high S2 and TOC values and low Tmax values (Figure 5). The average Tmax value for the least disturbed pyrograms is 426.1±3.2°C (Table 1).

Anomalous pyrograms have been identified for 46% of the Richards Sequence samples and 54% of the Taglu Sequence samples (Table 1). Most, but not all, of these pyrograms show obvious distortions in their shape due to contamination. There are a few pyrograms that appear to be relatively undisturbed but have very low Tmax values and elevated TOC and S2 values relative to the majority of the least disturbed samples. These Tmax values are significantly lower than expected for the observed sample burial depths and present temperatures and therefore some form of contamination is suspected. Figure 5 shows many examples where elevated TOC is associated with reduced Tmax and, in many cases, contamination can be demonstrated clearly. Analysis of extracts from selected samples from the Richards and Taglu sequences (8010 (2441.4), 8340 (2542), 9480 (2889.5), 11830 (3605.8) and 12930 (3941.1) feet (m); Table 1) indicate the presence of migrated oil (see below). Many of these oil-stained samples are associated with higher PI values and therefore the higher PI values below 11,800 feet (3597 m) suggest that there is a zone of migrated oil (Figure 5). Average Tmax values for the least disturbed pyrograms are 427.6±3.1°C and 431.0±3.7°C for the Richards and Taglu sequences, respectively (Table 1). Thermally mature sediments have Tmax values up to 440°C near the base of the well.

Figure 6 shows plots of HI versus OI and HI versus Tmax. As expected, these plots indicate that the well contains immature to mature, type III (terrestrially-derived) organic matter. However, these plots also show evidence of sample contamination through the presence of anomalously high OI values (up to 700 in the Kugmallit Sequence; Table 1), high HI values (7 samples have HI > 200) and low Tmax values (<410°C). Samples with HI > 300 tend to have high S1 and S2 values, low Tmax and multimodal S2 curves that are associated with oil (Table 1).

Parsons N-10

Similar to the Mallik A-06 well, unwashed cuttings samples had to be used for the Parsons N-10 well due to the low volume of material available for sampling. This greatly increases the potential for sample contamination by drilling mud additives. The daily drilling reports in the well history files list a number of additives that have the potential to affect Rock-Eval parameters. These include: Ben-Ex (mud viscosifier made of a blend of polyacrylate and polyacrylamide polymers), Q-Broxin (ferrochrome lignosulphonate mud thinner), Kwik-Seal (lost circulation material made from vegetable and polymer fibres), walnut shells (lost circulation material), CMC (carboxymethyl cellulose mud filtrate reducer) and Kelzan (carbohydrate biopolymer mud viscosifier). Table 2 contains Rock-Eval 6 data for the Parsons N-10 well and selected Rock-Eval parameters are plotted with respect to depth (in feet and metres) in Figure 7. Extensive sample contamination is clearly indicated from the top of the well down to a depth of 7200 feet (2195 m) by the highly variable and low Tmax (< 400°C), high PI (> 0.2) and high TOC values (Figure 7) and this is confirmed by examination of sample pyrograms (Table 2).

For the Iperk Sequence, 85% of sample pyrograms show obvious effects of contamination; the least disturbed pyrograms are probably affected to some degree as well and yield an average Tmax of 418.7±5.7°C (Table 2). The Iperk Sequence is thermally immature and the higher Tmax values (highlighted in orange in Table 2) reflect recycled organic matter. For the Aklak Sequence, at least 78% of pyrograms show evidence of sample contamination; the least affected pyrograms give an average Tmax of 425.2±4.0°C (Table 2). Below approximately 2000 feet (610 m) to the base of the Aklak Sequence, anomalous pyrograms are associated with high PI (approximately 0.2 to 0.5) and highly variable Tmax (296°C to 436°C) values (Figure 7). This trend continues into the Upper Cretaceous Mason River Formation and the Smoking Hills and Boundary Creek sequences where all samples are believed to be contaminated. The average Tmax for each of these Upper Cretaceous rock sequences is close to 415°C (Table 2).

Similar contamination occurs in the upper part of the Lower Cretaceous Arctic Red Formation (low Tmax, high PI) but this disappears abruptly at approximately 7200 feet (2195 m) (Figure 7). The reasons for this are unclear because there is no casing point at this depth or an obvious lithology change. Possibly the mud system was changed but this is not obvious in the drilling report. Most pyrograms are normal below 7200 feet. Average Tmax values for normal pyrograms are 432.4±1.8°C (Arctic Red Fm.), 431.8±3.2°C (Mount Goodenough Fm.), 434.0±0.9°C (Siku Member), 433.6±5.0°C (Kamik Fm.), 437.0±2.8°C (McGuire Fm.) and 438.5±1.4°C (Husky Fm.) (Table 2). Contamination is suspected for most of the samples in the Franklin Mountain Formation. Most samples show reduced Tmax, anomalous pyrograms and high PI values (0.2 to 0.5; Table 2). In addition to additives, caved material from the overlying Mesozoic section may also affect Rock-Eval parameters. For example, the Franklin Mountain Formation is a dolomite but it has mineral carbon values of < 10 wt% for most of the samples whereas this same unit has typical mineral carbon values of 10 to 13 wt% in the Kugaluk N-02 well (see below). It is possible that the carbonate is being diluted by caved material and organic petrology supports this (see section below on vitrinite reflectance results). Walnut shells were added to the mud system at the base of the well and this accounts for the high TOC (6.82 wt %) and low Tmax (311°C) for the deepest sample at 10490 feet (3197 m) (Table 2).

Plots of HI versus OI and HI versus Tmax (Figure 8) show that the well contains immature to mature, Type III organic matter. Tmax values approach 440°C in mature strata near the base of the well. There are Cretaceous marine stratigraphic units in the well and therefore there is probably a mix of type II and III organic matter. However, it is difficult to make definitive conclusions concerning organic matter type given the extent of sample contamination. Some of the highest HI values (> 200) are associated with contaminated samples in the Iperk, Aklak and Smoking Hills sequences, and the Mason River, Arctic Red, Husky and Franklin Mountain formations (Table 2). Contamination is also evident by the presence of anomalously low Tmax values (< 410°C) and high OI values (> 200) in the Iperk and Aklak sequences (Figure 8; Table 2).

Kugaluk N-02

Samples were collected from one inch diameter core from the Kugaluk N-02 well for Rock-Eval 6 analysis. Rock-Eval results are listed in Table 3 and selected parameters are plotted with respect to depth in Figure 9. Unfortunately, Rock-Eval parameters for all samples show evidence for substantial contamination due to the oil-based mud system used to drill the well (Table 3). According to the well history report, the following mud systems were used: invert (oil-based) mud for the 146 to 3855 foot interval (44.5 – 1175 m), invermul mud (oil-mud emulsion) for the 3855 to 4360 foot interval (1175 – 1328.9 m) and polymer mud for the 4360 to 8045 foot interval (1328.9 – 2452 m). The daily drilling report indicates that Kitwell oil was added to the polymer mud system during drilling.

The severity of sample contamination is evident by the anomalously low Tmax values (< 400°C) and anomalously high PI (0.2-0.76) values throughout the well (Figure 9). Most of the pyrograms are bimodal or highly asymmetric in shape and typically have a smaller high temperature S2 peak between 530 and 610°C (Table 3). For the Imperial Formation, Tmax averages 312.3±9.8°C and this is consistent with oil contamination. Only one sample yields a higher Tmax value of 532°C which indicates an overmature section. Similarly, five out of seven samples from the Canol Formation give an average Tmax of 306.6±9.8°C whereas two samples give a very high Tmax value of 606.5±0.7°C which is also consistent with an oil-contaminated, overmature section. Similar conclusions can be drawn for the Bluefish Member which has one low (327°C) and one high (601°C) Tmax value (Table 3).

TOC is generally quite low through the underlying carbonate succession (mainly < 0.2 wt%; Table 3). Three anomalously high TOC values in the Landry Formation are associated with very low Tmax (approximately 310-340°C) and high PI values (0.35-0.62). In spite of the very low TOC values, Tmax values are consistent and generally fall into two arbitrarily selected modes (300+°C and 400+°C). Both modes indicate drilling contamination because organic petrology shows that the entire well sequence is overmature (see below). Average Tmax values for mode 1 are 324.3±22.2°C (4 samples, Hume Fm.), 329.3±19.1°C (6 samples, Landry Fm.), 341.0±2.8°C (2 samples, Tatsieta Fm.), 354.4±19.2°C (10 samples, Peele Fm.), 351.8±13.8°C (4 samples, Mt. Kindle Fm.) and 376.0±8.5°C (2 samples, Franklin Mountain Fm.). Tmax values for mode 2 show a much narrower range of variation and are based on more samples. Average Tmax values for mode 2 are 440°C (1 sample, Hume Fm.), 430.8±4.6°C (28 samples, Landry Fm.), 432.1±3.3°C (7 samples, Arnica Fm.), 425.0±12.2°C (3 samples, Tatsieta Fm.), 418.6±12.9°C (16 samples, Peele Fm.), 421.3±7.7°C (33 samples, Mt. Kindle Fm.) and 425.6±6.0°C (38 samples, Franklin Mountain Fm.).

Severe sample contamination means that very little can be concluded from analysing the HI versus OI and HI versus Tmax plots (Figure 10). For example, almost all Tmax values are less than 440°C which is too low to reflect the true maturity of this overmature section. Given the high level of organic maturity, no firm conclusions can be given concerning organic matter type because pre-existing labile organic matter has been completely thermally degraded. Much of the organic matter in this marine succession was likely Type II based on what is known from equivalent but less mature Paleozoic successions examined elsewhere but this is not evident in Figure 10. For example, the Canol and Bluefish Member of the Hare Indian Formation are known to have good oil source rock characteristics in areas to the south (e.g. Snowdon *et al*., 1987).

Gas Chromatography and Gas Chromatography-Mass Spectrometry

Based on the results of Rock-Eval pyrolysis, samples with variably disturbed pyrograms were selected from the Mallik A-06 (14 samples) and Parsons N-10 (13 samples) wells for solvent extraction and organic geochemical analysis (Table 4). All samples are from well cuttings except for the deepest sample (2843.5 m, McGuire Formation; Table 4) from the Parsons N-10 well which is a coaly core sample.

Mallik A-06 – Rock-Eval Pyrograms

Figure 11 shows 14 Rock-Eval pyrograms for samples from the Iperk (a and b), Mackenzie Bay (c), Kugmallit (d and e), Richards (f-j), and Taglu (k-n) sequences from the Mallik A-06 well that were selected for GC and GC-MS analysis (Table 4). The FID response (in millivolts) depends on the organic richness and pyrolysis yield of each sample. Therefore, vertical axis scales were adjusted for each panel in Figure 11 (1.5 to 40 mV) to maximize the display area of the pyrolysis curves. The selected pyrograms show S2 curves with multi-modal peaks (Figure 11a, b, i, j and l), a broad peak (Figure 11d), and asymmetric peaks with left (Figure 11c, f-h, k and n) and right (Figure 11e) shoulders. The least disturbed pyrogram at 3941.1 m (12930 ft) in the Taglu Sequence has a relatively wide and asymmetric S2 peak with a low Tmax and elevated TOC value (Figure 11m; Table 4). Petrographic observations indicate that this sample is oil-stained (see below).

Mallik A-06 – GC and GC-MS Data

The saturate fraction gas chromatograms display several distinctive patterns (Figure 12). The upper interval (Iperk, Mackenzie Bay and Kugmallit sequences and upper part of Richards Sequence (222.5 – 1825.8 m); Figure 12a-g) is characterized by a broad distribution of C_{15}-C_{32} normal alkanes with a small unimodal or bimodal baseline hump. The n-alkane maxima are quite variable, from C_{15} (Kugmallit sample at 1274.1 m; Figure 12e) to C_{27} (Iperk sample at 222.5 m; Figure 12a). Isoprenoids are present in relatively lower concentrations with the pristane/phytane ratios typically greater than 1.0. A large baseline hump occurs in the samples from the middle interval (lower part of Richards Sequence and Taglu Sequence (2441.4 – 2889.5 m); Figure 12h-j). Smaller n-alkane peaks overprint the front slope of this hump. Below this interval, the Taglu sample at 3200.4m (Figure 12k) shows a unimodal distribution of n-alkanes with an almost flat baseline, high concentrations of C_{20}-C_{23} members (C_{21} maximum) and relative amounts of C_{23+} decreasing rapidly with increasing carbon number. Although the distinctive baseline hump observed in the middle interval re-appears below the Taglu sample at 3200.4 m (interval 3605.8 - 3941.1 m; Figure 12l and m), it is smaller than in the samples above. The lowermost Taglu sample (4096.5 m; Figure 12n) shows a more regular n-alkane profile centered at C_{19}-C_{22}, with a C_{20} maximum and much lower front and back ends, somewhat similar to that of the Taglu sample at 3200.4 m (Figure 12k).

The terpane (Figure 13) and sterane (figures 14 and 15) biomarker signatures are variable. The m/z 191 chromatograms show major C_{29} norhopane and C_{30} hopane peaks, especially in samples from the lower section (Richards and Taglu samples at 2441.4 m and below; Figure 13h-n) which, in general, show some differences compared with samples from shallower depths (Figure 13a-g). For example, the upper section has much higher concentrations of C_{21}-C_{25} tricyclic terpanes. Moretanes also occur in higher amounts relative to hopanes in the uppermost section (Iperk and Mackenzie Bay samples at 222.5 – 530.4 m; Figure 13a-c), indicating low thermal maturity. Samples from 1274.1 m (Kugmallit; Figure 13e) and 1347.2 m (Richards; Figure 13f) show a large peak at approximately 24 minutes which may belong to 25-norhopane. Moreover, unidentified large peaks that are present within the range of extended hopanes (C_{31}-C_{35}) might indicate the presence of unaltered biological configurations (Figure 13a-c and e-g). The hopane profiles of samples from the lower section (2441.4 m and below; Figure 13h-n) show signatures fairly typical for naturally occurring organic matter and petroleum. The C_{30} hopane is typically the dominant peak with the exception of the Taglu sample at 3941.1 m (Figure 13m). Whereas C_{21}-C_{24} tricyclic terpanes are present in relatively higher amounts in the Taglu samples at 3200.4 m (Figure 13k) and 4096.5 m (Figure 13n), C_{28}-C_{29} members are more pronounced in the other samples from that interval. Trisnorhopanes occur in relatively lower amounts with Ts/Tm ratios of less than 1.0. The Taglu sample from 3200.4 m (Figure 13k) shows a distinctive oleanane peak (an angiosperm marker) at 25.5 minutes. The homohopane profiles are fairly smooth with minor C_{35} predominance in several samples (Figure 13h-j and l).

Sterane fingerprints (m/z 217 and m/z 218) show high pregnane (C_{20}) and homopregnane (C_{21}) peaks for samples in the upper section (222.5 – 1825.8 m; figures 14a-g and 15a-g) and for several Taglu samples in the lower section at 3200.4 m (figures 14k and 15k) and

4096.5 m (figures 14n and 15n). Regular C_{27}-C_{29} steranes are more pronounced in the lower section, amounts of C_{27}, C_{28} and C_{29} being almost equal or slightly dominated by higher C_{29} (Figure 15h-n). Many of the samples show distinctive large peaks eluting after C_{29} sterane and these may represent unsaturated hopanes (Figure 15).

Mallik A-06 – Evidence for Biodegraded, Upper Cretaceous-Derived Oil

Overall, Rock-Eval parameters and GC and GC-MS data indicate that the Tertiary succession in the Mallik A-06 well contains immature to mature, terrestrially-derived organic matter. However, disturbed Rock-Eval pyrograms imply that the samples contain variable mixtures of heterogeneous organic components that may include contaminants from drilling mud additives. The upper section (222.5 – 1825.8 m; Figure 11a-g) is characterised by low thermal maturity (low Tmax in Table 1 and Figure 5; higher moretanes in Figure 13) and presence of possible unaltered biological components (large peaks in C_{31}-C_{35} range; Figure 13). The extent of drilling contamination is difficult to assess without other analytical methods such as pyrolysis GC but such contamination is likely to be significant because carbohydrates were added to the drilling mud and the samples were unwashed. Drilling contamination may be the source of the GC humps that occur at less than 30 minutes (Figure 12). Samples from the lower section (2441.4-4096.5 m; Figure 11h-n) also contain indigenous organic matter with higher plant material (Figure 13k) that ranges from immature to mature near the base of the well (Table 1 and Figure 5). However, the large GC humps (Figure 12h-j, l, and m) and C_{27}-C_{29} regular sterane distribution (Figure 15h-j, l, and m) suggest the presence of migrated and biodegraded oil derived from a marine source rock.

The Upper Cretaceous Boundary Creek and Smoking Hills formations are marine bituminous shales interpreted to be the source for oils discovered in reservoirs on the south and southeastern basin margin at Wagnark C-23 (Tertiary), Atkinson H-25, Imnak J-29, Kugpik O-13 and L-24 (Lower Cretaceous), and West Atkinson L-17 and Mayogiak J-17 (Paleozoic) (Brooks, 1986; McCaffrey et al., 1994) (Figure 1). Additional unpublished data suggest that the oils from the onshore Tuk and Tuktuk (mainly Tertiary on Tuktoyaktuk Peninsula south of Mayogiak) and Unak L-28 (south of Kugpik) discoveries, and the offshore Uviluk P-66 and Havik B-41 discoveries (north of Atkinson) were derived from Upper Cretaceous bituminous shale as well (Li et al., 2008a, b) (Figure 1). Although biomarker signatures show a clear association between Upper Cretaceous bituminous shale and oils on Tuktoyaktuk Peninsula, C and H stable isotope values for individual n-alkanes in these oils suggest that marine source rocks in the Upper Jurassic Husky Formation and Lower Cretaceous Kamik Formation have also contributed to these oils (Li et al., 2010).

Figure 16 shows GC and GC-MS data for an extract from a thermally mature outcrop sample from the Upper Cretaceous Boundary Creek Formation in the Yukon. The sample has a unimodal distribution of C_{13}-C_{28} normal alkanes with a maximum at C_{16} and a pristane/phytane ratio greater than 1 (Figure 16a). There is a major C_{30} hopane peak, a smooth homohopane profile, and trisnorhopanes give a Ts/Tm ratio greater than 1 (Figure 16b). There are major C_{27} and C_{29} diasterane peaks (Figure 16c) and regular C_{27}-C_{29} steranes occur in almost equal amounts (Figure 16d). Although the hydrocarbons at Mallik A-06 are significantly biodegraded, the samples retain some key chemical features. Similar to the Boundary Creek extract (Figure 16), they have smooth C_{31}–C_{35} homohopane profiles and relatively low tricyclic terpanes (Figure 13h-j, l and m) and nearly equal amounts of C_{27}, C_{28} and C_{29} regular steranes (Figure 15h-j, l and m). This suggests that the hydrocarbons could have been generated and expelled from a mature Upper Cretaceous bituminous source, migrated vertically into the lower maturity Tertiary succession containing terrestrial organic matter, and were subsequently biodegraded. As a result, gas chromatograms have mixed biomarker signatures that show contributions from immature Tertiary terrestrial organic matter and mature Cretaceous-derived petroleum. This is consistent with the interpretations of Li et al. (2006, 2008a,b, 2009, 2010) who conclude that the Upper Cretaceous Smoking Hills/Boundary Creek successions are a major source for many of the Tertiary-reservoired oils in offshore wells of the Beaufort-Mackenzie Basin. These results imply that Upper Cretaceous bituminous shales are likely more widespread in the Beaufort-Mackenzie region than mapped initially in Dixon (1996).

Parsons N-10 – Rock-Eval Pyrograms

Figure 17 shows Rock-Eval pyrograms for samples from the Iperk (a) and Aklak (b and c) sequences, the Mason River Formation (d-f), the Smoking Hills (g) and Boundary Creek (h and i) sequences, and the Arctic Red (j and k), Kamik (l) and McGuire (m) formations from the Parsons N-10 well that were selected for extract analysis (Table 4). Vertical axis scales were adjusted for each panel in Figure 17 (2 to 70 mV) to maximize the display area of the pyrolysis curves. In general, the pyrograms of Figure 17 appear to be less distorted than those of Figure 11. The selected pyrograms show S2 curves with a bimodal peak (Figure 17c), a broad peak (Figure 17b), and asymmetric peaks with right (Figure 17a) and left (Figure 17d-k) shoulders. A coaly sample of core material from the McGuire Formation at 2843.5 m (9329 ft) yields a normal, unimodal S2 peak (Figure 17m). A sample from the overlying Kamik Formation at 2825.5 m (9270 ft) yields an apparently normal pyrogram with a low Tmax (425) and elevated TOC (7.5%) value (Figure 17l; Table 4).

Parsons N-10 – GC and GC-MS Data

Several distinctive patterns are observed on the saturate fraction gas chromatograms (Figure 18). In the upper interval (Iperk and Aklak samples at 112.8 m and 338.3 m; Figure 18a and b), the Iperk sample shows an irregular n-alkane profile dominated by C_{21}-C_{23} members and some odd/even predominance in the C_{25}-C_{29} range. There is a characteristic cluster of peaks at around 25 minutes that most likely belongs to diterpenoids. These compounds are quite prominent in the Aklak sample below (338.3 m) and they dominate the gas chromatogram. The Aklak sample has another peak cluster at around 15 minutes that most likely represents sesquiterpenoids. The lower interval (Aklak, Mason River, Smoking Hills, Boundary Creek and Arctic Red samples at 1011.9 – 2084.4 m; Figure 18c-j) is characterized by a unimodal baseline hump that shows a systematic increase with increasing depth. This is associated with a slight shift in the profiles of the overprinting normal alkanes from the front towards the back end. The hump intensity diminishes towards the bottom of the sampled interval, especially in the deepest sample (McGuire sample at 2843.5 m; Figure 18m) which shows a broad n-alkane profile with an odd/even predominance within the C_{19}-C_{29} range. The McGuire sample also shows the highest pristane/phytane ratio of all Parsons N-10 samples. Overall, chromatograms with a baseline hump most likely reflect contamination by drilling additives.

The m/z 191 chromatograms (Figure 19) are dominated by C_{19}-C_{24} tricyclic terpanes (with typically a major peak belonging to the C_{23} member), except for the two shallowest (Figure 19a and b) and two deepest (Figure 19l and m) samples. The early eluting compounds visible in the two shallowest samples (Figure 19a and b) are likely diterpanes. Hopanes are present in relatively lower amounts with concentrations increasing with depth. The deepest sample (McGuire at 2843.5 m; Figure 19m) has the highest quantity of hopanes, at least an order of magnitude higher compared with other samples. This feature is also reflected in the m/z 217 and 218 chromatograms which show distinctive hopane peaks (figures 20m and 21m).

Similar to Mallik A-06 samples, pregnane (C_{20}) and homopregnane (C_{21}) form major peaks on m/z 217 and m/z 218 gas chromatograms (figures 20c-l and 21c-l). The C_{27}:C_{28}:C_{29} regular sterane profiles display a shift from C_{27} to C_{29} dominance with increasing depth. The Mason River samples (1627.6-1929.4 m) are dominated by the C_{27} member (Figure 21c-f), C_{27} and C_{28} are nearly equal for the Smoking Hills and shallower Boundary Creek sample (2011.7 m and 2030 m; Figure 21g and h), C_{28} is slightly dominant for the deeper Boundary Creek and shallower Arctic Red samples (2075.7 m and 2084.8 m; Figure 21i and j) and C_{29} is dominant for the Kamik sample (2825.5 m; Figure 21l). The distribution of steranes appears immature, with the αααR isomer (Figure 20) typically occurring in higher amounts compared to αααS and αββ isomers. This characteristic is best seen in the two deepest samples (2825.5 m and 2843.5 m; Figure 20l and m; Figure 21l and m). Therefore, biodegradation rather than maturity is the probable reason for the high relative concentration of tricyclic terpanes compared to hopanes (Figure 19c-k) because these compounds are more resistant to microbial degradation than hopanes.

Parsons N-10 – Implications for Interpreting Rock-Eval Data

The geochemical signature of the two uppermost samples (Iperk and Aklak; a and b in figures 18-21) is common for carbonaceous or coaly shales, indicating that some proportion of the indigenous organic matter is derived from gymnosperm plants. This is further confirmed by petrographic observations of coals in Iperk and Aklak samples and their high TOC values (tables 2 and 4). Although drilling contamination may be a factor, the very low Tmax values (Table 4) and the irregular shapes of the pyrograms (Figure 17a and b) are probably related to the low thermal maturity of these Tertiary coals. Samples in the intermediate interval (1011.9-2170.2 m) are generally immature with respect to oil generation and appear to be contaminated by drilling additives. This is consistent with the baseline GC hump at <30 minutes (Figure 18c-k), the high PI values (0.23-0.52; tables 2 and 4, Figure 7) and the asymmetric Rock-Eval pyrograms (17c-k). Drilling contamination seems to be more severe for the upper part of Parsons N-10 well (<2200 m; Figure 7) than for the Mallik A-06 well (Figure 5), probably because more organic-based mud additives were used and the samples were unwashed. The two deepest samples show much less contamination (Figure 18l and m) and contain mostly plant-derived organic matter. These Lower Cretaceous extracts have a dominance of C_{29} steranes (Figure 20l and m; Figure 21l and m) and a hopane distribution (Figure 19l and m) that is similar to Parsons/Siku/Kamik oils that are thought to be derived from Jurassic-Lower Cretaceous source rocks (Brooks, 1986; McCaffrey et al., 1994).

Vitrinite Reflectance

Table 5 lists codes and definitions for the organic matter types examined in this study and tables 6 to 8 contain vitrinite reflectance results for the three study wells. Tabulated information includes sample curation number, organic petrology lab pellet number, sample depth (in feet (original) and metres (converted)) with respect to Kelly Bushing and ground level elevations, stratigraphic unit, and mean random percent vitrinite reflectance in oil plus the standard deviation and number of measurements. Measurements were made on both core and cuttings samples and some samples contain multiple measurements corresponding to different vitrinite populations (caved, recycled) or organic matter types. Colour coding is used to highlight values that are plotted in figures 22 to 24. Yellow highlighting corresponds to primary vitrinite in cuttings (tables 6 and 7) or core samples (Table 8) whereas green highlighting indicates primary vitrinite in core samples (tables 6 and 7) or isotropic pyrobitumen %Ro_R converted to vitrinite-equivalent %Ro_R (Table 8).

Mallik A-06

Table 6 contains the results of %Ro_R measurements on primary vitrinite from core and cuttings samples from the Mallik A-06 well. Recycled vitrinite exists in both cuttings and core samples. In addition, woody material is observed in cuttings samples throughout the well, indicating probable contributions from caving and drilling mud contamination. Oil staining is known to decrease measured vitrinite reflectance and this was observed for samples at depths of 2897.1 mKB (9500-9510 feet) and 3939.5 mKB (12920-12930 feet) (Table 6). Suppressed %Ro_R values were interpreted for these two samples and results were confirmed by Rock-Eval (Table 1), GC (Figure 12j and m) and GC-MS (figures 13-15, j and m) analysis. The cuttings sample (2889.5m, 9480 feet; Table 1) immediately above the sample at 2897.1 mKB (9500-9510 feet) was extracted and indicates the presence of oil. Both of these samples have similar Rock-Eval parameters (high HI, high TOC, high PI; Table 1). Two other samples (3793.2 (12440-12450 feet) and 4104.1 (13460-13470 feet) mKB; Table 6) are inferred to have suppressed %Ro_R values; they occur in a zone of elevated PI values below 3597 m (11,800 feet) (Figure 5) and have anomalous pyrograms that may indicate oil staining (Table 1). It is possible that the core samples at 3599.7 mKB (11810 feet) and 3607.3 mKB (11835 feet) (Table 6) have suppressed %Ro_R values although their Rock-Eval parameters appear to be normal (Table 1). Analysis of an extract from a nearby cuttings sample (11830 feet or 3605.8 m) indicates oil staining (figures 12-15, panel l) and other nearby samples have Rock-Eval parameters consistent with oil staining (Table 1). The sample with the slightly low %Ro_R value at 3500.6 mKB (Table 6; Figure 22a) has a broad S2 curve with a reduced Tmax (Table 1; 11490 feet) which may be associated with oil staining.

The %Ro_R results of Table 6 are plotted with respect to drilled depth (Figure 22a) and estimated true vertical depth (corrected using the well deviation survey in the well history report; Figure 22b). There are only minor differences between Figure 22a and b but Figure 22b is included to provide a better estimate of maturity gradient because there is nearly a 176 m difference between measured depth and true vertical depth at the base of the Mallik A-06 well. Measured %Ro_R increases from 0.23 in the Iperk Sequence to 0.65 in the Taglu Sequence near the base of the well. An exponential curve was fitted to the %Ro_R-depth data for the Mackenzie Bay and older sequences (excluding suppressed values) and calculated vitrinite reflectance varies from 0.24 %Ro_R at 300 m near the top of the Mackenzie Bay Sequence to 0.69 %Ro_R at 3950 m near the base of the well (Figure 22b). Seismic and well log data indicate that there has been some erosion prior to the deposition of the Iperk Sequence and therefore a small maturity discontinuity may exist between the Iperk and Mackenzie Bay Sequences. Extrapolation of the exponential trend in Figure 22b to an initial surface %Ro_R value of 0.2 gives an estimated erosion magnitude of approximately 700 m (estimate includes the thickness of the post-erosion Iperk Sequence overlying the unconformity). The extrapolation of shale compaction data as described by Issler (1992) yields a similar amount of pre-Iperk erosion for the Mallik A-06 well.

Vitrinite reflectance thermal maturity results can be assessed in comparison with Rock-Eval Tmax results for samples with the least disturbed pyrograms. Tmax values were converted to vitrinite reflectance equivalents using the polynomial equation in Issler *et al*. (2005) that was fitted to tabulated data for type III organic matter (MATOIL™, 1990). Average Tmax values for selected pyrograms from each stratigraphic sequence (Table 1) give the following equivalent $\%Ro_R$ values: 0.39 (426°C; Iperk), 0.27 (423°C; Mackenzie Bay), 0.39 (426°C; Kugmallit), 0.47 (428°C; Richards), 0.57 (431°C; Taglu). The average of measured vitrinite reflectance values (excluding suppressed values) are 0.23 (Iperk), 0.26 (Mackenzie Bay), 0.28 (Kugmallit), 0.46 (Richards) and 0.56 $\%Ro_R$ (Taglu). Corresponding interpolated values at the mid-depth point for four of the stratigraphic sequences are 0.26 (Mackenzie Bay), 0.30 (Kugmallit), 0.42 (Richards) and 0.61 $\%Ro_R$ (Taglu).

In general, there is very good agreement between the thermal maturity estimates from edited Tmax values (excluding contributions from samples with anomalous Rock-Eval pyrograms; Table 1) and measured vitrinite reflectance. Discrepancies occur where a dominance of recycled organic matter increases Tmax values. For the Iperk Sequence, a reworked population of vitrinite has a measured reflectance value of 0.35±0.05 $\%Ro_R$ (Table 6) which is close to the level of maturity inferred from Tmax (0.39 $\%Ro_R$). Similarly, for the Kugmallit Sequence, there are a range of higher Tmax values (427 to 434°C; Table 1) with vitrinite reflectance equivalent values (0.43 to 0.66 $\%Ro_R$) that closely match the range of measured recycled vitrinite populations (0.43 to 0.67 $\%Ro_R$; Table 6). As a further check on organic maturity, a sandstone sample from the Richards Sequence at approximately 3211 mKB yields two apatite populations with different chemical compositions and annealing kinetic parameters that have AFT ages of 45.6±2.7 Ma and 70.1±4.7 Ma and corresponding mean AFT lengths of 10.89±1.43 μm and 11.67±1.19 μm. Qualitatively, the observed amount of AFT annealing is consistent with the measured maturity (0.55 $\%Ro_R$) based on the analysis of other samples in the region with similar characteristics that have been successfully modelled (unpublished work; Issler and Grist, 2008). Detailed AFT data and thermal modelling results will be published elsewhere.

Parsons N-10

Table 7 contains the results of $\%Ro_R$ measurements on primary vitrinite from core and cuttings samples from the Parsons N-10 well. Recycled and caved vitrinite occur over the depth of the well. Two core samples previously collected in 2001 (2752.3 (9030 feet) and 2799.6 (9185 feet) mKB) and analysed by Maria Tomica at GSC Calgary are included in Table 7. The sample at 2752.3 mKB was reanalysed and yielded very similar results to the original analysis (0.57±0.02 $\%Ro_R$ (new) versus 0.55±0.03 $\%Ro_R$ (original)). The original analysis for the sample at 2799.6 mKB is used in Table 7. Also included in Table 7 are $\%Ro_R$ measurements on core samples done by Paul Gunther at GSC Calgary during 1974 (included in NEB well history report). These older data are in close agreement with the more recent measurements. Vitrinite reflectance measurements for the sample from Cambro-Ordovician dolomite of the Franklin Mountain Formation (3195.8 mKB (10480-10490 feet); Table 7) are believed to be affected by caving from the overlying Cretaceous section and are excluded from further analysis (see above section describing Rock-Eval data).

The $\%Ro_R$ results (Table 7) are plotted with respect to drilled depth in Figure 23. Measured $\%Ro_R$ increases from 0.25 in the Iperk Sequence to 0.66 at the base of the Husky Formation. The Plio-Pleistocene Iperk Sequence rests unconformably on the Late Paleocene-Early

Eocene Aklak Sequence. Seismic and well data indicate significant erosion that resulted in a maturity discontinuity across this unconformity. Therefore, an exponential curve was fitted to the $\%Ro_R$-depth data for the Aklak to Husky interval and calculated vitrinite reflectance varies from 0.29 $\%Ro_R$ at the top of the Aklak Sequence (204 mKB) to 0.64 $\%Ro_R$ at the base of the Husky Formation (3077 mKB) (Figure 23). The $\%Ro_R$-depth curve provides a reasonable fit to the data but underestimates thermal maturity in the Kamik to Husky interval. Extrapolation of the exponential trend in Figure 23 to an initial surface $\%Ro_R$ value of 0.2 gives an estimated erosion magnitude of approximately 1290 m (estimate includes the thickness of the post-erosion Iperk Sequence). Shale compaction data gives approximately 600 to 900 m of pre-Iperk erosion at this well location.

Rock-Eval Tmax results for samples with the least disturbed pyrograms provide an independent measure of thermal maturity that can be compared with vitrinite reflectance results. Tmax values were converted to vitrinite reflectance equivalents using tabulated data for type II and III organic matter (MATOIL^{TM}, 1990). In general, Cenozoic strata contain type III organic matter whereas Cretaceous strata were deposited mainly in a marine environment and contain type II organic matter except for the Kamik Formation which contains coaly intervals. Average representative Tmax values for selected stratigraphic intervals (Table 2) give the following equivalent $\%Ro_R$ values: <0.20 (419°C; Iperk, type III), 0.35 (425°C; Aklak, type III), 0.55 (432°C; Arctic Red, type II), 0.55 (432°C; Mount Goodenough, type II), 0.60 (434°C; Siku, type II), 0.66 (434°C; Kamik, type III), 0.66 (437°C; McGuire, type II) and 0.69 (438.5°C; Husky, type II). Average Tmax values could not be determined for the Mason River, Smoking Hills and Boundary Creek formations because all pyrograms are affected by contamination (Table 2). The average of measured vitrinite reflectance values are 0.25 (Iperk), 0.35 (Aklak), 0.48 (Arctic Red), 0.53 (Mount Goodenough), 0.59 (Kamik), 0.63 (McGuire) and 0.66 $\%Ro_R$ (Husky). Corresponding interpolated values at the mid-depth point for six of the stratigraphic sequences are 0.34 (Aklak), 0.50 (Arctic Red), 0.53 (Mount Goodenough), 0.58 (Kamik), 0.60 (McGuire) and 0.62 $\%Ro_R$ (Husky).

There is good agreement between the thermal maturity estimates based on Tmax values from normal pyrograms and measured vitrinite reflectance. For the Iperk Sequence, all pyrograms are affected to some degree by drilling contamination and therefore maturity may be underestimated using Tmax. For the Aklak sequence, average thermal maturity is consistent between Tmax and vitrinite reflectance. For the Lower Cretaceous units, Tmax thermal maturity estimates are slightly higher than those based on vitrinite reflectance. These thermal maturity results are further supported by AFT data. A sandstone core sample from the Kamik Formation (approximately 135 Ma; Valanginian - Hauterivian) at approximately 2758 mKB yields two apatite populations with AFT ages of approximately 47 and 83 Ma. Unfortunately, there are no compositional or AFT length data for this sample but the AFT ages imply two populations with different compositions and annealing kinetics. Qualitatively, the observed amount of AFT age reduction indicates substantial but incomplete annealing that is consistent with the measured maturity (0.57-0.60 $\%Ro_R$; Table 7) based on a comparison with other AFT data for the region. Two slightly deeper samples (2861.7 and 2886.2 mKB) in the Martin Creek Formation (approximately 141 Ma; Berriasian) also contain two different apatite populations with different annealing kinetics. The less track retentive apatite populations in both samples have very young AFT ages (18.7 and 23.9 Ma) and short mean AFT lengths (9.54 and 9.37 μm) that imply complete thermal annealing during maximum burial, consistent with the measured vitrinite reflectance values directly above and below the samples (0.63-0.65 $\%Ro_R$; Table 7).

Kugaluk N-02

Table 8 contains the results of $\%Ro_R$ measurements on primary vitrinite and isotropic pyrobitumen from core samples from the Kugaluk N-02 well. Although cavings are not an issue, the samples contain both low and high reflecting organic material. The main source of sample contamination is from the oil-based mud used to drill the well which affected all Rock-Eval parameters. In general, due to the low TOC content, it was difficult to obtain very many measurements. Measurements were obtained mainly from vitrinite and vitrinite-like macerals in the Imperial, Canol and Landry formations and co-existing bitumen and isotropic pyrobitumen gave similar vitrinite-equivalent reflectance values (Table 8). Below the Landry Formation, measurements are deemed to be unreliable due to the limited amount of suitable organic material and the dominance of anisotropic pyrobitumen.

The $\%Ro_R$ results of Table 8 are plotted with respect to drilled depth in Figure 24. Measured $\%Ro_R$ increases from approximately 1.6 in the Imperial Formation to 2.0 in the Landry Formation over a depth range of 960 m. An exponential curve was fitted to the $\%Ro_R$-depth data (Figure 24) and extrapolated vitrinite reflectance values vary from 1.5 $\%Ro_R$ at the top of the Imperial Formation to 2.7 $\%Ro_R$ at 2452 m within the Franklin Mountain Formation at the base of the well. The very high maturity levels indicate high paleotemperatures and substantial erosion; vitrinite reflectance values > 1.5 $\%Ro_R$ imply maximum burial temperatures > 150°C (Morrow and Issler, 1993). Extrapolation of the exponential $\%Ro_R$-depth curve in Figure 24 to an initial surface $\%Ro_R$ value of 0.2 gives an estimated erosion magnitude of approximately 8 km. This estimate may be an upper limit and is subject to significant error due to the limited depth range of the data. The modest $\%Ro_R$ gradient suggests deep burial under a modest geothermal gradient (approximately 21 ºC/km according to the method of Middleton, 1982).

It is not possible to compare vitrinite reflectance thermal maturity estimates with Rock-Eval Tmax values due to severe sample contamination by oil-based drilling mud. However, many Rock-Eval pyrograms are multi-modal with high temperature peaks in the 500 to 600°C range (Table 3), indicating that the samples are overmature which is in general agreement with the reflectance microscopy results. The high level of organic maturity is further supported by two AFT samples collected from the Imperial Formation at depths of approximately 384 and 610 mKB. These samples have AFT ages of 216.2±13.8 Ma and 199.2±16.0 Ma, respectively, with corresponding mean AFT lengths of 12.68±1.51 and 12.26±1.83 μm. The relatively young AFT ages of the samples compared with their stratigraphic age (approximately 375 Ma; Figure 3) and their relatively long mean lengths indicates that the samples experienced total thermal annealing (>110°C) during maximum burial followed by cooling during Triassic and later times. Estimated thermal maturity for these samples is 1.63 $\%Ro_R$ (384 mKB) and 1.72 $\%Ro_R$ (610 mKB), implying that the samples were at temperatures significantly higher than their total AFT annealing temperatures.

DISCUSSION

NEB drill cuttings samples from the Mallik A-06 and Parsons N-10 wells were depleted considerably by sampling in previous years. Given the limited sample volumes available, unwashed samples were analysed and this raises concerns about sample quality and the potential effects of contamination from drilling mud additives. Samples with anomalous

Rock-Eval pyrograms (broad, asymmetric and/or multi-modal S2 curves) were identified as being contaminated and extracts from a subset of these (figures 11 and 17) were analysed using GC and GC-MS analysis to investigate the source of the contamination. Samples with unimodal and symmetric S2 pyrograms are considered normal and these were used to obtain average Tmax values for the various stratigraphic successions (tables 1 to 3). In spite of the widespread nature of sample contamination, useful new paleotemperature constraints have been obtained for the Mallik A-06, Parsons N-10 and Kugaluk N-02 wells. The integration of multiple thermal indicators (vitrinite reflectance, Rock-Eval Tmax, AFT annealing) and their overall agreement gives us confidence in the thermal maturity results presented here.

Rock-Eval, GC and GC-MS data provide new evidence for early petroleum generation, migration and biodegradation at the Mallik A-06 well location. The Taglu Sequence and part of the Richards Sequence contain biodegraded oil that is correlated with an Upper Cretaceous source (Smoking Hills/Boundary Creek formations) and that coincides with a zone of overpressure (Issler et al., 2002, 2011). In a study of pore water chemistry, Grasby et al. (2009) inferred that there is a zone of biodegradation in association with high alkalinity, overpressured fluids at Mallik A-06 and at other nearby wells north of the Taglu Fault Zone. They suggested that deep meteoric water invasion occurred during Late Miocene uplift and erosion of the basin margin and that subsequent rapid burial and overpressuring allowed for high alkalinity fluids to develop in a closed system through anaerobic methanogenesis. Although detailed timing relationships concerning oil generation, migration and biodegradation still need to be worked out, our results confirm that there is a zone of biodegradation in the lower part of the Mallik A-06 well. Furthermore, our results are compatible with the interpretations of Li et al. (2006, 2008a,b, 2009, 2010) that the Upper Cretaceous Smoking Hills/Boundary Creek successions may be a major source for Tertiary-reservoired oils in many wells in the central and eastern offshore areas of the Beaufort-Mackenzie Basin.

Stasiuk *et al.* (2005, 2009) have published two GSC open file reports on thermal maturity for selected Beaufort-Mackenzie wells. This publication represents the third in a series of five planned open file reports on thermal maturity for selected wells from the Beaufort-Mackenzie Basin. All of the new thermal maturity results will be used in the preparation of regional maps and cross sections showing thermal maturity trends and erosion magnitudes across the study area. Also, these data will be used as constraints for integrated thermal history and petroleum generation models involving AFT and other geological data as part of a basin-scale study of petroleum systems of the Beaufort-Mackenzie Basin.

CONCLUSIONS

Rock-Eval and vitrinite reflectance data were obtained for unwashed cuttings and core samples from the Mallik A-06 and Parsons N-10 wells (Beaufort-Mackenzie Basin), and for core samples from the Kugaluk N-02 well (Anderson Plain). Many samples have disturbed pyrograms that imply significant sample contamination. GC and GC-MS analyses of selected sample extracts were undertaken to investigate the nature of the sample contamination. Results indicate that organic drilling mud additives have significantly affected Rock-Eval parameters in the upper sections of the Mallik A-06 (Iperk to Richards sequences) and Parsons N-10 (mainly upper Cretaceous and younger successions) wells. The lower part of the Mallik A-06 well (Richards and Taglu sequences) shows extensive contamination by migrated and biodegraded oil believed to be derived from mature, Upper Cretaceous bituminous shale (Boundary Creek/Smoking Hills formations). Most samples from the Jurassic-Lower Cretaceous succession in the Parsons N-10 well have normal pyrograms. All samples in the Kugaluk N-02 well have been contaminated severely by oil-based drilling mud. Samples with the least disturbed pyrograms yield Tmax thermal maturity values that are in close agreement with measured vitrinite reflectance values for the Mallik A-06 and Parsons N-10 wells. Thermal maturity varies from immature (0.2-0.3%Ro) to mature (0.65-0.7 %Ro) in both wells whereas the sedimentary succession is overmature (>1.5%Ro) in the Kugaluk N-02 well. Measured maturity values are in qualitative agreement with the observed degree of apatite fission track annealing in samples collected from these wells and maturity gradients yield net erosion magnitudes of 0.7, 1.3 and 8 km for the Mallik A-06, Parsons N-10 and Kugaluk N-02 wells, respectively.

ACKNOWLEDGEMENTS

We thank Krista Boyce of GSC Calgary for sample collection, preparation and curation. Ross Stewart (contractor) did the Rock-Eval analysis using a Rock-Eval 6 instrument at GSC Calgary. Sneh Achal of the organic geochemistry laboratory at GSC Calgary prepared the samples for GC and GC-MS analysis. This study was funded by the Beaufort-Mackenzie consortium of companies (BP Canada Energy Company, Chevron Canada Limited, ConocoPhillips Canada Resources Corporation, Imperial Oil Resources Ventures Limited, MGM Energy Corporation and Shell Exploration and Production Company), the Program of Energy Research and Development (PERD) and Natural Resources Canada through the Earth Sciences Sector Secure Canadian Energy Supply and Geo-Mapping for Energy and Minerals (GEM) programs. The authors thank Dr. Roger Macqueen for his thorough and constructive review of the manuscript.

REFERENCES

Behar, F., Beaumont, V. and De B. Penteado, H.L. 2001. Rock-Eval 6 Technology: Performances and Developments. Oil & Gas Science and Technology – Revue de l'Institut Français du Pétrole, v. 56, no. 2, p. 111-134.

Brooks, P.W. 1986. Biological marker geochemistry of oils from the Beaufort-Mackenzie region, Arctic Canada. Bulletin of Canadian Petroleum Geology, v. 34, no. 4, p. 490-505.

Dahl, B., Bojesen-Koefoed, J., Holm, A., Justwan, H., Rasmussen, E. and Thomsen, E. 2004. A new approach to interpreting Rock-Eval S2 and TOC data for kerogen quality assessment. Organic Geochemistry, v. 35, p. 1461-1477.

Dallimore, S.R., Uchida, T. and Collett, T.S., editors, 1999. Scientific results from JAPEX/JNOC/GSC Mallik 2L-38 gas hydrate research well, Mackenzie Delta, Northwest Territories, Canada. Geological Survey of Canada, Bulletin 544, 403 p.

Dallimore, S.R., and Collett, T.S., editors, 2005. Scientific results from the Mallik 2002 Gas Hydrate Production Research Well Program, Mackenzie Delta, Northwest Territories, Canada. Geological Survey of Canada, Bulletin 585, 140 p. (1 CD-ROM)

Dixon, J., editor, 1996. Geological Atlas of the Beaufort-Mackenzie Region. Geological Survey of Canada, Miscellaneous Report 59, 173p.

Dixon, J., Morrel, G.R., Dietrich, J. R., Taylor, G.C., Procter, R.M., Conn, R.F., Dallaire, S.M. and Christie, J. A. 1994. Petroleum resources of the Mackenzie Delta and Beaufort Sea. Geological Survey of Canada, Bulletin 474, 52 p.

Espitalié, J., Madec, M., Tissot, B., Mennig, J.J. and Leplat, P. 1977. Source rock characterization method for petroleum exploration. Proceedings of the 9th Annual Offshore Technology Conference, v. 3, p. 439-448.

Espitalié, J., Madec, M. and Tissot, B. 1980. Role of mineral matrix in kerogen pyrolysis: influence on petroleum generation and migration. American Association of Petroleum Geologists Bulletin, v. 64, no. 1, p. 59-66.

Espitalié, J., Marquis, F. and Barsony, I. 1984. Geochemical Logging. *In*: Voorhees, K.J. (ed.). Analytical Pyrolysis – Techniques and Applications. Boston, Butterworth, p. 276-304.

Gallagher, K., Brown, R. and Johnson, C. 1998. Fission track analysis and its applications to geological problems. Annual Reviews of Earth and Planetary Science, v. 26, p. 519-572.

Gleadow, A.J.W., Belton, D.X., Kohn, B.P. and Brown, R.W. 2002. Fission track dating of phosphate minerals and the thermochronology of apatite. In: Phosphates; Geochemical, Geobiological and Materials Importance. M. J. Kohn, J. Rakovan and J.M. Hughes (eds.). Reviews in Mineralogy and Geochemistry, v. 48, p. 579-630.

Grasby, S.E., Chen, Z., Issler, D. and Stasiuk, L. 2009. Evidence for deep anaerobic biodegradation associated with rapid sedimentation and burial in the Beaufort-Mackenzie basin, Canada. Applied Geochemistry, v. 24, p. 536-542.

Issler, D.R. 1992. A new approach to shale compaction and stratigraphic restoration, Beaufort-Mackenzie Basin and Mackenzie Corridor, northern Canada. American Association of Petroleum Geologists Bulletin, v. 76, no. 8, p. 1170-1189.

Issler, D.R., Katsube, T.J., Bloch, J.D. and McNeil, D.H. 2002. Shale compaction and overpressure in the Beaufort-Mackenzie Basin of northern Canada. Geological Survey of Canada, Open File 4192, 10 p.

Issler, D.R., Grist, A.M. and Stasiuk, L.D. 2005. Post-Early Devonian thermal constraints on hydrocarbon source rock maturation in the Keele Tectonic Zone, Tulita area, NWT, Canada, from multi-kinetic apatite fission track thermochronology, vitrinite reflectance and shale compaction. Bulletin of Canadian Petroleum Geology, v. 53, no. 4, p. 405-431.

Issler, D.R. and Grist, A.M. 2008. Integrated thermal history analysis of the Beaufort-Mackenzie basin using multi-kinetic apatite fission track thermochronology. Geochimica et

Cosmochimica Acta, v. 72, no. 12S, p. A413 (Special Supplement, Awards Ceremony Speeches and Abstracts of the 18th Annual V.M. Goldschmidt Conference, Vancouver, Canada, July 13-18, 2008).

Issler, D.R., Hu, K., Lane, L.S. and Dietrich, J.R. 2011. GIS Compilations of Depth to Overpressure, Permafrost Distribution, Geothermal Gradient, and Regional Geology, Beaufort Mackenzie Basin, Northern Canada. Geological Survey of Canada, Open File 5689.

Jacob, H. 1989. Classification, structure, genesis and practical importance of natural solid oil bitumen (“migrabitumen”). International Journal of Coal Geology, v. 11, p. 65-79.

Lafargue, E., Marquis, F. and Pillot, D. 1998. Rock-Eval 6 Applications in Hydrocarbon Exploration, Production and Soil Contamination Studies. Oil & Gas Science and Technology – Revue de l’Institut Français du Pétrole, v. 53, no. 4, p. 421-437.

Li, M., Xiong, Y., Snowdon, L.R. and Issler, D.R. 2006. Cross-formational hydrocarbon fluid flows in the Tertiary deltaic system of the Beaufort-Mackenzie Basin. Journal of Geochemical Exploration, v. 89, Issues 1-3, p. 214-217.

Li, M., Chen, Z., Achal, S., Milovic, S., Robinson, R., Snowdon, L. and Issler, D. 2008a. New geological and geochemical constraints for the petroleum systems in the Beaufort-Mackenzie Basin, Canada. Book of Extended Abstracts, 7th International Conference and Exhibition on Petroleum Geochemistry and Exploration in the Afro-Asian Region, Association of Afro-Asian Petroleum Geochemists, Shehu Musa Yar’Adua Centre, Abuja, Nigeria (October 19-20), p. 14-18.

Li, M., Zhang, S., Snowdon, L. and Issler, D. 2008b. Oil-source correlation in the Tertiary deltaic petroleum systems: a comparative study of the Beaufort-Mackenzie Basin in Canada and the Pearl River Mouth Basin in China. Organic Geochemistry, v. 39, p. 1170-1175.

Li, M., Chen, Z., Hu, K., Achal, S., Milovic, M., Robinson, R. and Issler, D. 2009. Recognition of deep Upper Cretaceous marine petroleum source rocks in the offshore region of the Beaufort-Mackenzie Basin and implications for the thermal history and hydrocarbon generation models of Tertiary deltaic sequences. Abstract volume, 24th International Meeting on Organic Geochemistry, Bremen, Germany (September 6-11).

Li, M., Chen, Z., Issler, D., Achal, S., Milovic, M. and Robinson, R. 2010. New insights into the effective petroleum source rocks in the Beaufort-Mackenzie Basin from an integrated molecular and isotope approach. AAPG Search and Discovery Article #40669 (2010), Adapted from oral presentation at American Association of Petroleum Geologists International Conference and Exhibition, Calgary, Alberta, Canada, September 12-15, 2010. http://www.searchanddiscovery.com/documents/2010/40669li/ndx_li.pdf

MATOIL™ 1990. A quantitative model of hydrocarbon generation for the personal computer. Bureau d’Etudes Industrielles et de Coopération de l’Institut Français du Pétrole. Rueil-Malmaison, France.

McCaffrey, M.A., Dahl, J.E., Sundararaman, P., Moldowan, J. M. and Schoell, M. 1994. Source rock quality determination from oil biomarkers II – a case study using Tertiary-reservoired Beaufort Sea oils. American Association of Petroleum Geologists Bulletin, v. 78, no. 10, p. 1527-1540.

Middleton, M.F. 1982. Tectonic history from vitrinite reflectance. Geophysical Journal of the Royal Astronomical Society, v. 68, p. 121-132.

Morrow, D.W. and Issler, D.R. 1993. Calculation of vitrinite reflectance from thermal histories: a comparison of some methods. American Association of Petroleum Geologists Bulletin, v. 77, no. 4, p. 610-624.

Morrow, D.W., Jones, A.L. and Dixon, J. 2006. Infrastructure and Resources of the Northern Canadian Mainland Sedimentary Basin. Geological Survey of Canada, Open File 5152, 59 p.

NEB, 1998. Probabilistic estimate of hydrocarbon volumes in the Mackenzie Delta and Beaufort Sea discoveries. Report by National Energy Board of Canada (Cat. No. NE23-78/1998E, ISBN 0-662-27455-5), Calgary, 8 p.

Obermajer, M., Stewart, K. R. and Dewing, K. 2007. Geological and Geochemical Data from the Canadian Arctic Islands, Part II: Rock-Eval/TOC Data. Geological Survey of Canada, Open File 5459, 27 (+ fig.) p. (CD-ROM)

Peters, K.E. 1986. Guidelines for evaluating petroleum source rock using programmed pyrolysis. American Association of Petroleum Geologists Bulletin, v. 70, no. 3, p. 318-329.

Riediger, C., Carrelli, G.G. and Zonneveld, J.-P. 2004. Hydrocarbon source rock characterization and thermal maturity of the Upper Triassic Baldonnel and Pardonet formations, northeastern British Columbia, Canada. Bulletin of Canadian Petroleum Geology, v. 52, no. 4, p. 277-301.

Robertson Group 1989. A Manual of the Geochemical and Palynological Properties of Selected Mud Additives. Publication by The Roberston Group plc, 209 p.

Snowdon, L.R., Brooks, P.W., Williams, G.K. and Goodarzi, F. 1987. Correlation of the Canol Formation source rock with oil from Norman Wells. Organic Geochemistry, v. 11, no. 6, p. 529-548.

Stach, E., Mackowsky, M.-Th., Teichmüller, M., Taylor, G.H., Chandra, D., Teichmüller, R. 1982. Stach's Textbook of Coal Petrology. 3rd edition, Gebrüder Borntraeger, Berlin, 535 p.

Stasiuk, L.D., Issler, D.R., Tomica, M. and Potter, J. 2005. Re-evaluation of thermal maturation - vitrinite reflectance profiles for Cretaceous and Tertiary strata, Beaufort-Mackenzie basin, Northwest Territories (Adlartok P-09, Amerk O-09, Edlok N–56, Ikhil K-35, Sarpik B-35, Hansen G-07 and Havik B-41). Geological Survey of Canada, Open File 4665. (CD-ROM)

Stasiuk, L.D., Issler, D.R., Dixon, J. and McNeil, D.H. 2009. Thermal maturity of Cretaceous and Tertiary strata in the Itiginkpak F-29, Napartok M-01, Kurk M-15, Tuk B-02 and Tuk M-18 wells, Beaufort-Mackenzie Basin, Northwest Territories. Geological Survey of Canada, Open File 5639. (CD-ROM)

Sweeney, J.J. and Burnham, A.K. 1990. Evaluation of a simple model of vitrinite reflectance based on chemical kinetics. American Association of Petroleum Geologists Bulletin, v. 74, p. 1559-1570.

Wagner, G.A. and Van den Haute, P. 1992. Fission track dating. Klewer Academic Publishers, Dordrecht, 285p.

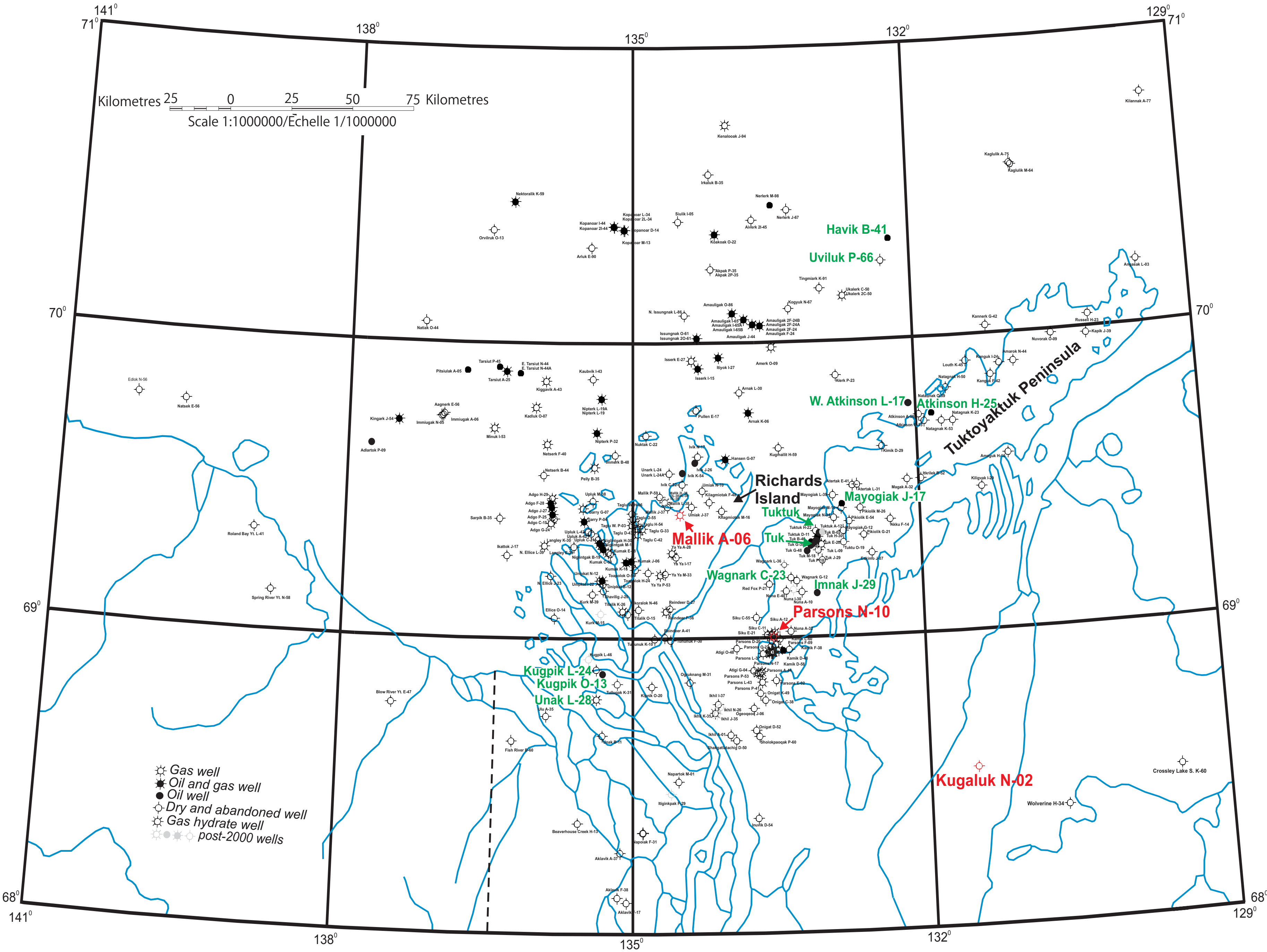

Figure 1. Map showing location of the three study wells (in red), Beaufort-Mackenzie Basin, Northwest Territories. Other wells mentioned in text are in green.

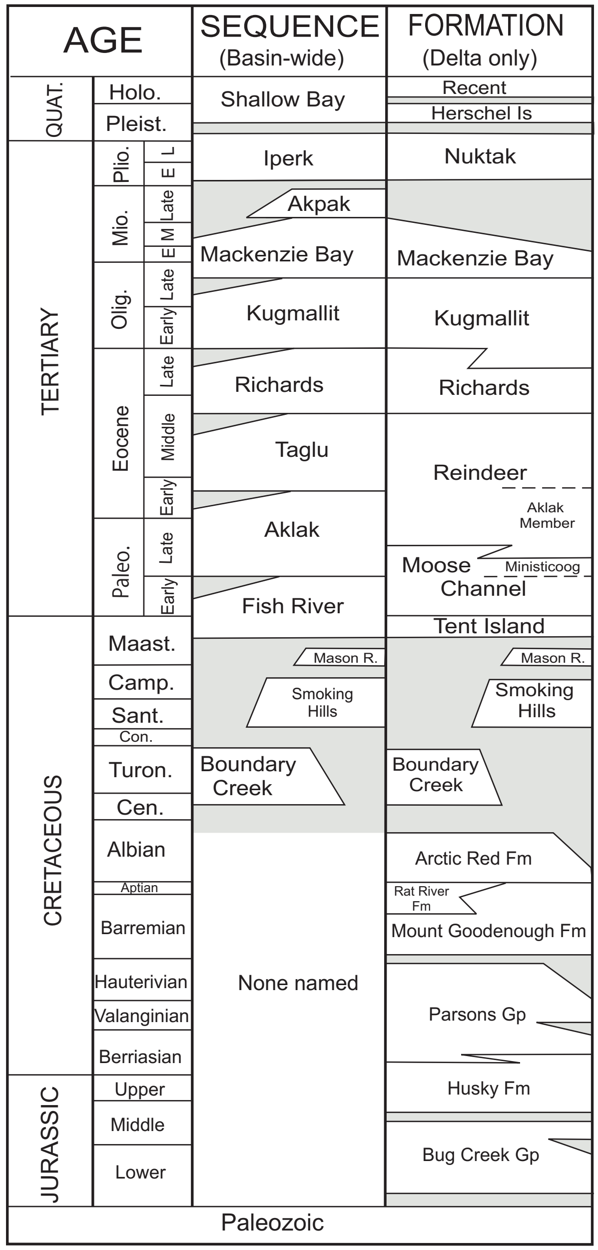

Figure 2. Stratigraphy of the Beaufort-Mackenzie region (J. Dixon, personal communication, 2009).

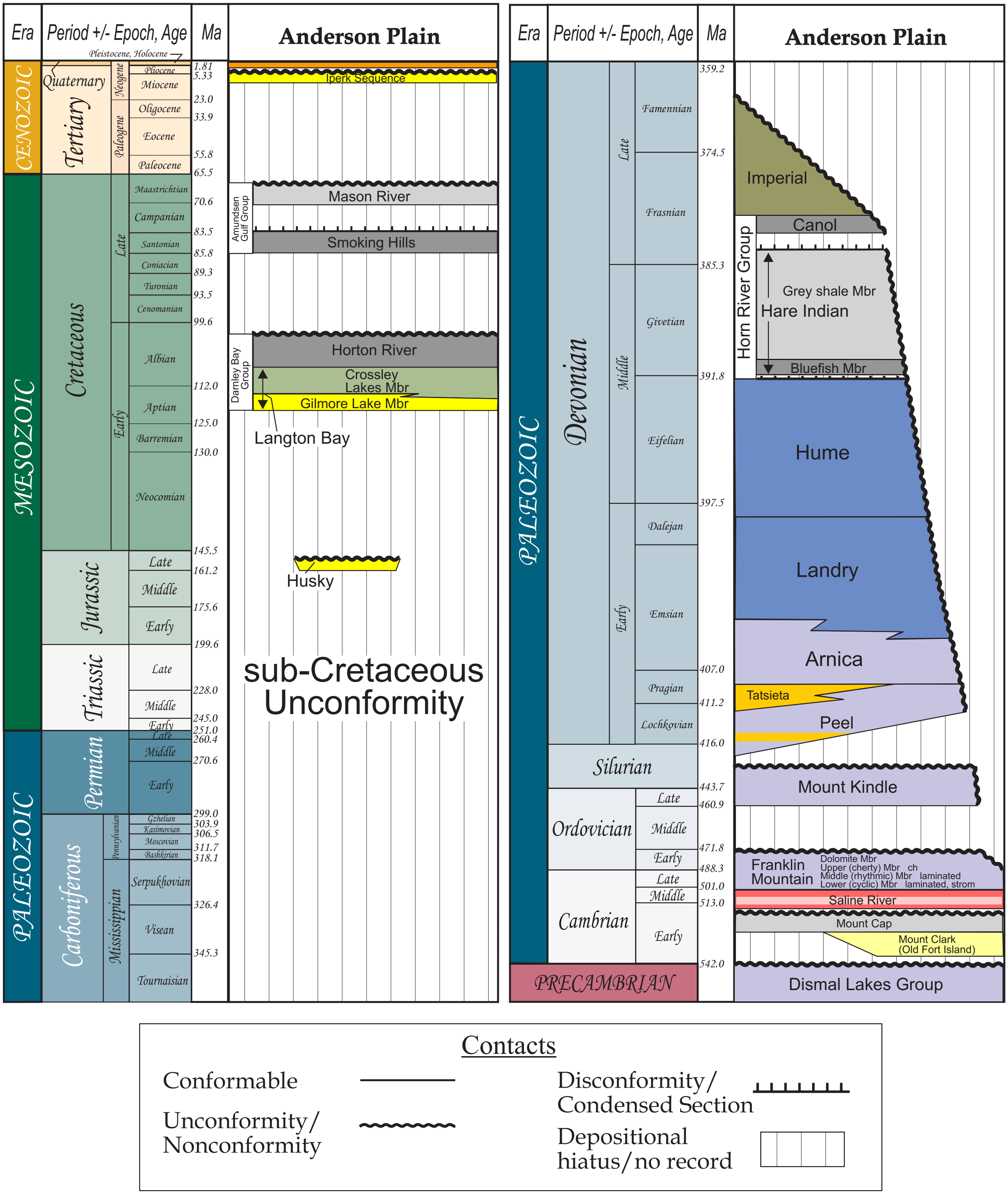

Figure 3. Stratigraphy of the Anderson Plain region (modified after Morrow *et al.*, 2006).

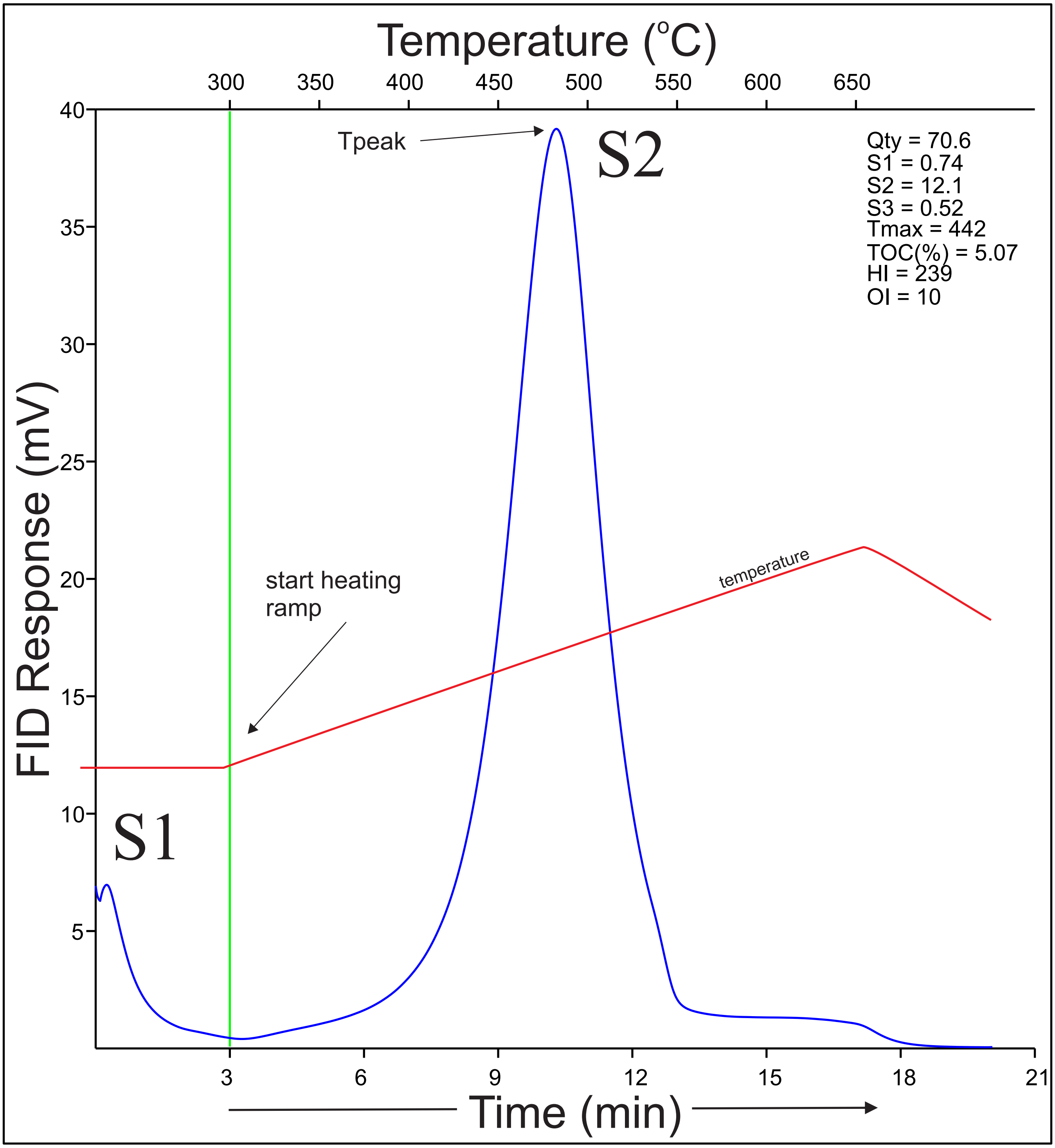

Figure 4. Rock-Eval 6 pyrogram showing the S1 and S2 curves for Rock-Eval standard 9107. Hydrocarbons are measured using a flame ionization detector (FID).

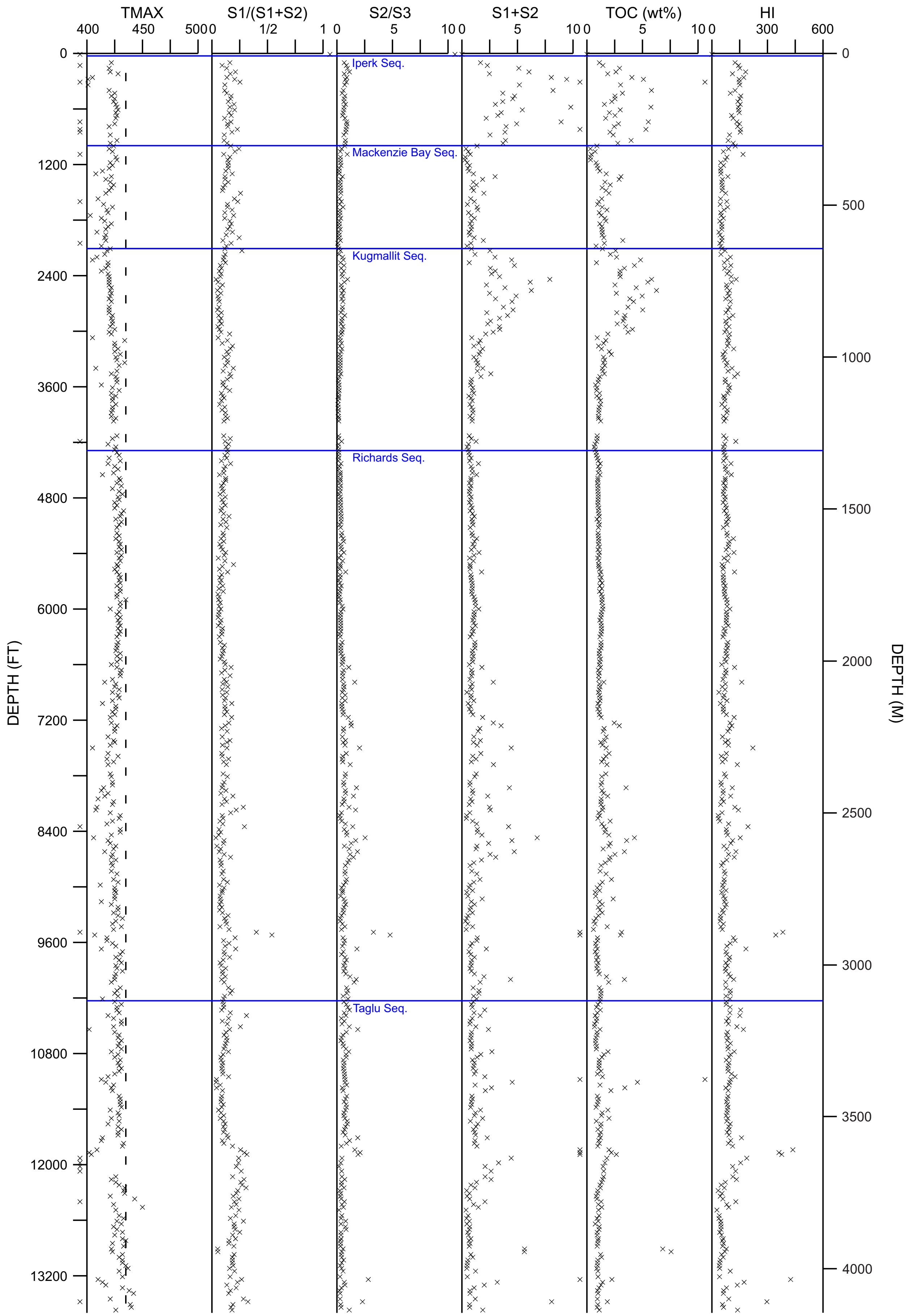

Figure 5. Selected Rock-Eval 6 parameters versus depth for the Mallik A-06 well (see text for parameter definitions).

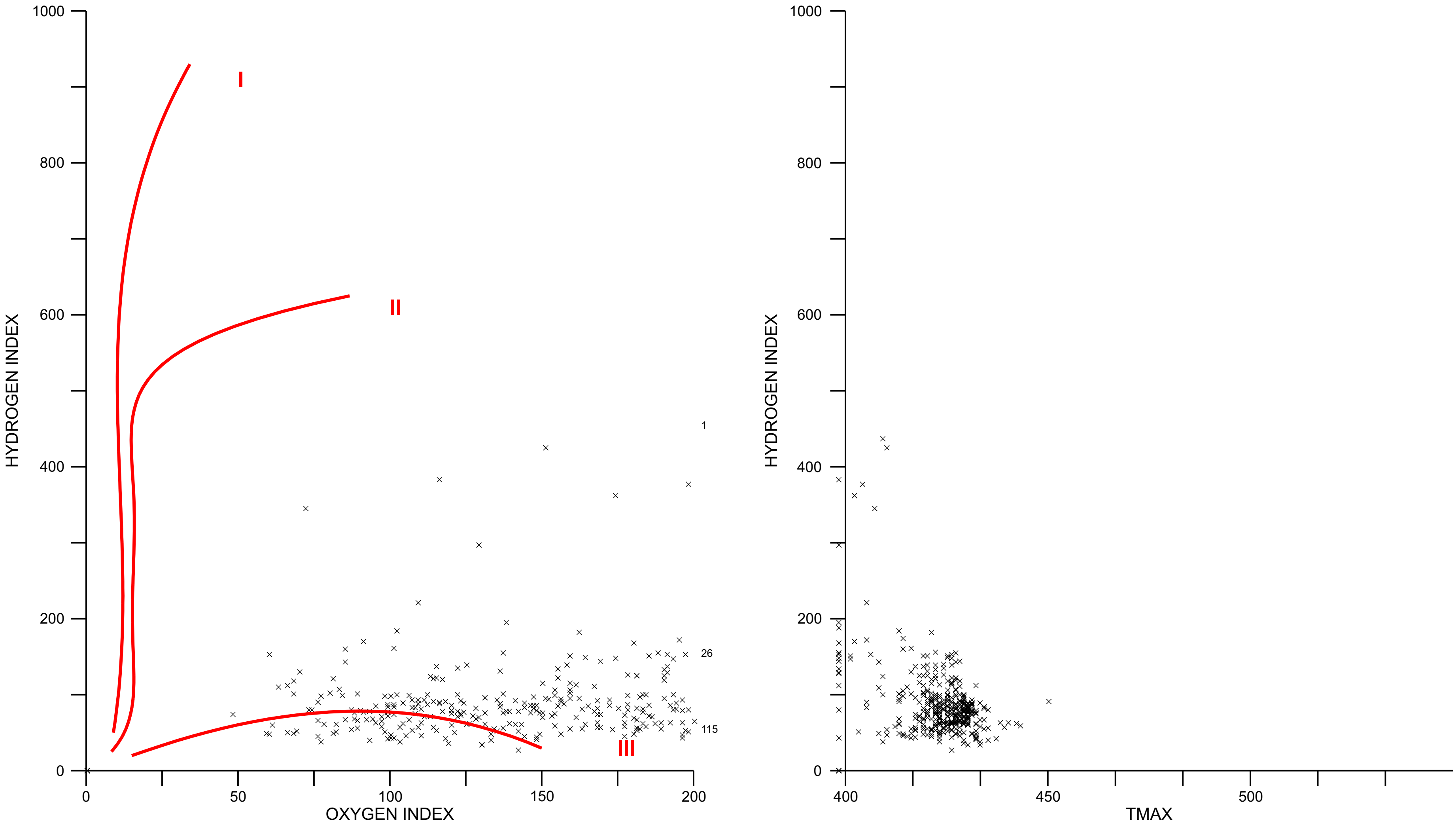

Figure 6. Whole rock HI versus OI (left) and HI versus Tmax (right) for the Mallik A-06 well (see text for parameter definitions). Organic maturation pathways (red curves) are shown for different end member organic matter types - Type I (oil-prone, usually lacustrine), Type II (oil-prone, marine) and Type III (gas-prone, terrestrial).

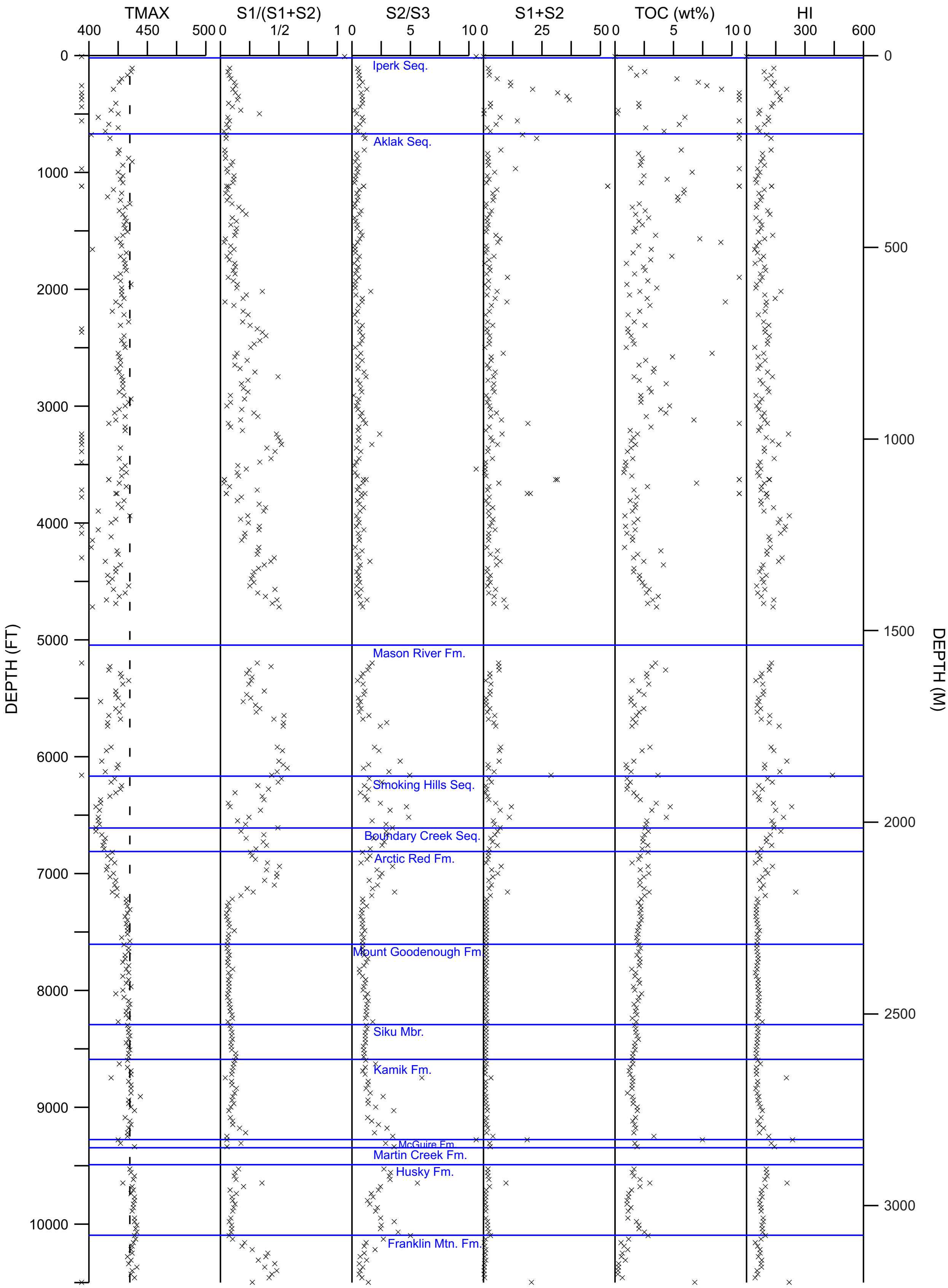

Figure 7. Selected Rock-Eval 6 parameters versus depth for the Parsons N-10 well (see text for parameter definitions).

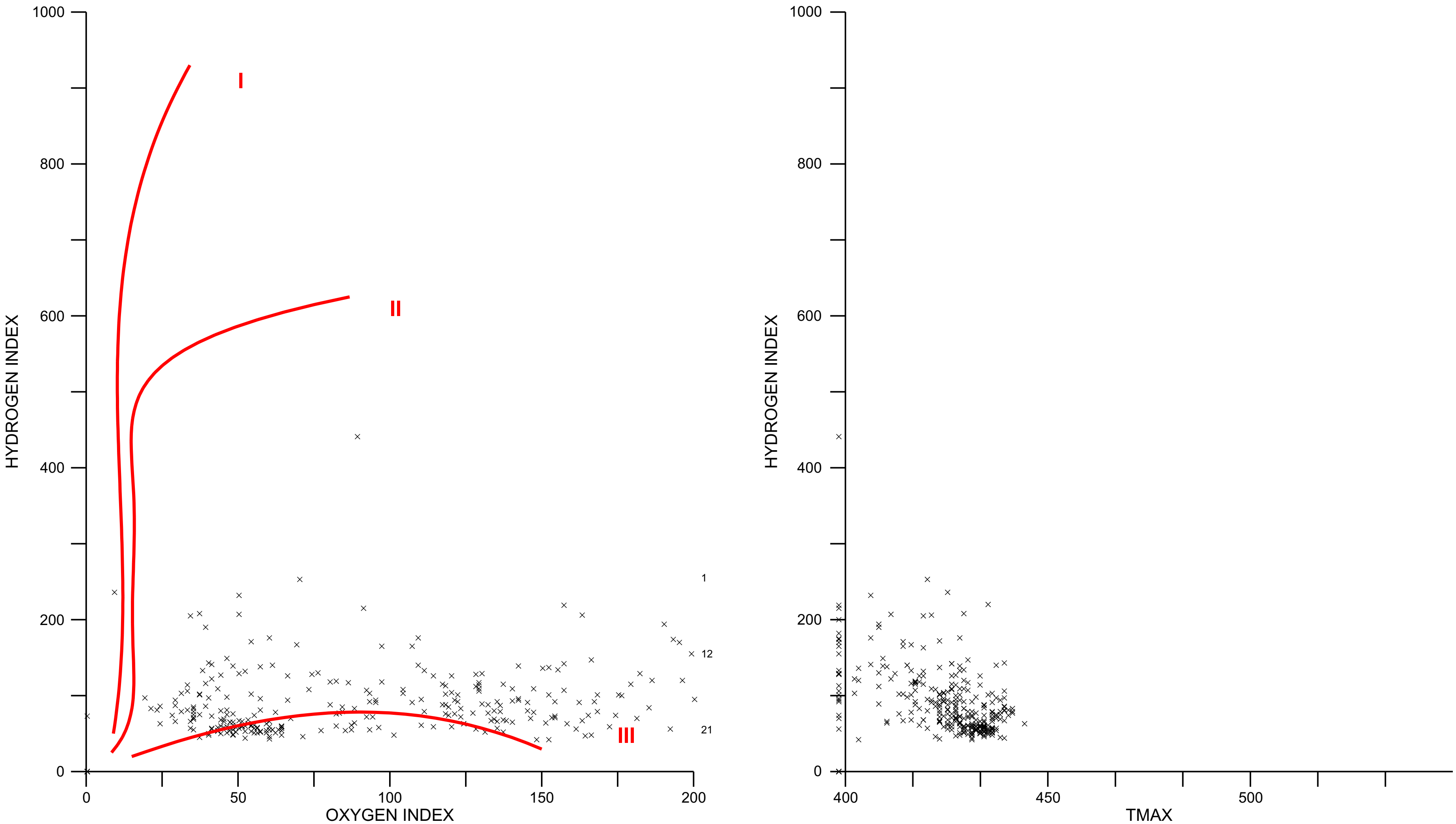

Figure 8. Whole rock HI versus OI (left) and HI versus Tmax (right) for the Parsons N-10 well (see text for parameter definitions). Organic maturation pathways (red curves) are shown for different end member organic matter types - Type I (oil-prone, usually lacustrine), Type II (oil-prone, marine) and Type III (gas-prone, terrestrial).

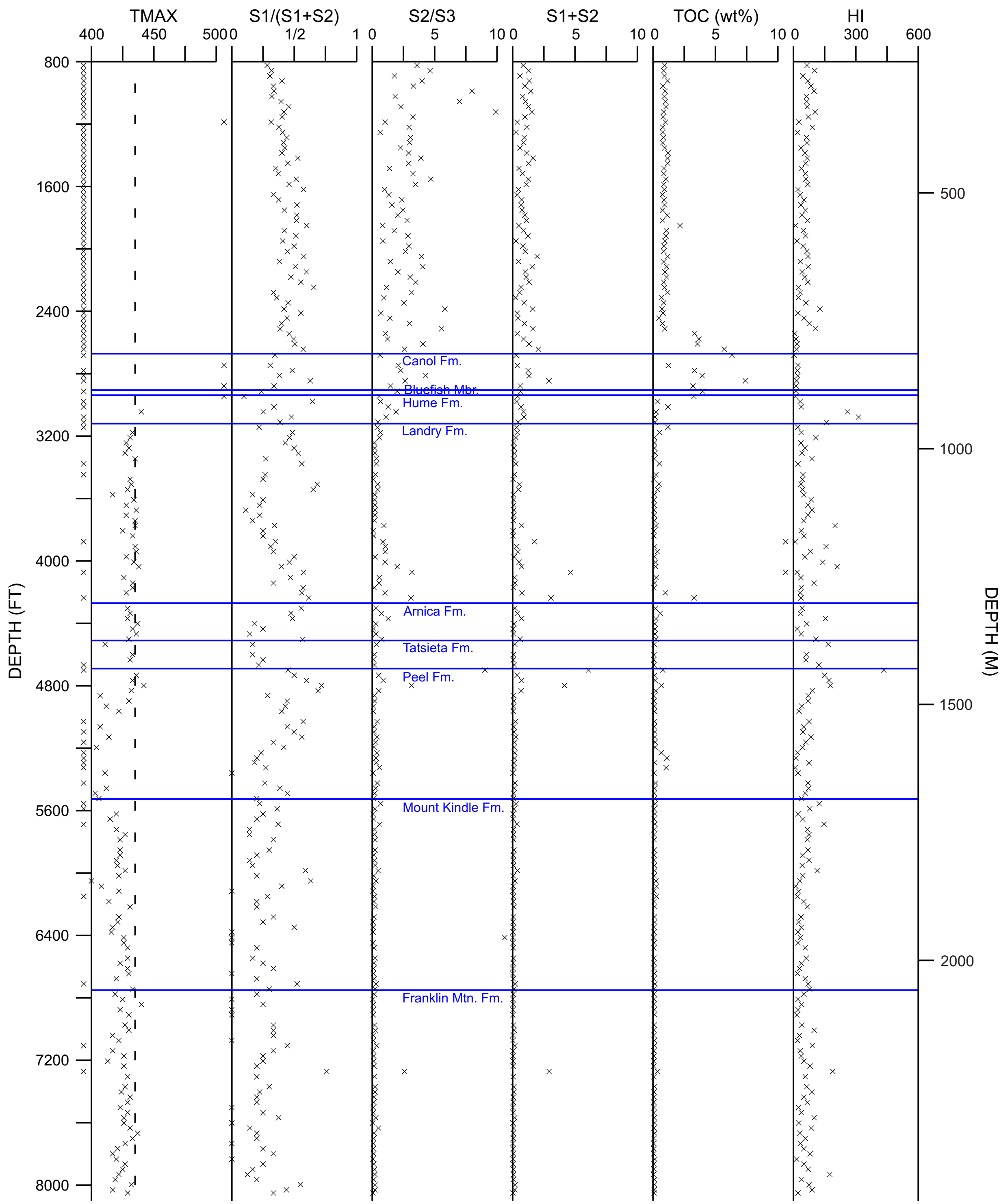

Figure 9. Selected Rock-Eval 6 parameters versus depth for the Kugaluk N-02 well (see text for parameter definitions).

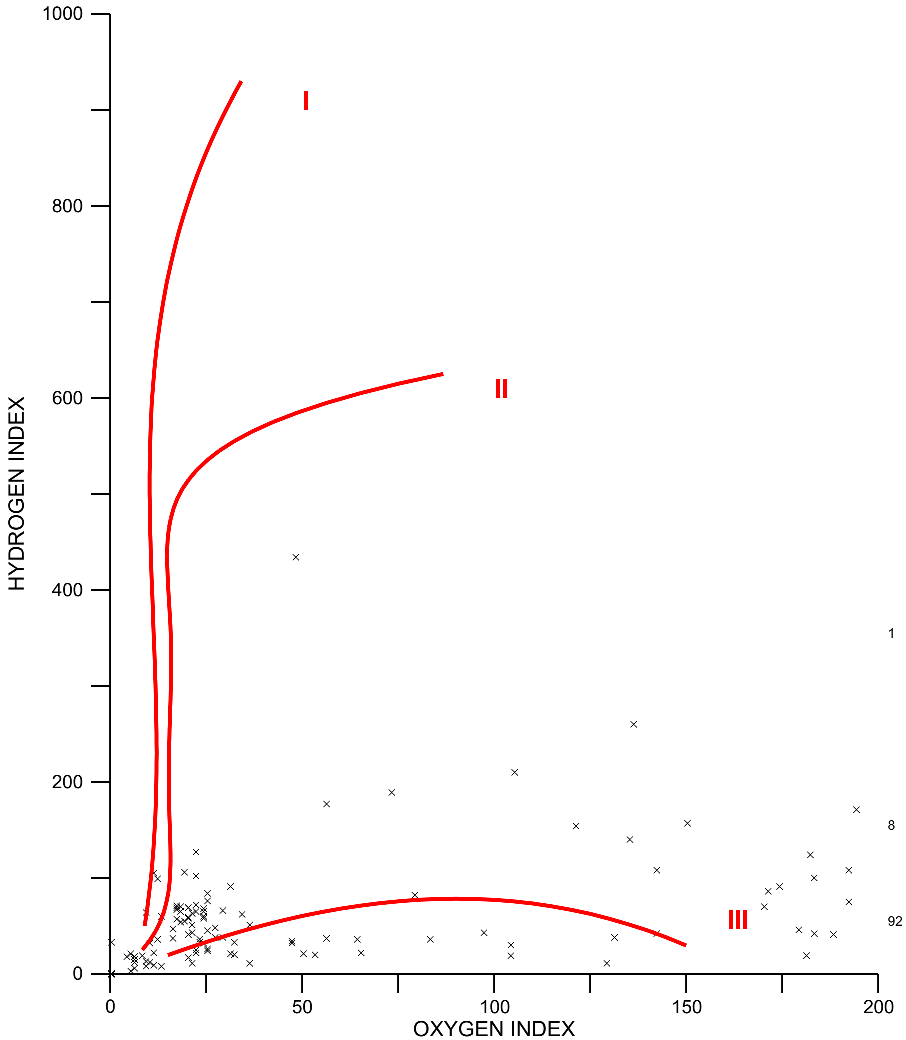

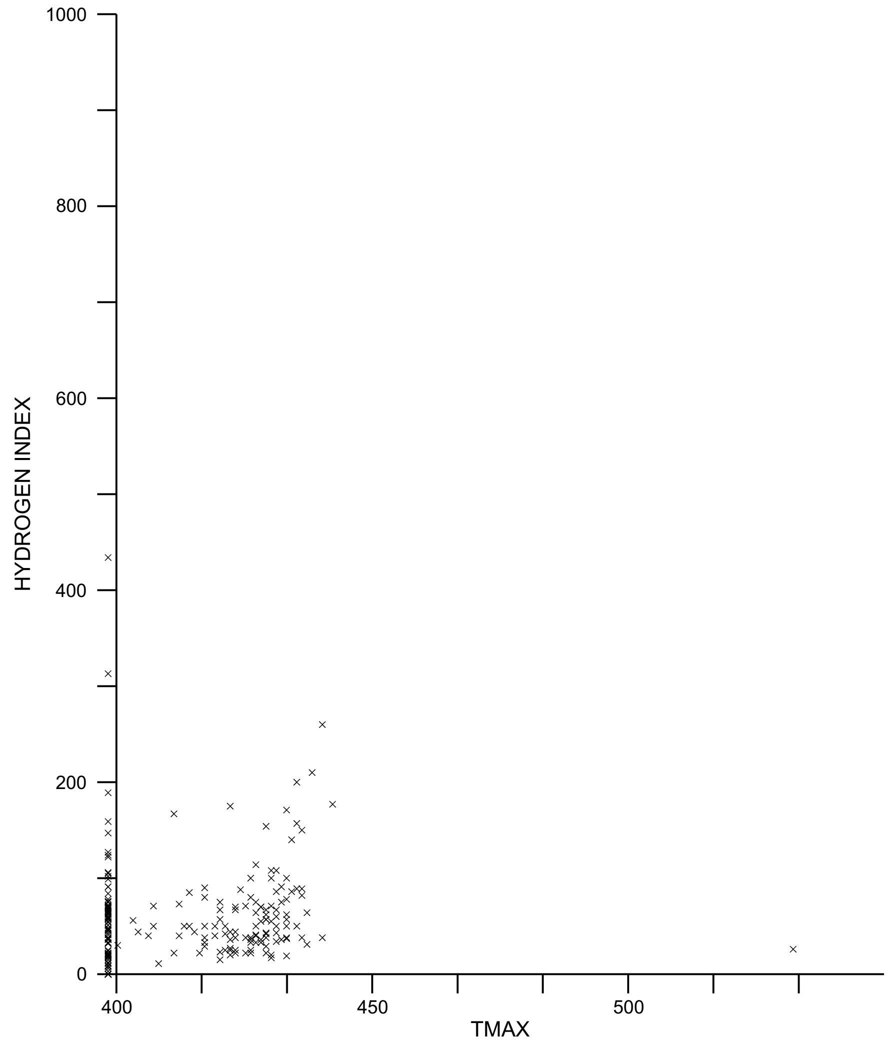

Figure 10. Whole rock HI versus OI (left) and HI versus Tmax (right) for the Kugaluk N-02 well (see text for parameter definitions). Organic maturation pathways (red curves) are shown for different end member organic matter types - Type I (oil-prone, usually lacustrine), Type II (oil-prone, marine) and Type III (gas-prone, terrestrial).

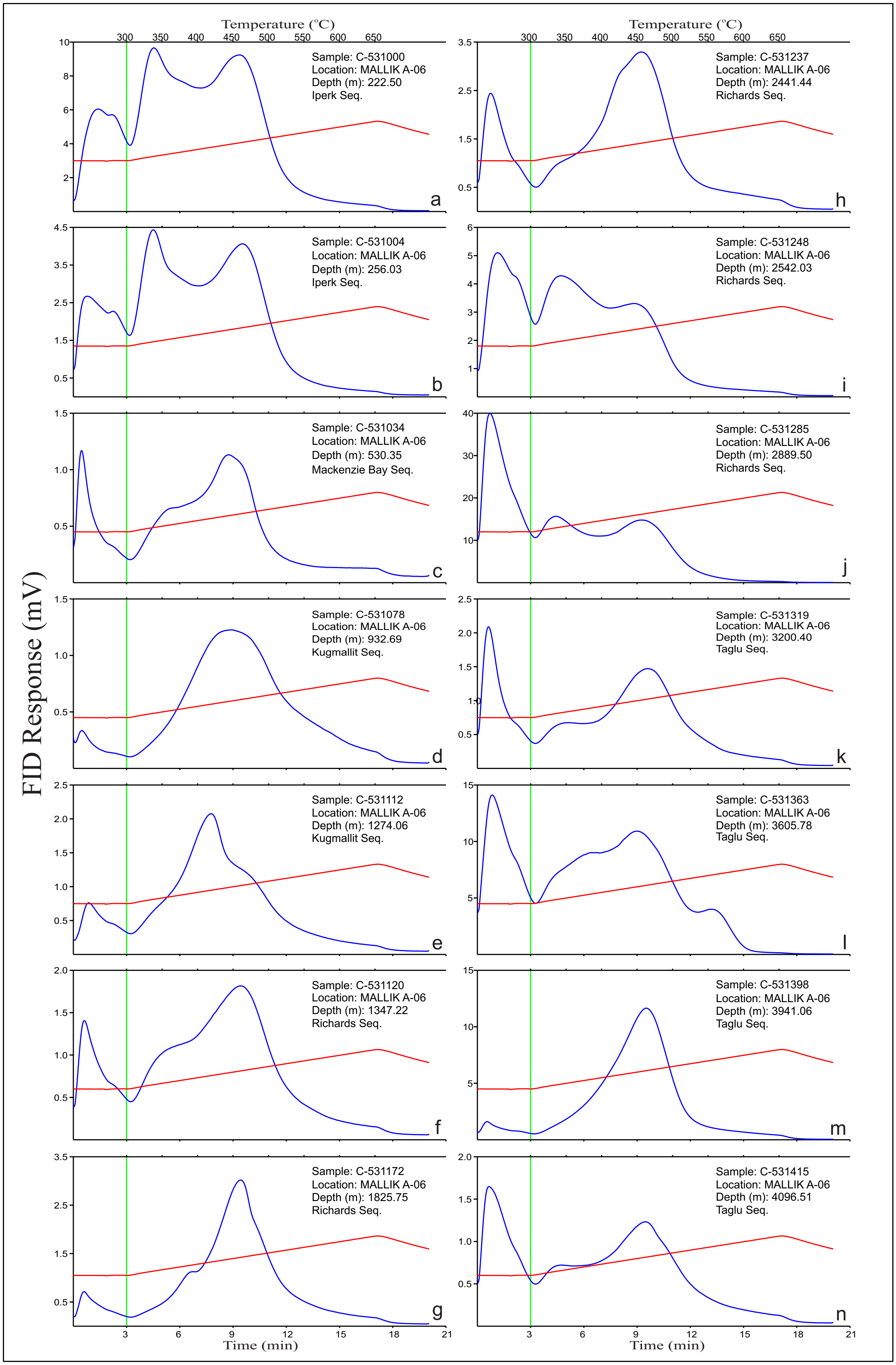

Figure 11. Rock-Eval pyrograms for samples from the Mallik A-06 well that were selected for solvent extraction and GC and GC-MS analysis.

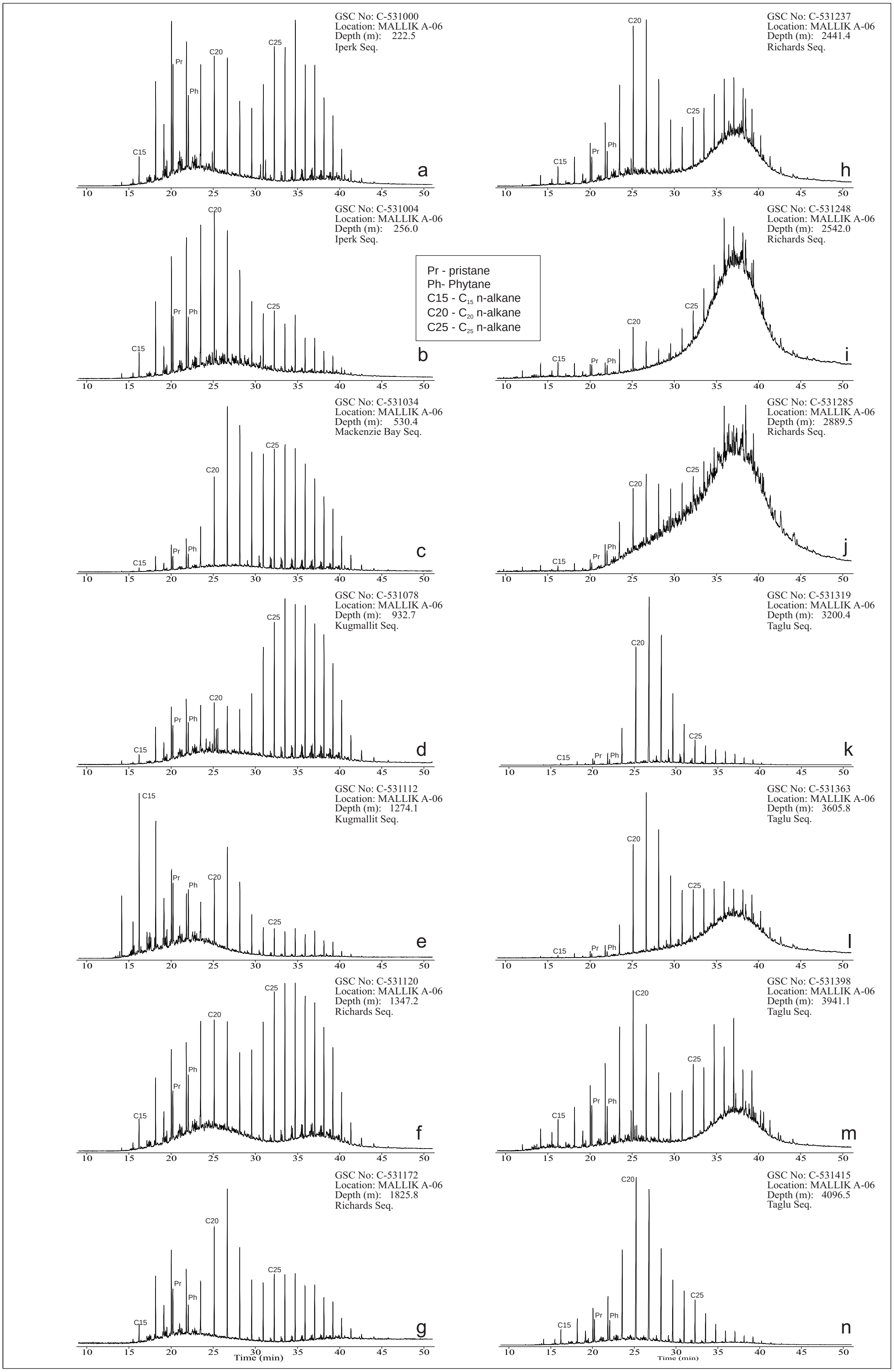

Figure 12. Saturate fraction gas chromatograms for selected samples from the Mallik A-06 well.

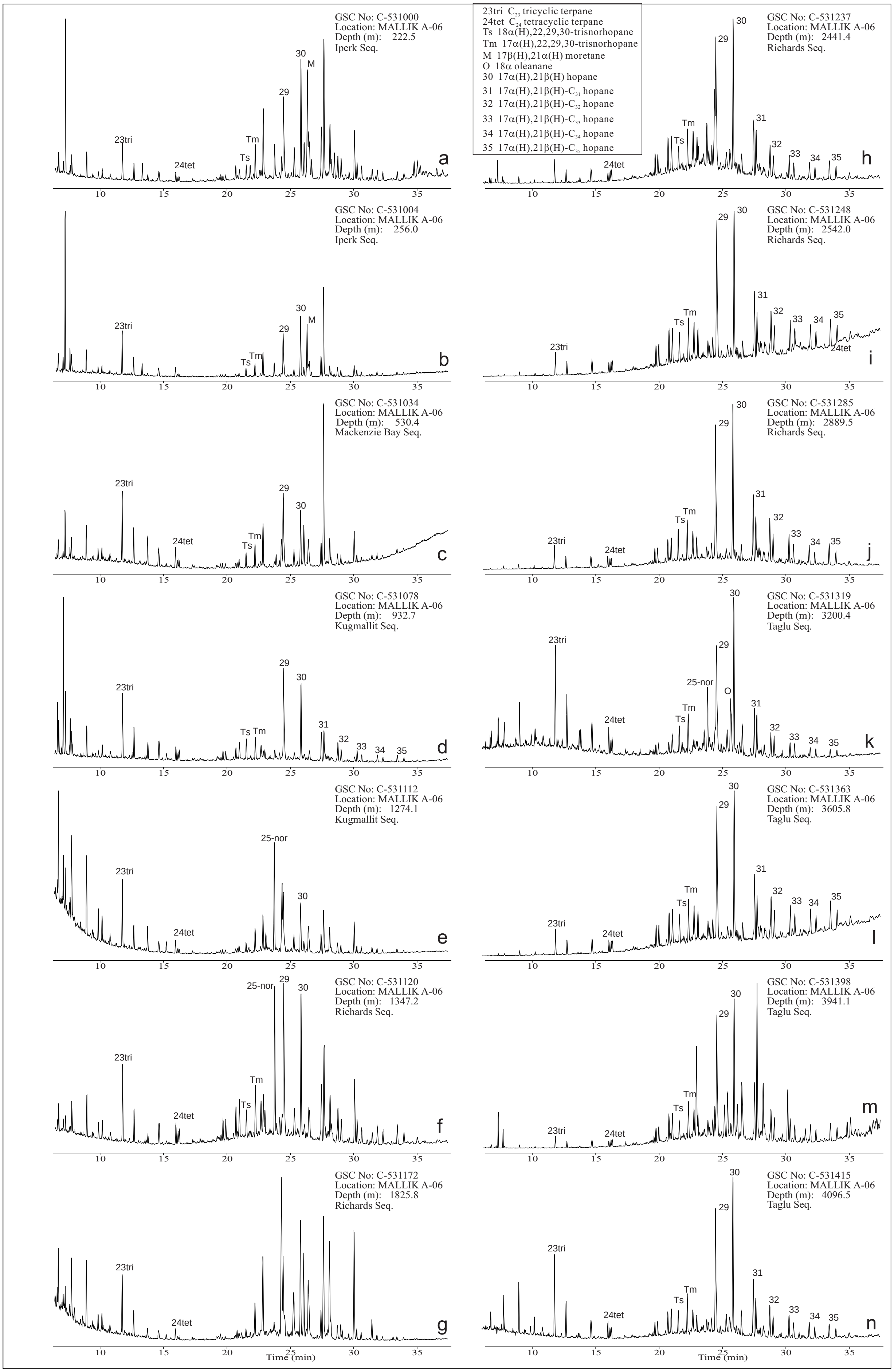

Figure 13. M/z 191 saturate fraction gas chromatograms for selected samples from the Mallik A-06 well.

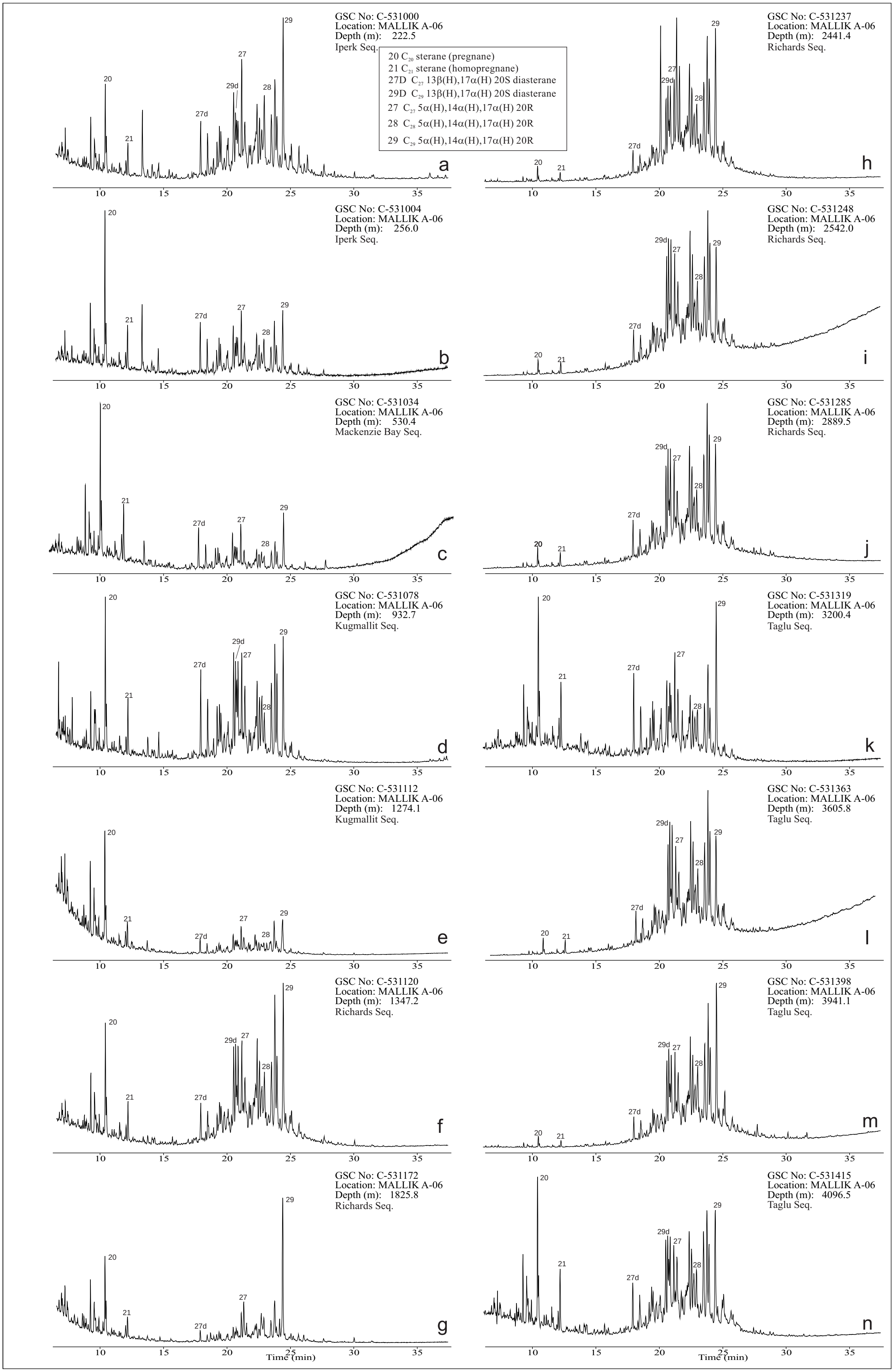

Figure 14. M/z 217 saturate fraction gas chromatograms for selected samples from the Mallik A-06 well.

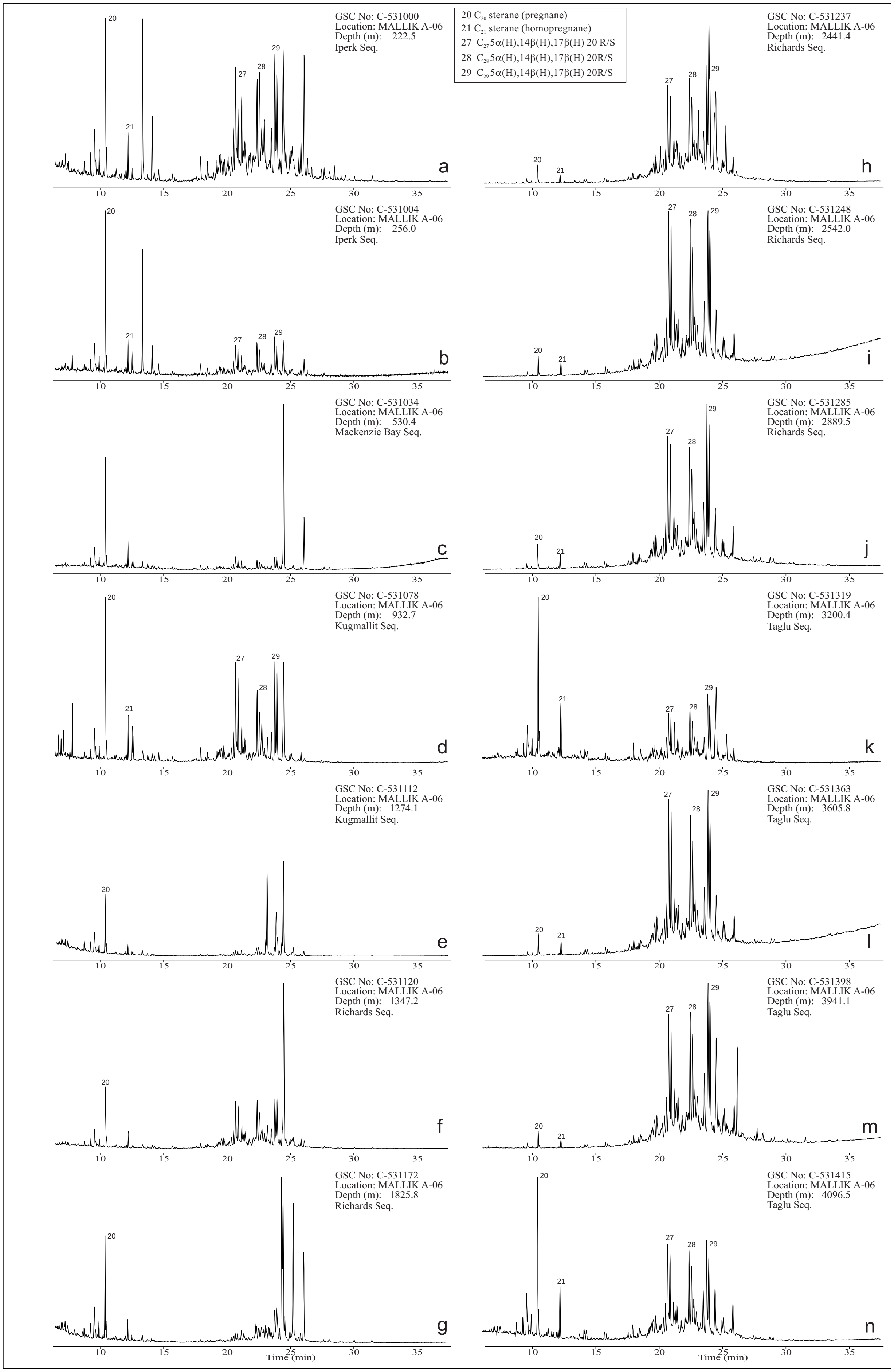

Figure 15. M/z 218 saturate fraction gas chromatograms for selected samples from the Mallik A-06 well.

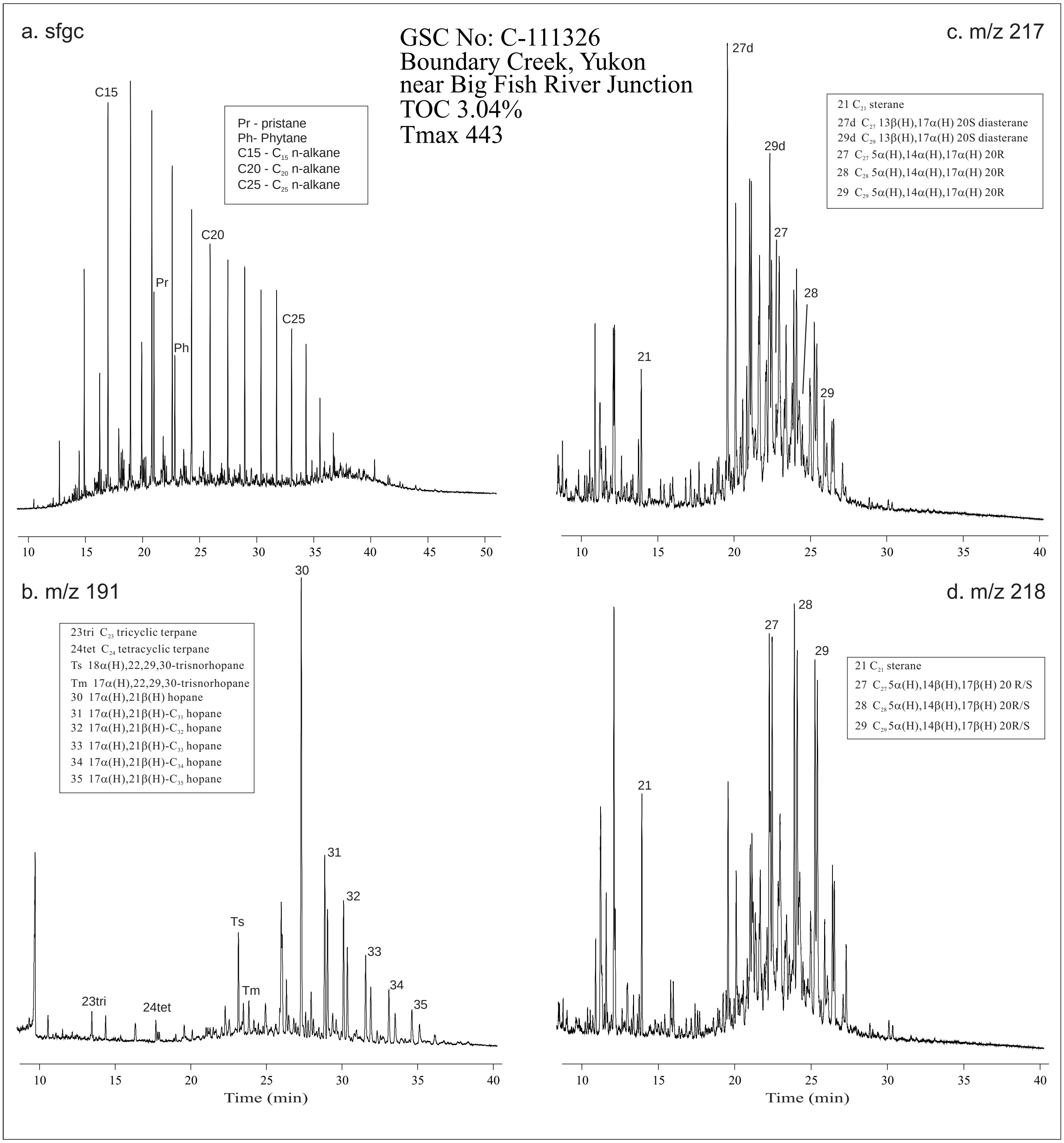

Figure 16. Conventional GC and GC-MS data for an extract from an outcrop sample of the Upper Cretaceous Boundary Creek Formation. (a) Saturate fraction gas chromatogram and (b) m/z 191, (c) 217 m/z and (d) m/z 218 saturate fraction gas chromatograms.

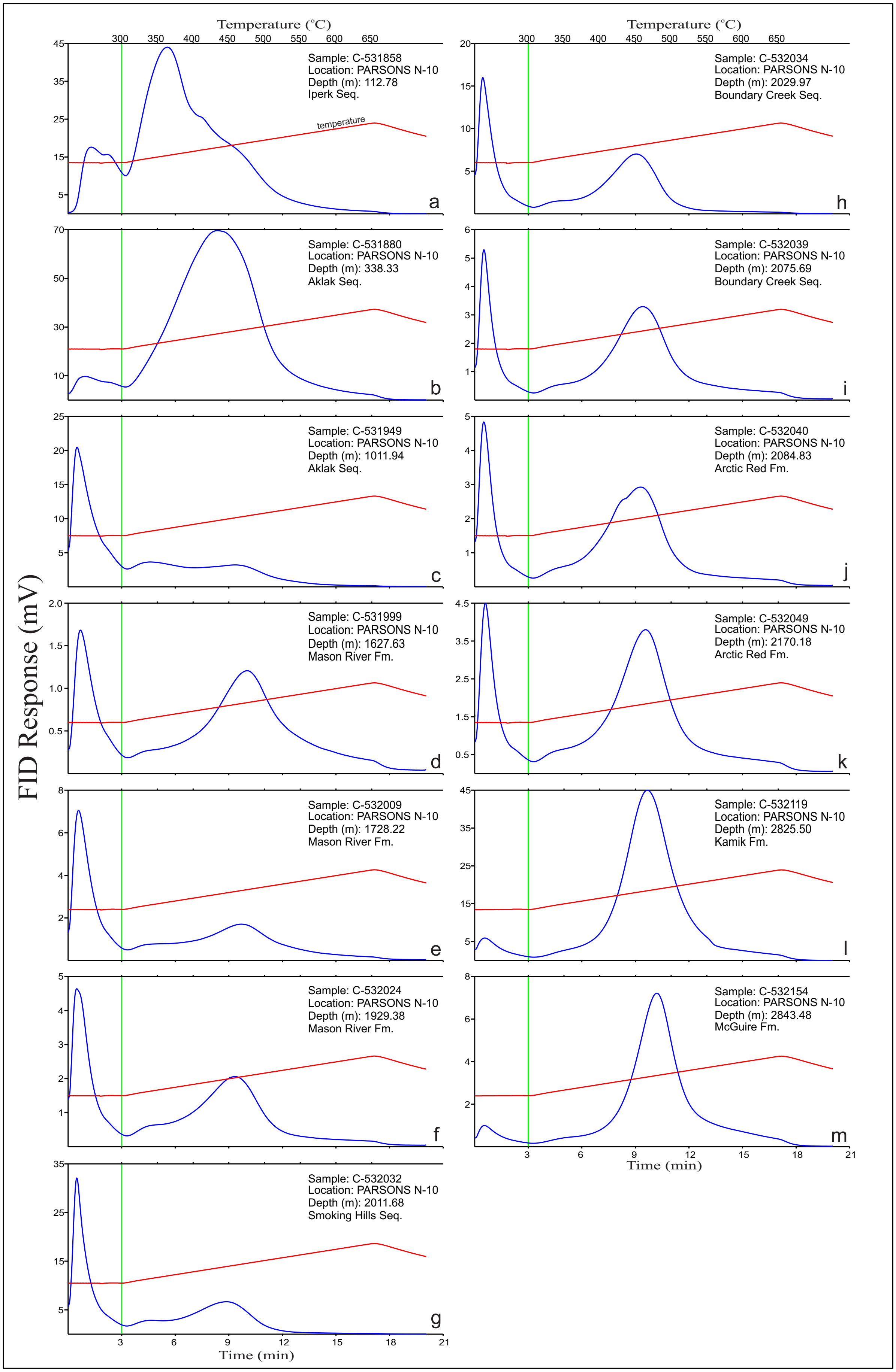

Figure 17. Rock-Eval pyrograms for samples from the Parsons N-10 well that were selected for solvent extraction and GC and GC-MS analysis.

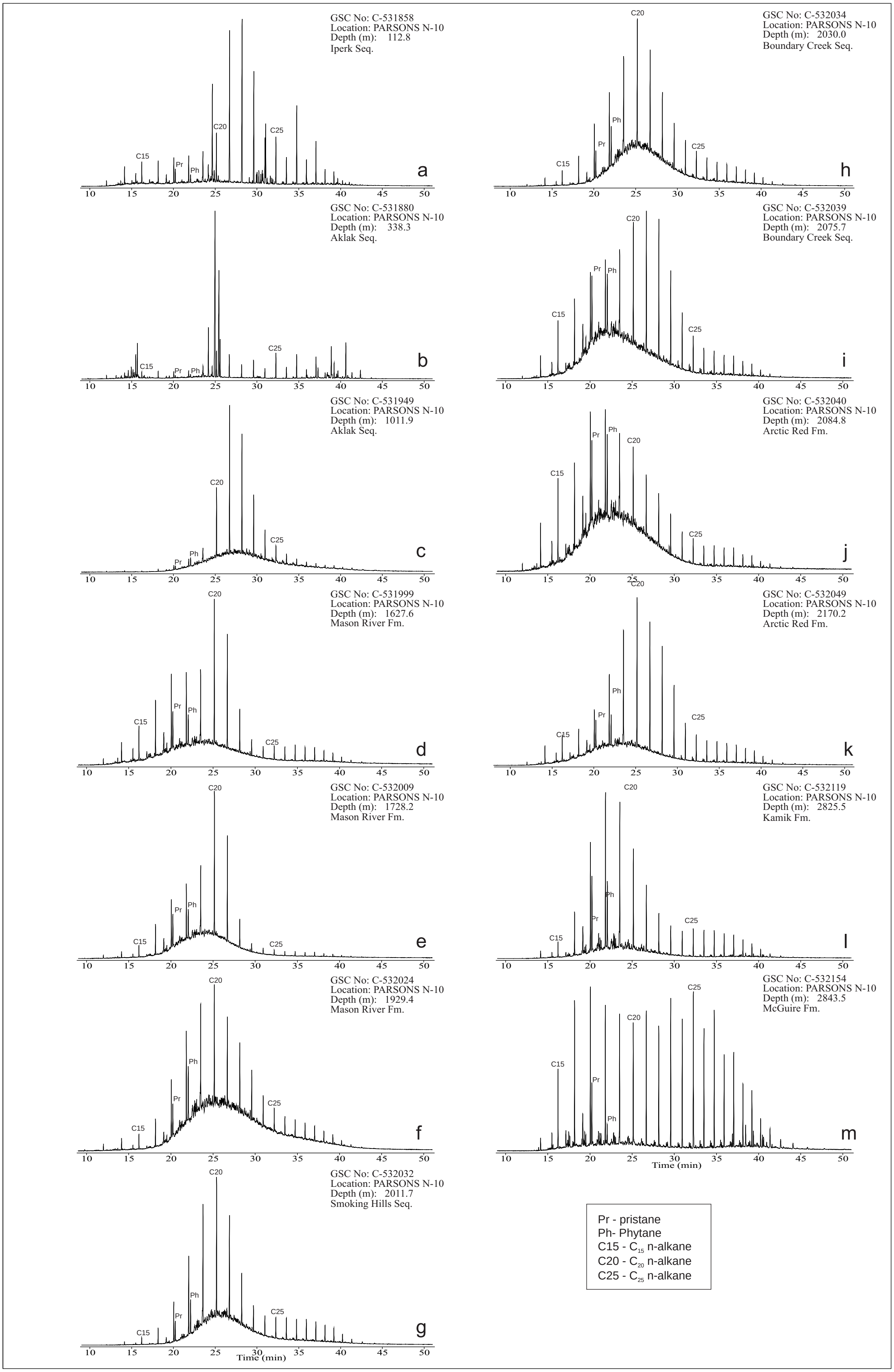

Figure 18. Saturate fraction gas chromatograms for selected samples from the Parsons N-10 well.

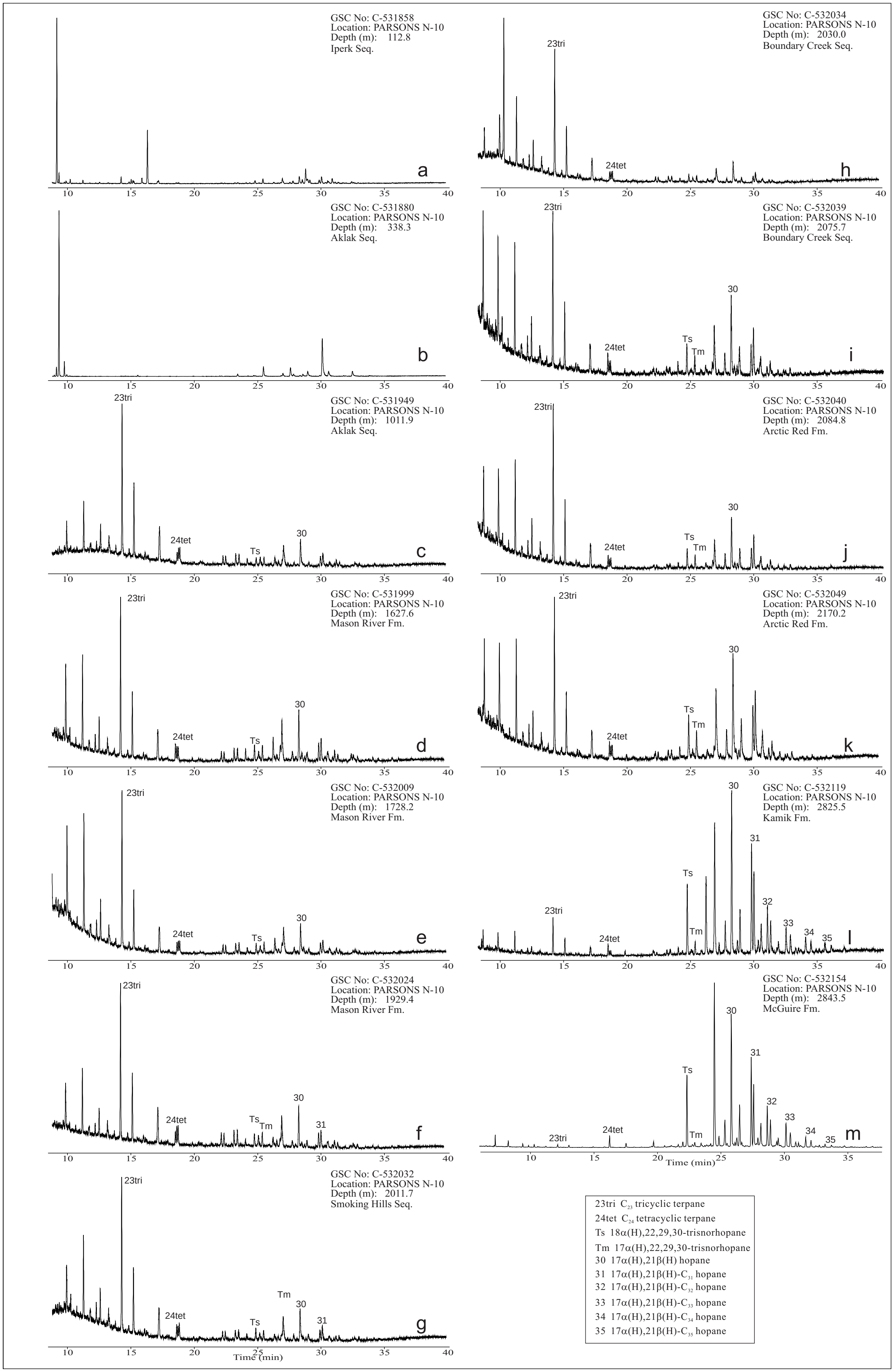

Figure 19. M/z 191 saturate fraction gas chromatograms for selected samples from the Parsons N-10 well.

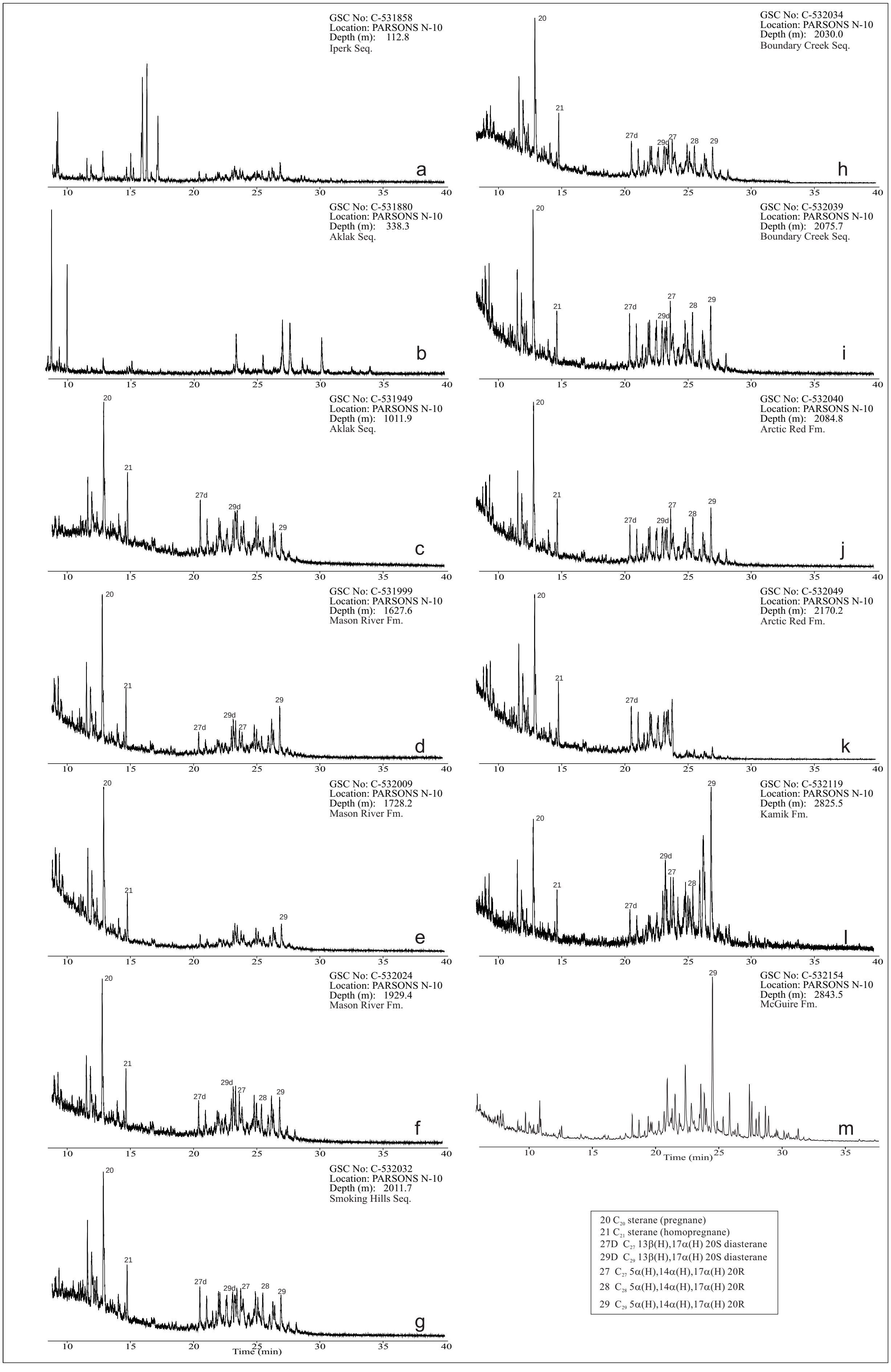

Figure 20. M/z 217 saturate fraction gas chromatograms for selected samples from the Parsons N-10 well.

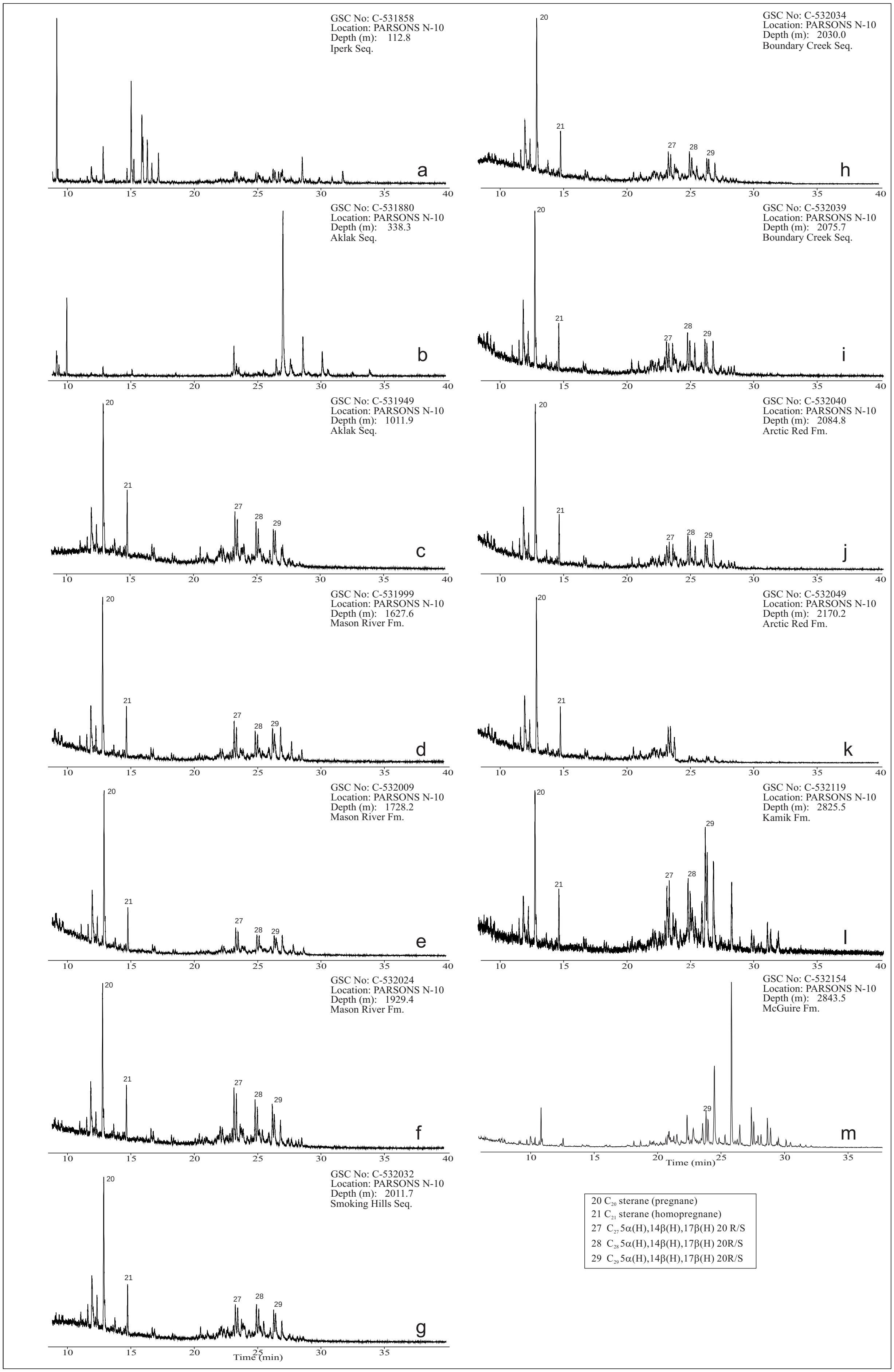

Figure 21. M/z 218 saturate fraction gas chromatograms for selected samples from the Parsons N-10 well.

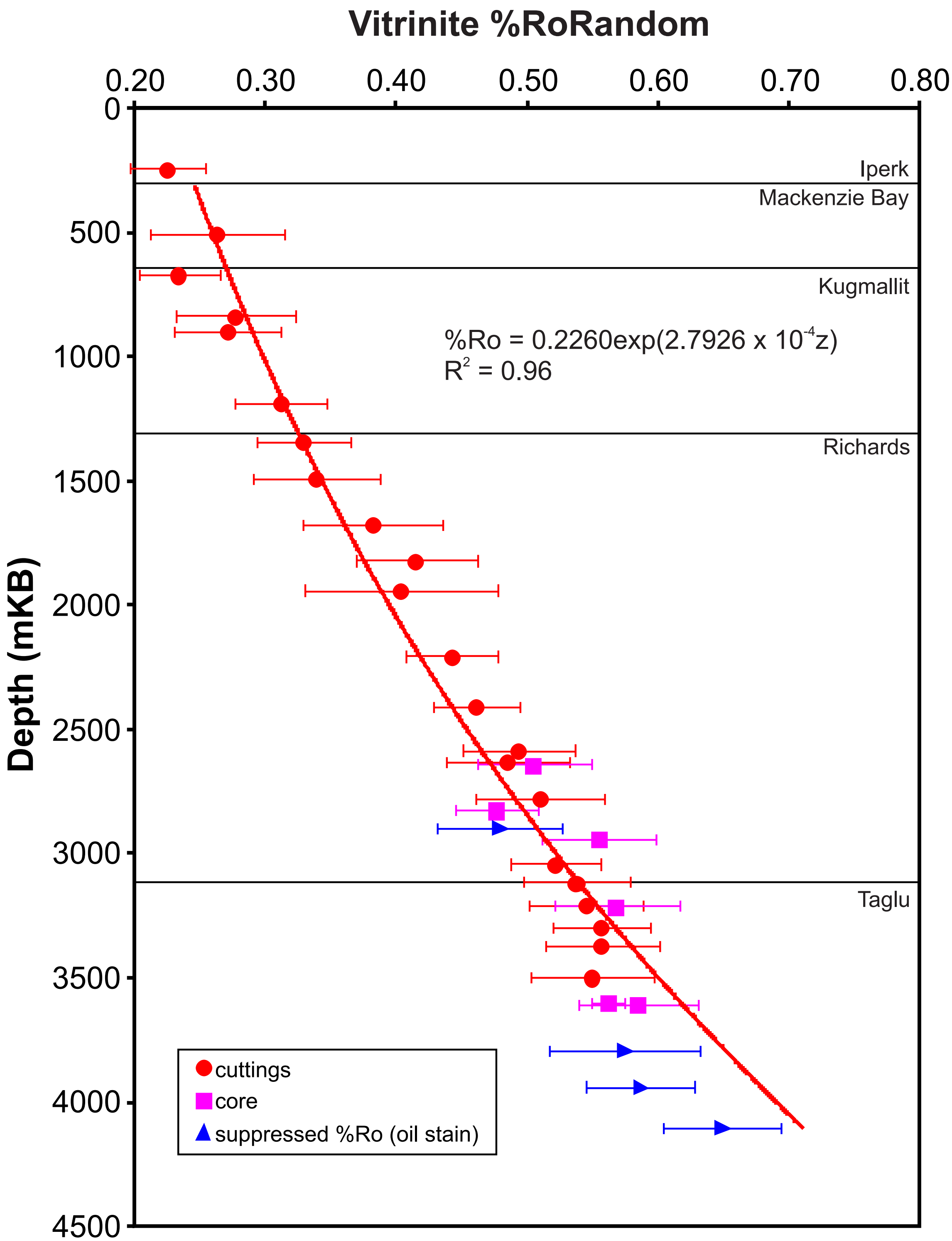

Figure 22a. Random percent vitrinite reflectance in oil (%Ro_R) for the Mallik A-06 well. Vertical axis is drilled depth with respect to Kelly Bushing elevation.

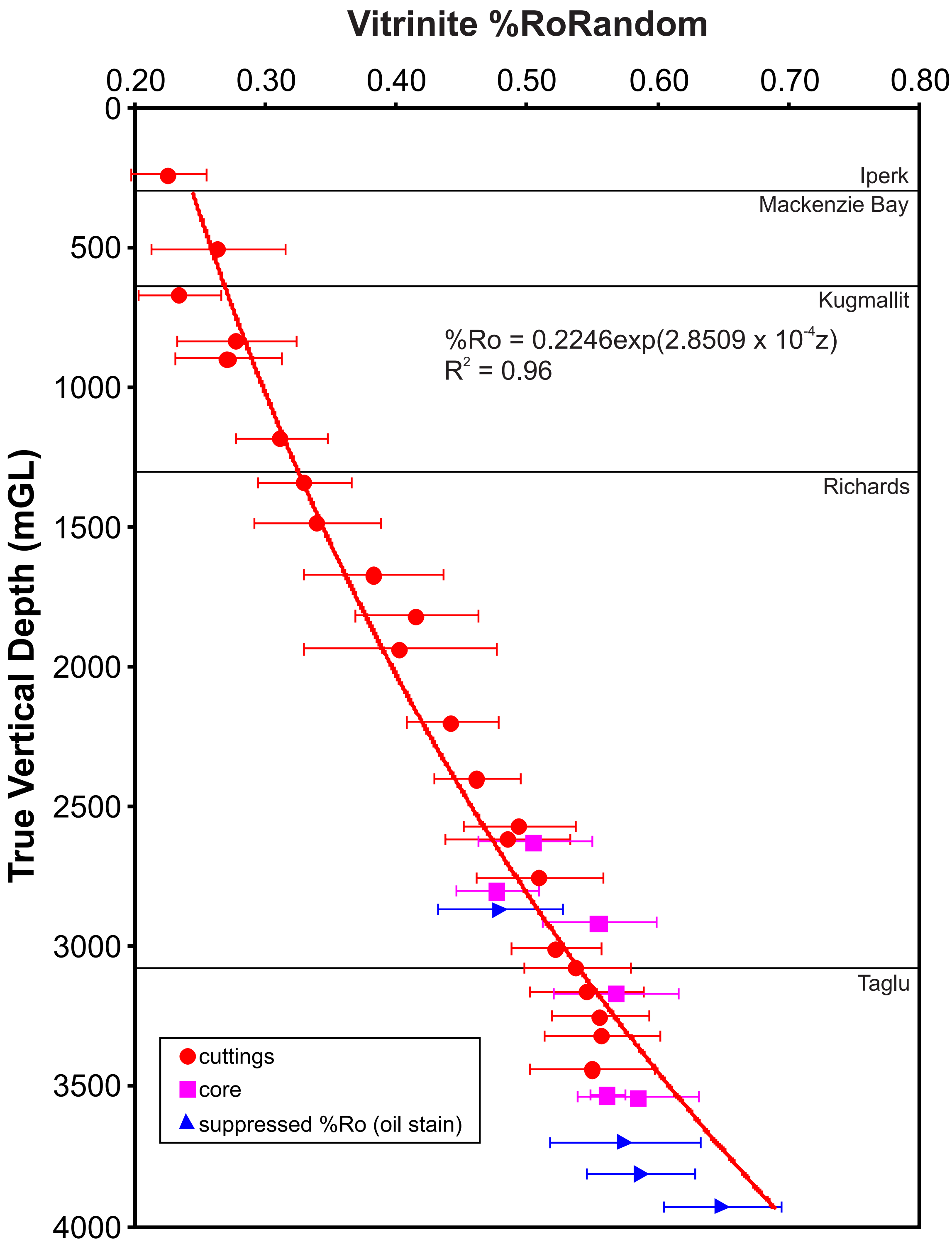

Figure 22b. Random percent vitrinite reflectance in oil (%Ro_R) for the Mallik A-06 well. Vertical axis is estimated true vertical depth with respect to ground surface elevation.

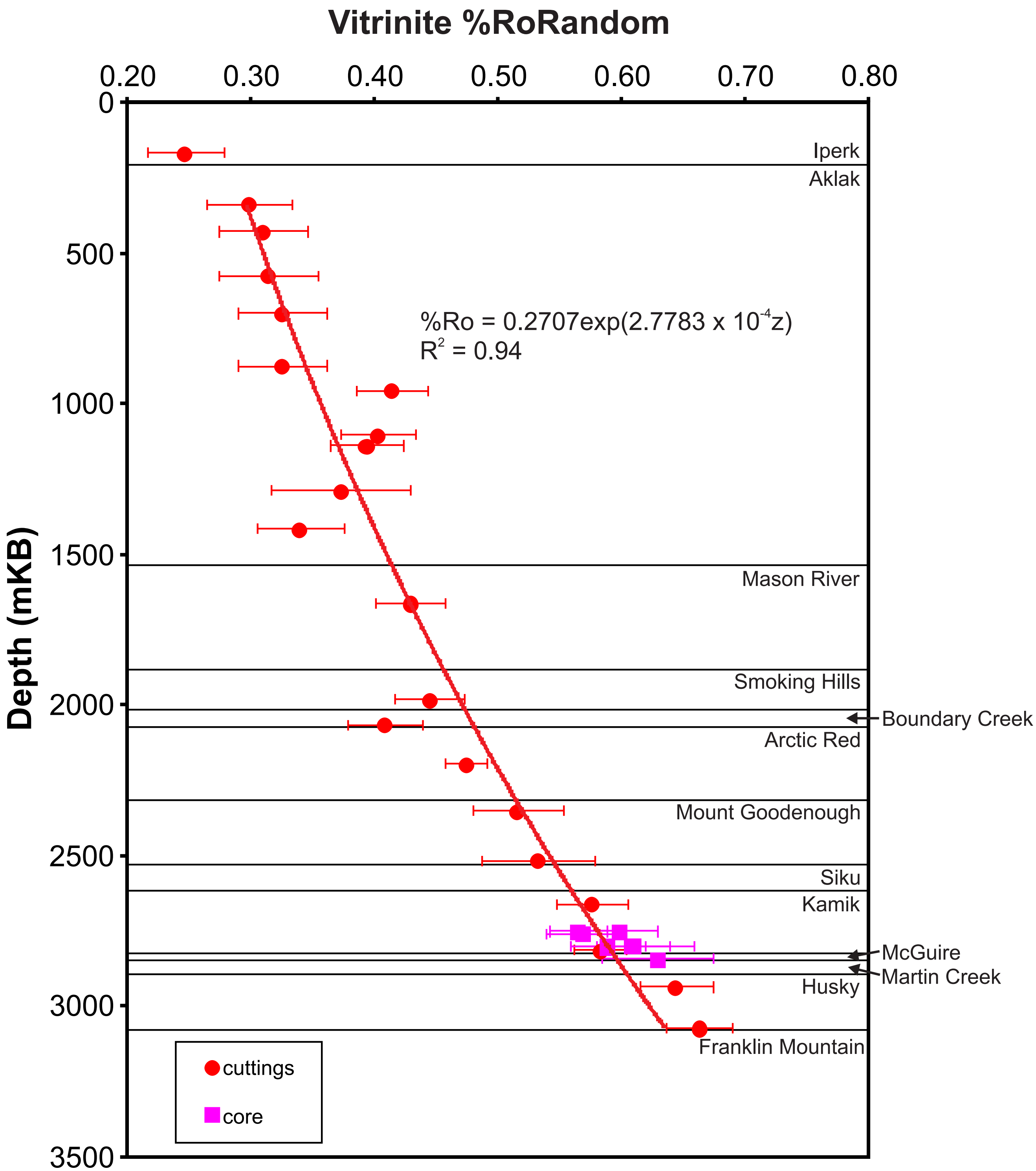

Figure 23. Random percent vitrinite reflectance in oil (%Ro_R) for the Parsons N-10 well. Vertical axis is drilled depth with respect to Kelly Bushing elevation.

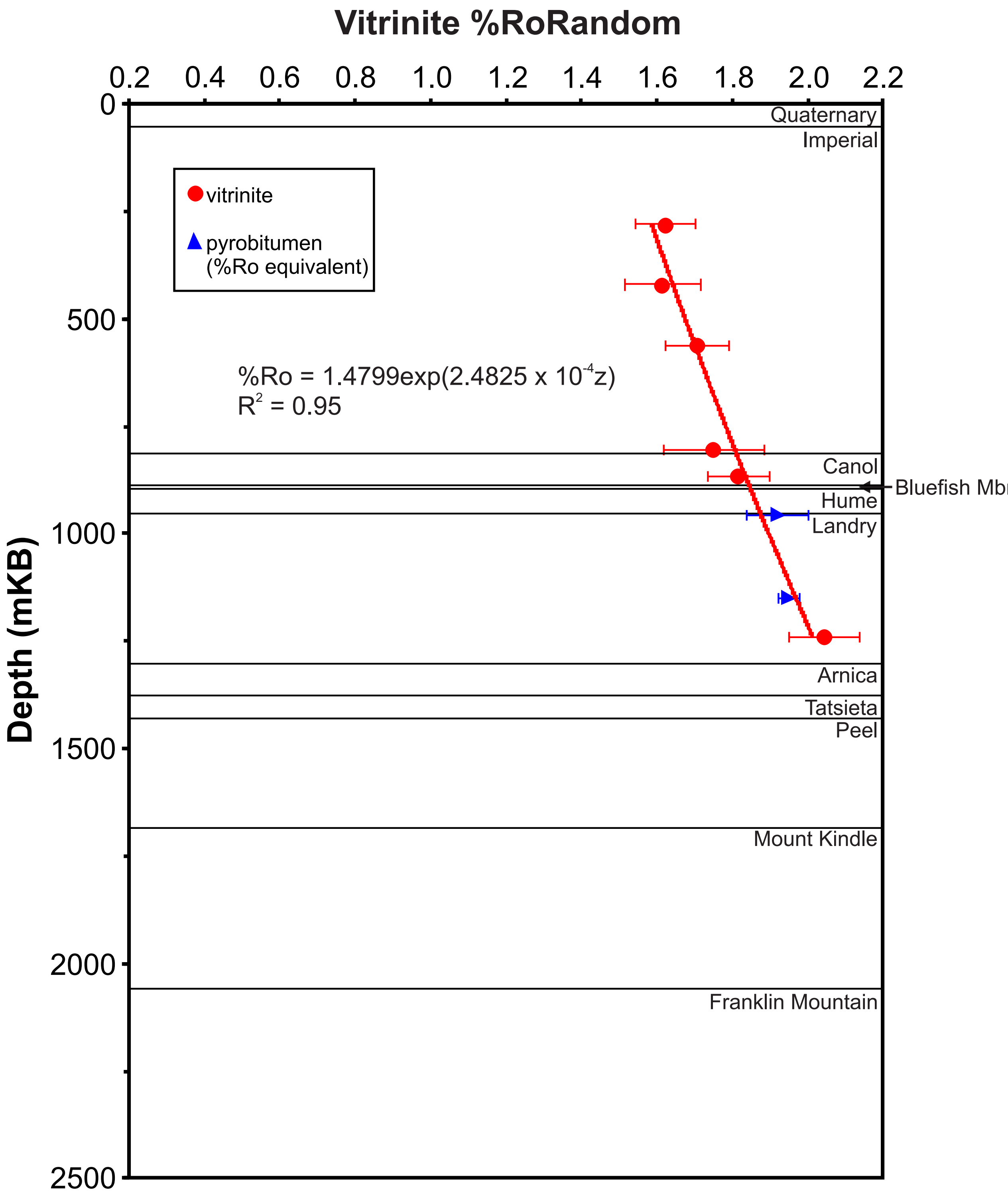

Figure 24. Random percent vitrinite reflectance in oil (%Ro_R) for the Kugaluk N-02 well. Vertical axis is drilled depth with respect to Kelly Bushing elevation.

Table 1. Mallik A-06 Rock-Eval 6 data (Rock-Eval 2 format).

(green)	acceptable pyrogram
(purple)	anomalous pyrogram
(yellow)	%Ro analysis

Depth ft	Depth m	Qty	Tmax	S1	S2	S3	PI	S2/S3	PC(%)	TOC(%)	HI	OI	MINC	Comments
										Iperk Sequence				
90	27.4	70.1	422	0.27	1.40	2.13	0.16	0.66	0.23	1.12	125	190	0.9	S1 2/3 recovery, small left shoulder on S2
120	36.6	70.3	396	0.21	2.08	2.44	0.09	0.85	0.29	1.44	144	169	0.6	S1 2/3 recovery, left shoulder on S2, double peak Tmax
150	45.7	70.4	420	0.68	4.44	4.66	0.13	0.95	0.63	2.94	151	159	0.5	S1 2/3 recovery, small left peak on S2
190	57.9	70.8	421	1.28	4.76	4.23	0.21	1.13	0.69	2.61	182	162	0.9	S1 2/3 recovery, large left peak on S2
210	64.0	70.5	428	0.41	2.07	3.13	0.17	0.66	0.35	1.87	111	167	0.9	S1 2/3 recovery, small left peak on S2
250	76.2	70.9	405	1.09	6.96	7.89	0.13	0.88	1.00	4.05	172	195	1.3	S1 1/2 recovery, large left shoulder on S2
270	82.3	70.0	401	1.93	7.50	9.81	0.20	0.76	1.19	5.09	147	193	0.8	S1 2/3 recovery, large left peak on S2
300	91.4	20.4	299	14.30	42.38	49.91	0.25	0.85	6.98	28.69	148	174	1.8	bimodal S1, 60% recovery, large asymmetric S2 peak+ right shoulder
330	100.6	70.3	401	0.60	4.57	6.53	0.12	0.70	0.68	3.03	151	216	0.9	S1 2/3 recovery, left shoulder on S2
390	118.9	70.3	420	0.94	7.26	12.53	0.11	0.58	1.20	5.81	125	216	1.1	bimodal S1 peak, 30% recovery, large left shoulder on S2
420	128.0	70.2	425	0.49	3.19	6.78	0.13	0.47	0.57	3.20	100	212	1.1	S1 2/3 recovery, left shoulder on S2
450	137.2	70.7	422	0.82	3.92	5.48	0.17	0.72	0.62	2.52	156	217	0.9	S1 3/4 recovery, left shoulder on S2
480	146.3	70.7	425	0.77	3.81	5.89	0.17	0.65	0.60	2.52	151	234	0.9	S1 3/4 recovery, left shoulder on S2, min effect on Tmax
510	155.4	70.7	424	0.54	3.13	4.97	0.15	0.63	0.51	2.24	140	222	1.0	S1 2/3 recovery, left shoulder on S2
540	164.6	70.8	426	0.60	2.41	3.11	0.20	0.77	0.37	1.58	153	197	1.0	S1 3/4 recovery, left shoulder on S2, min effect on Tmax
570	173.7	70.2	427	1.58	8.22	12.80	0.16	0.64	1.34	5.76	143	222	1.3	bimodal S1, 60% recovery, large left peak on S2
600	182.9	70.8	428	1.11	4.33	6.85	0.20	0.63	0.72	3.00	144	228	0.8	S1 80% recovery, left shoulder on S2
630	192.0	70.7	426	0.55	2.99	5.34	0.15	0.56	0.49	2.02	148	264	1.0	S1 2/3 recovery, left shoulder on S2
660	201.2	71.0	427	0.56	2.67	5.23	0.17	0.51	0.48	2.53	106	207	0.7	S1 80% recovery, left shoulder on S2
690	210.3	70.4	426	0.25	1.94	2.68	0.11	0.72	0.29	1.69	115	159	0.5	S1 2/3 recovery, left shoulder on S2, min effect on Tmax
730	222.5	70.8	299	1.53	7.40	8.55	0.17	0.87	1.13	5.53	134	155	0.6	bimodal S1, 1/3 recovery, bimodal S2
750	228.6	70.3	425	0.69	4.24	4.67	0.14	0.91	0.62	2.84	149	164	0.5	bimodal S1 40% recovery, left shoulder on S2
780	237.7	70.5	420	0.57	3.41	3.88	0.14	0.88	0.50	2.46	139	158	0.3	S1 50% recovery, large left peak on S2
810	246.9	70.4	302	2.45	8.24	10.00	0.23	0.82	1.32	5.31	155	188	0.6	similar to 300, bimodal S2 with 2nd peak ~60% of first
840	256.0	70.4	298	0.70	3.18	3.97	0.18	0.80	0.49	2.08	153	191	0.3	similar to 730
870	265.2	70.6	421	0.28	2.25	3.57	0.11	0.63	0.37	2.36	95	151	0.3	S1 1/2 recovery, large left shoulder on S2
930	283.5	70.0	427	0.43	3.50	4.60	0.11	0.76	0.53	3.98	88	116	0.4	S1 60% recovery, large left shoulder on S2
960	292.6	70.9	421	0.50	3.20	4.18	0.13	0.77	0.50	2.78	115	150	0.4	S1 40% recovery, large left peak on S2
990	301.8	70.3	424	0.23	1.13	1.60	0.17	0.71	0.18	0.90	126	178	0.2	S1 80% recovery, left shoulder on S2, min effect on Tmax
Ave			403.7											all values (29)
SD			43.2											
Ave			**425.7**											selected values (3 points)
SD			**0.6**											

Depth ft	m	Qty	Tmax	S1	S2	S3	PI	S2/S3	PC(%)	TOC(%)	HI	OI	MINC	Comments
										Mackenzie Bay				
1020	310.9	70.8	420	0.09	0.28	0.66	0.25	0.42	0.06	0.31	90	213	0.1	S1 80% recovery, left shoulder on S2
1050	320.0	70.9	423	0.12	0.46	1.51	0.21	0.30	0.11	0.74	62	204	0.2	S1 80% recovery, left shoulder on S2, min effect on Tmax
1080	329.2	70.4	397	0.08	0.67	0.72	0.11	0.93	0.09	0.40	168	180	0.1	S1 85% recovery, right shoulder on S2
1110	338.3	70.1	426	0.05	0.26	0.84	0.16	0.31	0.06	0.32	81	263	0.2	S1 70% recovery, left shoulder on S2, min effect on Tmax
1140	347.5	70.9	427	0.04	0.24	0.78	0.14	0.31	0.06	0.33	73	236	0.2	similar to 1110
1170	356.6	70.2	421	0.07	0.40	1.24	0.15	0.32	0.09	0.83	48	149	0.2	flat response at front of S2, left shoulder on S2
1200	365.8	70.0	423	0.10	0.59	1.65	0.15	0.36	0.13	0.93	63	177	0.2	double left shoulder on S2
1230	374.9	70.0	420	0.08	0.46	2.09	0.15	0.22	0.12	0.98	47	213	0.1	broad S2, left shoulder
1260	384.0	70.3	414	0.08	0.56	2.80	0.12	0.20	0.17	1.16	48	241	0.2	S1 75% recovery, large left shoulder on S2
1290	393.2	70.4	408	0.19	0.85	4.25	0.18	0.20	0.26	1.74	49	244	0.3	S1 60% recovery, large left peak on S2
1320	402.3	70.7	422	0.35	2.64	5.25	0.12	0.50	0.46	3.06	86	172	0.3	S1 75% recovery, small left shoulder on S2, min effect on Tmax
1350	411.5	70.7	417	0.22	1.64	4.88	0.12	0.34	0.38	2.90	57	168	0.3	S1 2/3 recovery, large left shoulder on S2
1380	420.6	70.1	421	0.15	0.87	3.21	0.14	0.27	0.22	1.63	53	197	0.2	S1 70% recovery, left shoulder on S2
1410	429.8	70.3	424	0.15	1.15	3.82	0.12	0.30	0.26	2.10	55	182	0.3	S1 70% recovery, left shoulder on S2, min effect on Tmax
1440	438.9	70.5	422	0.09	0.80	2.52	0.10	0.32	0.18	1.37	58	184	0.2	S1 70% recovery, left shoulder on S2, min effect on Tmax
1470	448.1	71.0	420	0.10	0.95	2.80	0.10	0.34	0.21	1.72	55	163	0.2	S1 70% recovery, left shoulder on S2, min effect on Tmax
1500	457.2	70.5	417	0.51	1.47	4.24	0.26	0.35	0.33	1.98	74	214	0.3	S1 75% recovery, large left shoulder on S2
1560	475.5	70.1	410	0.16	0.63	2.63	0.20	0.24	0.17	1.34	47	196	0.2	S1 75% recovery, large left shoulder on S2
1590	484.6	70.9	397	0.26	0.86	2.14	0.23	0.40	0.17	1.08	80	198	0.2	S1 80% recovery, large left shoulder on S2
1620	493.8	70.6	415	0.07	0.43	1.70	0.13	0.25	0.12	0.96	45	177	0.2	S1 70% recovery, large left shoulder on S2
1650	502.9	70.2	423	0.19	1.17	2.13	0.14	0.55	0.21	1.37	85	155	0.1	S1 80% recovery, left shoulder on S2, min effect on Tmax
1680	512.1	70.4	418	0.26	1.17	4.50	0.18	0.26	0.29	1.80	65	250	0.3	S1 80% recovery, large left shoulder on S2
1710	521.2	70.2	419	0.07	0.53	2.00	0.12	0.27	0.12	1.11	48	180	0.1	S1 75% recovery, large left shoulder on S2
1740	530.4	70.3	403	0.16	0.66	2.56	0.19	0.26	0.18	1.29	51	198	0.2	S1 80% recovery, large left shoulder on S2
1770	539.5	70.2	413	0.13	1.00	2.95	0.12	0.34	0.22	1.61	62	183	0.2	S1 75% recovery, left shoulder on S2
1800	548.6	70.5	416	0.14	0.73	3.35	0.16	0.22	0.20	1.71	43	196	0.2	S1 75% recovery, left shoulder on S2
1830	557.8	70.8	422	0.13	0.61	2.89	0.17	0.21	0.17	1.16	53	249	0.2	S1 75% recovery, left shoulder on S2, min effect on Tmax
1860	566.9	70.3	419	0.14	0.73	3.27	0.16	0.22	0.21	1.34	54	244	0.2	S1 75% recovery, large left shoulder on S2
1890	576.1	70.5	417	0.12	0.72	2.44	0.14	0.30	0.17	1.35	53	181	0.2	S1 2/3 recovery, large left shoulder on S2
1920	585.2	70.5	409	0.12	0.53	2.94	0.18	0.18	0.17	1.40	38	210	0.2	S1 70% recovery, large left shoulder on S2
1950	594.4	70.4	417	0.09	0.61	2.89	0.13	0.21	0.16	1.38	44	209	0.2	S1 70% recovery, large left shoulder on S2
1980	603.5	70.2	416	0.27	0.83	3.73	0.25	0.22	0.24	1.52	55	245	0.2	S1 80% recovery, large left shoulder on S2
2010	612.6	70.0	417	0.19	1.74	5.59	0.10	0.31	0.39	3.23	54	173	0.3	S1 70% recovery, large left shoulder on S2
2040	621.8	70.6	396	0.14	0.67	8.44	0.17	0.08	0.33	1.57	43	538	1.8	S1 2/3 recovery, large left shoulder on S2
2070	630.9	70.1	413	0.06	0.40	3.98	0.12	0.10	0.16	0.82	49	485	0.6	S1 2/3 recovery, large left shoulder on S2
2100	640.1	70.6	421	0.10	0.76	4.68	0.11	0.16	0.23	1.40	54	334	0.6	S1 70% recovery, left shoulder on S2, min effect on Tmax
Ave			416.2											all values (36)
SD			7.8											
Ave			**423.2**											selected values (9 points)

Depth ft	m	Qty	Tmax	S1	S2	S3	PI	S2/S3	PC(%)	TOC(%)	HI	OI	MINC	Comments
SD			2.2											
										Kugmallit Sequence				
2120	646.2	70.1	418	0.68	1.84	5.68	0.27	0.32	0.42	2.58	71	220	0.7	S1 80% recovery, large left shoulder on S2
2160	658.4	70.0	416	0.14	1.04	5.53	0.12	0.19	0.30	2.11	49	262	0.5	S1 70% recovery, large left shoulder on S2
2190	667.5	70.6	409	0.32	2.66	5.15	0.11	0.52	0.45	2.67	100	193	0.7	S1 80% recovery, broad S2
2220	676.7	70.4	405	0.46	4.02	6.94	0.10	0.58	0.67	4.83	83	144	0.6	bimodal S1, 60% recovery, large left shoulder on S2
2250	685.8	70.4	419	0.08	0.58	1.81	0.12	0.32	0.13	0.86	67	210	0.2	S1 70% recovery, left shoulder on S2
2280	694.9	70.3	419	0.36	4.36	6.80	0.08	0.64	0.68	4.28	102	159	0.4	S1 60% recovery, broad S2
2310	704.1	70.5	417	0.22	2.34	6.05	0.08	0.39	0.46	3.37	69	180	0.4	S1 70% recovery, left shoulder on S2
2340	713.2	70.6	413	0.20	2.80	4.54	0.07	0.62	0.44	2.99	94	152	0.5	S1 70% recovery, broad S2
2370	722.4	70.1	419	0.22	2.44	5.35	0.08	0.46	0.43	2.96	82	181	0.4	S1 70% recovery, asymmetric broad S2
2400	731.5	70.9	420	0.26	3.13	6.32	0.08	0.50	0.51	3.00	104	211	0.4	asymmetric broad S2
2430	740.7	70.4	420	0.30	7.61	7.93	0.04	0.96	0.98	5.82	131	136	0.8	asymmetric broad S2
2460	749.8	70.5	420	0.34	5.81	8.72	0.06	0.67	0.85	5.48	106	159	0.5	asymmetric broad S2
2490	759.0	70.4	420	0.21	2.00	5.22	0.09	0.38	0.38	2.53	79	206	0.3	asymmetric broad S2
2520	768.1	70.5	422	0.28	3.60	8.61	0.07	0.42	0.65	4.44	81	194	0.5	asymmetric broad S2
2550	777.2	70.5	421	0.31	5.94	10.14	0.05	0.59	0.93	6.26	95	162	0.5	asymmetric broad S2
2580	786.4	70.8	422	0.20	2.29	5.09	0.08	0.45	0.40	2.65	86	192	0.3	asymmetric broad S2
2610	795.5	70.8	421	0.26	4.62	8.57	0.05	0.54	0.75	4.97	93	172	0.4	asymmetric broad S2
2640	804.7	70.6	420	0.18	2.84	6.54	0.06	0.43	0.51	3.86	74	169	0.4	asymmetric broad S2
2670	813.8	70.6	422	0.30	4.21	7.74	0.07	0.54	0.68	4.20	100	184	0.4	asymmetric broad S2
2730	832.1	70.4	420	0.24	3.50	7.04	0.06	0.50	0.58	3.70	95	190	0.4	asymmetric broad S2
2760	841.2	70.6	420	0.23	4.37	8.92	0.05	0.49	0.73	5.02	87	178	0.4	asymmetric broad S2
2790	850.4	70.7	420	0.19	2.05	5.81	0.08	0.35	0.40	2.69	76	216	0.3	asymmetric broad S2
2820	859.5	70.5	423	0.25	3.86	5.52	0.06	0.70	0.56	3.42	113	161	0.3	
2850	868.7	70.2	422	0.28	3.11	6.58	0.08	0.47	0.53	3.35	93	196	0.5	asymmetric broad S2
2880	877.8	70.2	423	0.18	2.40	5.47	0.07	0.44	0.43	3.26	74	168	0.4	asymmetric broad S2
2910	887.0	70.1	423	0.20	2.12	5.66	0.09	0.37	0.42	2.73	78	207	0.4	
2940	896.1	70.7	421	0.18	3.20	5.85	0.05	0.55	0.51	3.48	92	168	0.3	asymmetric broad S2
2970	905.3	70.5	425	0.23	3.18	6.84	0.07	0.46	0.57	4.10	78	167	0.4	asymmetric broad S2
3000	914.4	70.5	420	0.23	2.58	5.56	0.08	0.46	0.46	3.70	70	150	0.4	asymmetric broad S2
3020	920.5	70.7	422	0.34	1.80	4.76	0.16	0.38	0.35	1.89	95	252	0.4	S1 80% recovery, small left shoulder on S2
3060	932.7	70.5	405	0.05	0.84	2.87	0.06	0.29	0.18	0.93	90	309	1.8	S1 70% recovery, broad S2
3090	941.8	70.0	434	0.23	1.42	4.51	0.14	0.31	0.32	1.70	84	265	2.0	S1 70% recovery, left shoulder on S2, highly asymmetric
3120	951.0	70.4	425	0.14	1.37	3.28	0.09	0.42	0.26	1.50	91	219	1.6	s1 2/3 recovery, bimodal S2
3125	952.5	70.6	387	0.13	0.78	2.58	0.15	0.30	0.17	1.07	73	241	0.5	asymmetric S2 with left/right shoulders; **core**
3150	960.1	70.6	425	0.20	0.88	3.27	0.19	0.27	0.21	1.05	84	311	2.5	S1 70% recovery, large left shoulder on S2
3180	969.3	71.1	428	0.31	1.55	3.40	0.17	0.46	0.29	1.31	118	260	2.3	S1 70% recovery, large left shoulder on S2, highly asymmetric
3210	978.4	70.3	425	0.22	1.42	3.74	0.13	0.38	0.29	2.01	71	186	1.5	
3240	987.6	70.3	430	0.23	1.32	4.97	0.15	0.27	0.31	2.20	60	226	1.4	S1 80% recovery, small left shoulder on S2, min effect on Tmax

Depth ft	m	Qty	Tmax	S1	S2	S3	PI	S2/S3	PC(%)	TOC(%)	HI	OI	MINC	Comments
3270	996.7	70.0	426	0.12	0.96	3.24	0.11	0.30	0.21	1.49	64	217	1.3	
3300	1005.8	70.7	427	0.18	1.11	3.51	0.14	0.32	0.23	1.60	69	219	1.2	
3330	1015.0	70.8	434	0.20	1.21	4.07	0.14	0.30	0.26	1.48	82	275	0.9	
3360	1024.1	70.4	429	0.17	1.25	4.25	0.12	0.29	0.27	1.60	78	266	1.0	
3390	1033.3	70.5	408	0.36	1.51	5.34	0.19	0.28	0.33	1.39	109	384	0.8	S1 80% recovery, left shoulder on asymmetric S2
3420	1042.4	70.0	427	0.14	1.25	4.68	0.10	0.27	0.27	1.43	87	327	0.9	
3450	1051.6	70.3	422	0.42	2.18	6.23	0.16	0.35	0.41	1.57	139	397	0.8	S1 70% recovery, large left shoulder on S2
3480	1060.7	70.4	426	0.29	1.42	6.21	0.17	0.23	0.34	1.16	122	535	0.6	
3510	1069.8	70.5	427	0.12	0.75	5.70	0.14	0.13	0.25	1.04	72	548	0.5	
3540	1079.0	70.1	427	0.08	0.73	4.83	0.10	0.15	0.22	1.01	72	478	0.4	asymmetric broad S2, left shoulder
3570	1088.1	70.2	413	0.08	0.71	3.50	0.11	0.20	0.18	0.78	91	449	0.4	S1 50% recovery, left shoulder on S2
3600	1097.3	70.4	423	0.12	0.86	4.76	0.12	0.18	0.23	0.90	96	529	0.6	S1 60% recovery, broad S2
3630	1106.4	70.8	429	0.15	0.79	4.02	0.16	0.20	0.21	0.87	91	462	0.6	S1 70% recovery, large left shoulder on S2
3660	1115.6	70.3	422	0.09	0.97	6.65	0.09	0.15	0.29	1.14	85	583	0.4	asymmetric broad S2
3690	1124.7	70.3	426	0.06	0.56	4.03	0.10	0.14	0.18	0.89	63	453	0.4	asymmetric broad S2, left shoulder
3710	1130.8	70.0	423	0.09	0.74	4.64	0.11	0.16	0.21	1.09	68	426	0.5	broad S2, left shoulder
3740	1140.0	70.1	423	0.08	0.85	8.41	0.08	0.10	0.32	1.22	70	689	0.5	
3780	1152.1	70.7	426	0.05	0.67	6.86	0.08	0.10	0.27	1.23	54	558	0.4	
3810	1161.3	70.6	423	0.10	0.77	7.13	0.12	0.11	0.29	1.11	69	642	0.4	asymmetric broad S2
3840	1170.4	70.7	423	0.09	0.90	5.86	0.09	0.15	0.26	1.08	83	543	0.7	
3870	1179.6	70.6	422	0.12	0.87	7.64	0.12	0.11	0.30	1.08	81	707	0.6	
3910	1191.8	70.9	422	0.09	0.64	5.15	0.13	0.12	0.23	1.03	62	500	0.5	S1 60% recovery, left shoulder on S2
3930	1197.9	70.2	426	0.13	0.80	4.76	0.14	0.17	0.23	1.05	76	453	0.5	left shoulder on S2
3960	1207.0	70.6	424	0.10	0.82	5.02	0.11	0.16	0.25	1.24	66	405	0.5	left shoulder on S2
4120	1255.8	70.6	427	0.07	0.59	4.01	0.10	0.15	0.18	0.92	64	436	0.5	S1 40% recovery, left shoulder on S2
4150	1264.9	70.6	423	0.14	0.71	4.07	0.17	0.17	0.20	0.93	76	438	0.5	S1 50% recovery, left shoulder on S2
4180	1274.1	70.0	379	0.15	1.12	2.67	0.12	0.42	0.20	0.87	129	307	0.5	S1 60% recovery, right shoulder on S2
4210	1283.2	70.4	419	0.09	0.51	3.32	0.15	0.15	0.17	0.74	69	449	0.4	S1 60% recovery, left shoulder on S2
4240	1292.4	70.5	426	0.06	0.41	3.45	0.14	0.12	0.15	0.66	62	523	0.4	S1 60% recovery, left shoulder on S2
4270	1301.5	70.6	425	0.08	0.49	2.93	0.14	0.17	0.14	0.75	65	391	0.4	S1 60% recovery, left shoulder on S2
Ave			420.9											all values (68)
SD			8.6											
Ave			**426.1**											selected values (15 points)
SD			**3.2**											
									Richards Sequence					
4300	1310.6	70.3	427	0.09	0.55	3.26	0.15	0.17	0.16	0.84	65	388	0.4	S1 60% recovery, left shoulder on S2
4330	1319.8	70.6	429	0.08	0.60	4.23	0.12	0.14	0.19	0.86	70	492	0.5	left shoulder on S2
4360	1328.9	70.6	420	0.11	0.72	4.10	0.13	0.18	0.20	0.95	76	432	0.4	left shoulder on S2
4390	1338.1	70.6	430	0.06	0.64	5.03	0.09	0.13	0.22	1.02	63	493	0.3	
4420	1347.2	70.6	419	0.25	1.24	3.47	0.17	0.36	0.24	1.20	103	289	0.5	S1 70% recovery, left shoulder on S2

Depth ft	m	Qty	Tmax	S1	S2	S3	PI	S2/S3	PC(%)	TOC(%)	HI	OI	MINC	Comments
4450	1356.4	70.5	425	0.10	0.73	3.27	0.12	0.22	0.18	1.02	72	321	0.4	left shoulder on S2
4470	1362.5	70.2	427	0.04	0.26	0.80	0.14	0.33	0.06	0.86	30	93	0.15	**core**; small left shoulder on S2
4480	1365.5	70.3	428	0.10	0.82	4.21	0.11	0.19	0.21	1.11	74	379	0.4	left shoulder on S2
4520	1377.7	70.9	424	0.10	0.84	2.82	0.11	0.30	0.18	1.02	82	276	0.3	2 left shoulders on S2
4540	1383.8	70.3	414	0.09	1.23	3.93	0.07	0.31	0.25	1.17	105	336	0.4	S1 60% recovery, bimodal S2
4580	1396.0	70.3	429	0.10	0.71	2.36	0.13	0.30	0.15	0.99	72	238	0.3	left shoulder on S2
4600	1402.1	70.4	430	0.10	0.71	2.36	0.12	0.30	0.16	0.99	72	238	0.3	left shoulder on S2
4630	1411.2	70.4	427	0.07	0.60	2.33	0.11	0.26	0.14	0.95	63	245	0.3	small left shoulder on S2
4660	1420.4	70.9	431	0.07	0.74	2.16	0.09	0.34	0.15	1.01	73	214	0.3	S1 60% recovery, small left peak on S2
4690	1429.5	70.2	423	0.07	0.68	2.33	0.10	0.29	0.15	0.98	69	238	0.3	broad S2, left shoulder
4720	1438.7	70.5	429	0.07	0.61	2.10	0.11	0.29	0.14	0.99	62	212	0.2	
4750	1447.8	70.2	432	0.05	0.63	2.99	0.07	0.21	0.16	1.02	62	293	0.7	
4780	1456.9	70.6	428	0.10	0.73	2.48	0.12	0.29	0.15	1.02	72	243	0.4	small left shoulder on S2
4810	1466.1	70.5	429	0.07	0.70	2.08	0.09	0.34	0.15	1.00	70	208	0.4	
4840	1475.2	71.0	425	0.07	0.61	2.06	0.10	0.30	0.13	1.00	61	206	0.3	
4870	1484.4	70.6	427	0.10	0.73	2.15	0.12	0.34	0.15	0.98	74	219	0.3	
4900	1493.5	70.8	425	0.08	0.83	2.61	0.09	0.32	0.17	1.06	78	246	0.2	left shoulder on S2
4930	1502.7	70.5	433	0.06	0.68	1.85	0.08	0.37	0.13	1.02	67	181	0.3	
4960	1511.8	70.6	431	0.10	0.85	2.56	0.11	0.33	0.17	1.07	79	239	0.3	
4990	1521.0	71.0	430	0.17	0.94	2.45	0.15	0.38	0.18	1.11	85	221	0.3	
5020	1530.1	70.0	426	0.09	0.81	2.19	0.10	0.37	0.15	0.91	89	241	1.4	S1 60% recovery, left shoulder on S2
5050	1539.2	70.5	431	0.12	0.83	2.18	0.12	0.38	0.16	1.07	78	204	0.3	
5080	1548.4	70.3	429	0.08	0.92	3.53	0.08	0.26	0.20	1.12	82	315	0.3	
5110	1557.5	70.9	427	0.10	0.65	1.94	0.13	0.34	0.14	1.04	62	187	0.3	
5170	1575.8	70.1	427	0.09	0.81	1.83	0.10	0.44	0.14	1.00	81	183	0.3	
5200	1585.0	70.7	429	0.10	0.85	2.12	0.11	0.40	0.15	1.02	83	208	0.3	small left shoulder on S2
5230	1594.1	70.6	426	0.11	1.22	2.20	0.09	0.55	0.19	1.05	116	210	0.2	
5260	1603.2	70.6	429	0.12	1.01	1.67	0.11	0.60	0.16	1.07	94	156	0.3	S1 80% recovery, left shoulder on S2
5290	1612.4	70.0	430	0.07	0.92	2.89	0.07	0.32	0.18	1.03	89	281	0.3	
5320	1621.5	70.2	429	0.09	1.00	2.70	0.09	0.37	0.20	1.12	89	241	0.5	
5350	1630.7	70.3	431	0.08	0.77	1.83	0.10	0.42	0.15	1.00	77	183	0.4	
5380	1639.8	70.6	427	0.19	1.35	2.15	0.12	0.63	0.22	1.13	119	190	0.4	S1 80% recovery, left peak on S2
5410	1649.0	70.8	431	0.12	0.97	2.76	0.11	0.35	0.19	1.09	89	253	0.4	
5440	1658.1	70.3	429	0.04	0.65	3.33	0.06	0.20	0.18	0.98	66	340	0.3	
5470	1667.3	70.1	430	0.12	0.91	1.77	0.12	0.51	0.16	1.07	85	165	0.4	small left shoulder on S2
5510	1679.4	70.4	427	0.14	0.58	1.98	0.20	0.29	0.13	1.05	55	189	0.4	irregular S2 peak
5530	1685.5	70.8	428	0.07	0.68	2.12	0.09	0.32	0.14	1.08	63	196	0.3	
5560	1694.7	70.9	425	0.05	0.68	2.73	0.07	0.25	0.15	1.14	60	239	0.3	
5590	1703.8	70.6	427	0.25	1.52	1.94	0.14	0.78	0.23	1.25	122	155	0.5	S1 80% recovery, left shoulder on S2
5620	1713.0	70.8	429	0.07	0.73	2.54	0.09	0.29	0.15	1.17	62	217	0.5	

Depth ft	m	Qty	Tmax	S1	S2	S3	PI	S2/S3	PC(%)	TOC(%)	HI	OI	MINC	Comments
5650	1722.1	70.3	430	0.06	0.79	2.61	0.07	0.30	0.17	1.29	61	202	0.4	
5680	1731.3	70.1	429	0.07	0.77	4.28	0.08	0.18	0.21	1.20	64	357	0.4	
5710	1740.4	70.4	430	0.07	0.86	3.29	0.08	0.26	0.19	1.36	63	242	0.4	
5740	1749.6	70.4	427	0.09	0.83	2.15	0.10	0.39	0.17	1.16	72	185	0.5	left shoulder on S2
5770	1758.7	70.6	430	0.06	0.88	3.00	0.06	0.29	0.18	1.34	66	224	0.4	
5800	1767.8	70.8	430	0.09	0.79	3.05	0.10	0.26	0.18	1.14	69	268	0.5	
5830	1777.0	70.4	427	0.05	0.87	4.47	0.05	0.19	0.22	1.30	67	344	0.5	
5860	1786.1	70.0	427	0.07	1.00	5.01	0.07	0.20	0.25	1.39	72	360	0.4	
5890	1795.3	70.5	435	0.07	1.09	3.56	0.06	0.31	0.22	1.36	80	262	0.5	
5920	1804.4	70.1	430	0.09	1.11	4.06	0.08	0.27	0.24	1.35	82	301	0.5	S1 70% recovery, small left shoulder on S2
5960	1816.6	70.2	430	0.08	1.16	2.49	0.06	0.47	0.19	1.42	82	175	0.4	
5990	1825.8	70.4	421	0.12	1.39	2.60	0.08	0.53	0.24	1.43	97	182	0.5	S1 70% recovery, left shoulder on S2
6020	1834.9	70.7	429	0.07	1.02	2.85	0.07	0.36	0.19	1.32	77	216	0.6	
6050	1844.0	70.0	427	0.07	1.04	3.23	0.06	0.32	0.21	1.29	81	250	0.5	
6080	1853.2	70.5	430	0.06	1.00	3.33	0.06	0.30	0.20	1.26	79	264	0.5	
6110	1862.3	70.6	428	0.08	0.90	2.76	0.08	0.33	0.17	1.16	78	238	0.4	
6140	1871.5	70.8	429	0.08	0.98	2.86	0.07	0.34	0.19	1.28	77	223	0.4	
6170	1880.6	70.9	430	0.07	1.14	3.36	0.06	0.34	0.22	1.29	88	260	0.4	small left shoulder on S2
6200	1889.8	70.0	428	0.09	0.86	2.64	0.09	0.33	0.17	1.32	65	200	0.3	
6230	1898.9	70.6	430	0.09	0.93	2.65	0.09	0.35	0.18	1.31	71	202	0.4	
6260	1908.0	70.8	429	0.08	0.82	3.27	0.09	0.25	0.20	1.26	65	260	0.4	
6290	1917.2	70.6	427	0.05	0.70	2.38	0.07	0.29	0.15	1.17	60	203	0.4	irregular S2 peak
6350	1935.5	70.4	428	0.09	1.09	2.35	0.08	0.46	0.18	1.27	86	185	0.3	
6380	1944.6	70.7	427	0.13	1.02	2.91	0.12	0.35	0.20	1.26	81	231	0.5	
6410	1953.8	70.5	427	0.11	1.06	3.08	0.09	0.34	0.21	1.26	84	244	0.5	
6440	1962.9	70.3	426	0.10	0.86	2.45	0.10	0.35	0.17	1.13	76	217	0.4	
6470	1972.1	70.1	430	0.09	0.85	2.31	0.10	0.37	0.16	1.11	77	208	0.4	
6500	1981.2	70.9	427	0.09	0.93	1.90	0.09	0.49	0.16	1.13	82	168	0.4	
6530	1990.3	70.6	430	0.07	0.86	1.57	0.08	0.55	0.14	1.22	70	129	0.3	
6560	1999.5	70.8	427	0.11	0.87	1.71	0.11	0.51	0.14	1.15	76	149	0.2	left shoulder on S2
6590	2008.6	70.4	422	0.08	0.59	1.29	0.12	0.46	0.11	1.12	53	115	0.2	asymmetric, left shoulder on S2
6620	2017.8	70.5	427	0.31	1.49	1.40	0.17	1.06	0.21	1.22	122	115	0.3	S1 70% recovery, left shoulder on S2, **Peltex added**
6650	2026.9	70.3	431	0.10	0.76	1.25	0.12	0.61	0.12	1.02	75	123	0.3	small left shoulder on S2
6680	2036.1	70.4	430	0.08	0.84	1.66	0.09	0.51	0.14	1.11	76	150	0.3	
6710	2045.2	70.1	430	0.14	0.72	1.36	0.16	0.53	0.13	1.06	68	128	0.3	left shoulder, asymmetric S2
6750	2057.4	70.5	423	0.08	0.64	1.28	0.11	0.50	0.11	1.07	60	120	0.3	
6780	2066.5	70.8	416	0.37	2.45	1.53	0.13	1.60	0.30	1.52	161	101	0.4	multipeak S1 30% recovery, large left shoulder on S2, **Peltex added**
6800	2072.6	70.5	426	0.09	0.83	1.39	0.10	0.60	0.14	1.13	73	123	0.2	left shoulder on S2
6830	2081.8	70.2	425	0.11	0.66	1.04	0.15	0.63	0.12	1.17	56	89	0.3	left shoulder on S2
6860	2090.9	70.4	429	0.08	0.79	1.35	0.09	0.59	0.13	1.11	71	122	0.2	

Depth ft	m	Qty	Tmax	S1	S2	S3	PI	S2/S3	PC(%)	TOC(%)	HI	OI	MINC	Comments
6890	2100.1	70.6	423	0.06	0.39	0.80	0.13	0.49	0.08	1.04	38	77	0.2	
6920	2109.2	70.2	428	0.08	0.75	1.01	0.10	0.74	0.12	1.13	66	89	0.3	
6950	2118.4	71.0	429	0.10	0.72	1.48	0.12	0.49	0.14	1.18	61	125	0.2	
6980	2127.5	70.8	423	0.12	0.94	1.28	0.12	0.73	0.14	1.16	81	110	0.3	
7010	2136.6	70.3	414	0.10	0.46	1.05	0.18	0.44	0.10	1.00	46	105	0.6	S1 80% recovery, wide asymmetric S2 peak
7040	2145.8	70.8	426	0.09	0.68	1.52	0.12	0.45	0.12	1.09	62	139	0.3	small left shoulder on S2
7070	2154.9	70.3	426	0.08	0.60	1.28	0.12	0.47	0.11	0.98	61	131	0.4	
7100	2164.1	70.9	423	0.11	0.71	1.23	0.13	0.58	0.12	1.12	63	110	0.2	S1 70% recovery, left shoulder on S2
7130	2173.2	70.0	425	0.11	0.87	1.56	0.11	0.56	0.15	1.12	78	139	0.3	S1 70% recovery, left shoulder on S2
7160	2182.4	70.3	421	0.33	1.53	1.50	0.18	1.02	0.21	1.28	120	117	0.5	S1 50% recovery, bimodal S2, smaller Tmax~330
7220	2200.7	70.8	422	0.43	2.40	1.90	0.15	1.26	0.32	2.46	98	77	0.6	left shoulder on S2
7250	2209.8	71.0	427	0.42	3.10	2.41	0.12	1.29	0.40	2.91	107	83	0.5	small left shoulder, asymmetric S2
7280	2218.9	70.7	425	0.14	1.47	2.46	0.09	0.60	0.24	1.55	95	159	0.6	
7310	2228.1	70.8	425	0.20	1.26	2.17	0.14	0.58	0.20	1.47	86	148	0.4	left shoulder on S2
7370	2246.4	70.7	419	0.10	0.98	1.98	0.10	0.49	0.19	1.73	57	114	0.8	S1 70% recovery, left skew asymmetric S2
7410	2258.6	70.2	424	0.27	1.39	1.79	0.16	0.78	0.22	1.60	87	112	0.4	S1 70% recovery, left shoulder on S2
7430	2264.7	70.7	425	0.14	0.90	1.59	0.14	0.57	0.16	1.25	72	127	0.5	
7460	2273.8	70.5	421	0.13	1.24	1.72	0.10	0.72	0.18	1.39	89	124	0.5	S1 70% recovery, large left shoulder on S2
7490	2283.0	70.6	405	0.60	3.84	1.89	0.14	2.03	0.45	1.74	221	109	0.6	S1 50% recovery, large left shoulder on S2
7550	2301.2	70.5	419	0.15	1.55	1.85	0.09	0.84	0.24	1.99	78	93	1.0	asymmetric S2
7580	2310.4	70.6	428	0.09	0.88	1.68	0.10	0.52	0.16	1.71	51	98	0.7	**Peltex added**
7610	2319.5	70.4	418	0.19	1.08	2.30	0.15	0.47	0.20	1.50	72	153	0.6	S1 80% recovery, wide asymmetric S2 peak, **Peltex added**
7640	2328.7	70.4	424	0.09	0.76	1.45	0.11	0.52	0.14	1.33	57	109	0.4	**Peltex added**
7670	2337.8	70.6	419	0.37	2.47	2.07	0.13	1.19	0.32	1.80	137	115	0.6	S1 60% recovery, large left shoulder
7770	2368.3	70.8	421	0.13	1.16	1.49	0.10	0.78	0.18	1.70	68	88	0.7	S1 70% recovery, left shoulder on S2
7800	2377.4	70.6	422	0.16	0.99	1.35	0.14	0.73	0.15	1.34	74	101	0.6	S1 75% recovery, left shoulder on S2
7860	2395.7	70.7	423	0.08	0.65	1.08	0.10	0.60	0.11	1.34	49	81	0.7	
7890	2404.9	70.2	423	0.07	0.65	1.04	0.10	0.63	0.11	1.27	51	82	0.6	asymmetric S2
7920	2414.0	70.4	415	0.39	3.88	2.20	0.09	1.76	0.47	3.52	110	63	0.7	asymmetric S2
7950	2423.2	71.0	413	0.12	0.83	1.11	0.13	0.75	0.14	1.36	61	82	0.8	S1 80% recovery, small left shoulder, symmetric S2 peak
7980	2432.3	70.4	419	0.08	0.91	1.17	0.09	0.78	0.15	1.50	61	78	0.8	S1 80% recovery, small left shoulder, asymmetric S2
8010	2441.4	70.6	416	0.44	1.89	1.27	0.19	1.49	0.27	1.87	101	68	0.7	S1 80% recovery, two left shoulders on S2 peak; **oil stain**
8040	2450.6	70.7	410	0.09	0.70	1.12	0.11	0.63	0.12	1.29	54	87	0.7	S1 70% recovery, asymmetric S2
8070	2459.7	70.3	424	0.12	0.79	1.20	0.13	0.66	0.14	1.26	63	95	0.7	small left shoulder on S2
8100	2468.9	70.5	423	0.06	0.60	1.27	0.09	0.47	0.12	1.27	47	100	0.8	
8130	2478.0	70.5	409	0.70	1.78	1.63	0.28	1.09	0.27	1.44	124	113	0.8	S1 70% recovery, asymmetric bimodal S2
8160	2487.2	70.2	408	0.56	2.00	1.19	0.22	1.68	0.27	1.40	143	85	0.6	S1 60% recovery, large left shoulder on S2
8190	2496.3	71.0	421	0.12	0.59	1.45	0.17	0.41	0.12	1.08	55	134	0.5	bimodal S1, small left shoulder on S2, **added Peltex**
8220	2505.5	70.0	430	0.04	0.39	1.49	0.09	0.26	0.10	1.15	34	130	0.7	
8250	2514.6	70.6	429	0.04	0.36	1.18	0.10	0.31	0.09	0.99	36	119	0.6	

Depth ft	m	Qty	Tmax	S1	S2	S3	PI	S2/S3	PC(%)	TOC(%)	HI	OI	MINC	Comments
8280	2523.7	70.6	423	0.07	0.89	2.12	0.07	0.42	0.19	2.09	43	101	0.8	bimodal S1
8310	2532.9	70.6	418	0.13	1.20	1.56	0.10	0.77	0.18	1.34	90	116	0.7	S1 80% recovery, large left shoulder on S2 peak
8340	2542.0	70.0	303	1.23	2.97	2.09	0.29	1.42	0.43	1.52	195	138	0.6	S1 peak ht > S2, 45% recovery, bimodal S2; **oil stain**
8370	2551.2	70.1	430	0.09	1.31	1.97	0.07	0.66	0.19	1.69	78	117	0.8	
8400	2560.3	70.4	430	0.11	1.28	1.46	0.08	0.88	0.18	1.62	79	90	0.7	
8430	2569.5	70.4	422	0.11	1.69	1.89	0.06	0.89	0.23	1.98	85	95	0.8	asymmetric S2
8460	2578.6	70.4	406	0.24	6.53	2.57	0.04	2.54	0.68	4.28	153	60	0.8	symmetric S2, broad peak
8490	2587.8	70.4	419	0.49	4.01	2.37	0.11	1.69	0.50	3.58	112	66	0.9	asymmetric S2
8520	2596.9	70.3	421	0.25	2.15	1.68	0.10	1.28	0.29	2.10	102	80	1.0	
8550	2606.0	70.0	426	0.06	1.29	1.92	0.04	0.67	0.21	1.98	65	97	1.0	
8580	2615.2	70.1	424	0.10	1.17	1.06	0.08	1.10	0.14	1.46	80	73	0.8	
8610	2624.3	70.2	416	0.31	4.40	2.38	0.07	1.85	0.52	3.38	130	70	1.0	
8640	2633.5	70.3	423	0.28	2.26	1.91	0.11	1.18	0.30	2.52	90	76	0.8	
8670	2642.6	70.2	422	0.51	2.53	1.70	0.17	1.49	0.33	2.09	121	81	0.8	asymmetric S2
8671	2642.9	70.7	423	0.45	8.19	5.43	0.05	1.51	1.03	11.92	69	46	0.39	**core**
8700	2651.8	70.6	426	0.13	1.63	1.50	0.07	1.09	0.23	2.03	80	74	0.7	
8730	2660.9	70.3	422	0.09	0.99	1.01	0.08	0.98	0.15	1.65	60	61	0.5	
8760	2670.0	70.3	423	0.06	0.67	0.88	0.08	0.76	0.11	1.28	52	69	0.4	
8820	2688.3	70.6	422	0.09	0.80	1.09	0.10	0.73	0.13	1.19	67	92	0.7	asymmetric S2 peak
8850	2697.5	70.5	427	0.12	1.22	1.67	0.09	0.73	0.19	1.72	71	97	0.7	**Peltex added**
8910	2715.8	70.8	424	0.17	1.45	1.69	0.10	0.86	0.22	2.21	66	76	0.6	left shoulder on S2
8940	2724.9	70.6	428	0.15	0.93	1.18	0.14	0.79	0.15	1.39	67	85	0.8	**Peltex added**
8970	2734.1	70.1	412	0.05	0.68	1.13	0.07	0.60	0.12	1.17	58	97	0.9	asymmetric S2 with right shoulder
9000	2743.2	70.2	425	0.07	0.57	1.33	0.11	0.43	0.11	0.93	61	143	0.7	
9030	2752.3	70.6	425	0.09	0.87	1.67	0.10	0.52	0.15	1.14	76	146	0.5	small left shoulder on S2
9050	2758.4	71.0	426	0.04	0.40	0.80	0.09	0.50	0.07	0.75	53	107	0.7	small left shoulder on S2
9090	2770.6	70.0	425	0.04	0.50	1.52	0.08	0.33	0.10	0.79	63	192	0.7	slightly asymmetric S2
9120	2779.8	70.2	425	0.14	1.68	2.66	0.07	0.63	0.26	2.36	71	113	0.7	**Peltex added**
9150	2788.9	70.4	413	0.07	0.78	1.08	0.08	0.72	0.12	1.15	68	94	0.8	asymmetric S2 with right shoulder, **Peltex added**
9180	2798.1	70.5	422	0.08	1.06	1.35	0.07	0.79	0.16	1.37	77	99	1.0	asymmetric S2 with left shoulder
9210	2807.2	70.5	428	0.07	0.72	1.13	0.08	0.64	0.12	1.02	71	111	0.9	
9240	2816.4	70.9	428	0.05	0.67	1.21	0.07	0.55	0.12	1.17	57	103	0.8	
9270	2825.5	70.3	424	0.09	0.86	1.44	0.09	0.60	0.14	1.38	62	104	0.8	asymmetric S2, broader peak, **Peltex**
9276	2827.3	70.4	423	0.04	0.36	0.31	0.10	1.16	0.05	1.00	36	31	0.12	**core**
9300	2834.6	70.1	428	0.08	0.47	1.13	0.14	0.42	0.10	1.03	46	110	0.4	**Peltex added**
9330	2843.8	70.1	432	0.05	0.39	1.28	0.12	0.30	0.09	0.82	48	156	0.4	
9360	2852.9	70.9	426	0.04	0.28	0.95	0.11	0.29	0.07	0.64	44	148	0.3	**Peltex at 9345-76 (400 lbs)**
9390	2862.1	70.6	423	0.07	0.46	0.93	0.13	0.49	0.08	0.74	62	126	0.5	small left shoulder, **Peltex at 9376-9404 (1600 lbs)**
9420	2871.2	70.7	431	0.07	0.89	1.24	0.07	0.72	0.15	1.83	49	68	0.5	asymmetric S2, skewed right, **Peltex at 9404-9423 (1200 lbs)**
9450	2880.4	70.9	424	0.06	0.33	0.81	0.14	0.41	0.07	0.59	56	137	0.4	small left shoulder, **Peltex at 9446-9456 (500 lbs)**

Depth ft	m	Qty	Tmax	S1	S2	S3	PI	S2/S3	PC(%)	TOC(%)	HI	OI	MINC	Comments
9480	2889.5	70.1	297	7.99	11.98	3.64	0.40	3.29	1.80	3.13	383	116	2.8	large S1, bimodal S2, **Peltex at 9468-94 (250); oil stain**
9510	2898.6	70.7	407	12.22	10.43	2.18	0.54	4.78	1.98	3.02	345	72	2.4	large S1, bimodal S2; oil stain
9540	2907.8	70.7	418	0.29	1.10	2.02	0.21	0.54	0.20	0.95	116	213	0.6	left shoulder on S2
9570	2916.9	70.2	418	0.14	1.20	1.74	0.10	0.69	0.19	0.96	125	181	0.6	left shoulder on S2
9600	2926.1	70.8	423	0.14	0.77	1.20	0.15	0.64	0.14	0.78	99	154	0.8	left shoulder on S2
9630	2935.2	70.0	426	0.09	0.67	1.35	0.12	0.50	0.12	0.83	81	163	0.9	left shoulder
9660	2944.4	71.0	413	0.47	1.73	0.96	0.22	1.80	0.22	0.94	184	102	0.4	large left shoulder on S2
9661	2944.7	70.2	435	0.09	0.91	0.51	0.09	1.78	0.11	0.97	94	53	0.30	**core**
9690	2953.5	70.1	432	0.07	0.57	0.98	0.11	0.58	0.10	0.75	76	131	0.6	left shoulder, irregular peak
9720	2962.7	70.3	430	0.09	0.70	1.68	0.12	0.42	0.14	0.87	80	193	1.1	small left shoulder
9750	2971.8	70.4	426	0.18	0.95	1.30	0.16	0.73	0.16	0.99	96	131	0.7	bimodal S2
9780	2980.9	70.3	429	0.09	0.80	0.94	0.10	0.85	0.11	0.86	93	109	0.6	small left shoulder
9810	2990.1	70.0	431	0.06	0.76	1.09	0.08	0.70	0.12	1.01	75	108	0.6	
9840	2999.2	70.1	426	0.07	0.77	1.25	0.08	0.62	0.13	0.92	84	136	0.7	irregular S2
9870	3008.4	70.2	427	0.09	0.64	0.88	0.12	0.73	0.10	0.89	72	99	0.5	left shoulder, **Peltex at 9842-73**
9900	3017.5	70.6	432	0.08	0.77	1.24	0.10	0.62	0.12	1.03	75	120	0.8	small left shoulder, **Peltex at 9873-9911**
9930	3026.7	70.4	426	0.11	1.02	1.28	0.10	0.80	0.16	1.12	91	114	0.8	left shoulder, asymmetric S2
9960	3035.8	70.4	425	0.24	1.75	1.48	0.12	1.18	0.24	1.76	99	84	0.7	left shoulder, **Peltex at 9950-86**
9990	3045.0	70.4	425	0.38	4.00	2.30	0.09	1.74	0.47	3.38	118	68	0.7	**Peltex at 9986-10022**
10020	3054.1	70.3	422	0.18	1.46	0.94	0.11	1.55	0.20	1.96	74	48	0.3	**Peltex at 9986-10054, 10067-74**
10080	3072.4	70.7	430	0.15	0.86	0.99	0.15	0.87	0.14	1.13	76	88	0.5	small left shoulder, **Peltex at 10074-10133**
10110	3081.5	70.6	427	0.28	1.26	1.29	0.18	0.98	0.18	1.26	100	102	0.5	left shoulder on S2, **Peltex at 10074-10133**
10140	3090.7	70.5	425	0.25	1.27	1.42	0.17	0.89	0.19	1.27	100	112	0.5	left shoulder on S2, **Peltex at 10133-10210**
10170	3099.8	70.4	428	0.12	0.93	1.67	0.11	0.56	0.15	1.22	76	137	0.6	small left shoulder peak on S2, **Peltex at 10133-10210**
10200	3109.0	70.5	414	0.14	1.19	1.19	0.11	1.00	0.17	1.21	98	98	0.6	slight asymmetric S2, **Peltex at 10133-10210**
10230	3118.1	70.7	425	0.10	0.92	1.44	0.10	0.64	0.15	1.18	78	122	0.5	left shoulder on S2, **Peltex at 10210-10252**
Ave			423.7											all values (191)
SD			13.9											
Ave			**427.6**											selected values (104 points)
SD			**3.1**											
										Taglu Sequence				
10260	3127.2	70.7	431	0.09	0.77	0.91	0.10	0.85	0.12	1.00	77	91	0.5	
10290	3136.4	70.9	427	0.10	0.84	0.86	0.11	0.98	0.12	0.86	98	100	0.6	left shoulder, **Peltex at 10263-10285**
10320	3145.5	70.3	427	0.18	1.87	1.66	0.09	1.13	0.24	1.21	155	137	0.6	odd shaped angular S2, **Peltex at 10302-10356**
10350	3154.7	70.6	429	0.18	0.91	1.38	0.16	0.66	0.15	0.94	97	147	0.6	left shoulder, **Peltex at 10302-10356**
10380	3163.8	70.5	419	0.51	1.13	1.39	0.31	0.81	0.19	0.75	151	185	0.5	bimodal S2
10410	3173.0	70.2	424	0.14	0.79	1.97	0.15	0.40	0.15	0.89	89	221	0.7	broad S2 with left shoulder, **Peltex at 10387-10423 (300)**
10440	3182.1	71.1	431	0.07	0.68	1.03	0.09	0.66	0.11	0.86	79	120	0.7	
10470	3191.3	70.8	431	0.10	0.62	1.36	0.14	0.46	0.11	0.70	89	194	0.8	small left shoulder, **Peltex at 10447-10488 (300)**
10500	3200.4	70.9	424	0.32	0.93	0.84	0.26	1.11	0.15	0.69	135	122	1.1	bimodal S2

Depth														
ft	m	Qty	Tmax	S1	S2	S3	PI	S2/S3	PC(%)	TOC(%)	HI	OI	MINC	Comments
10530	3209.5	70.9	402	0.38	2.01	1.07	0.16	1.88	0.26	1.18	170	91	0.7	large left shoulder on S2, **Peltex at 10519-10534 (150)**
10540	3212.6	70.2	434	0.05	0.30	0.45	0.14	0.67	0.08	0.44	68	102	1.04	left shoulder on S2; **core**
10560	3218.7	70.5	425	0.11	0.76	0.89	0.13	0.85	0.12	0.90	84	99	0.7	broad S2 with left shoulder
10590	3227.8	70.9	429	0.09	0.73	1.36	0.10	0.54	0.16	0.92	79	148	1.5	small left shoulder, **Peltex at 10561-10613 (350)**
10620	3237.0	71.0	428	0.11	0.72	1.73	0.13	0.42	0.15	0.82	88	211	1.2	broad S2 with left shoulder, **Peltex at 10613-10642 (150)**
10650	3246.1	70.8	431	0.10	0.64	1.78	0.14	0.36	0.14	0.78	82	228	1.1	small left shoulder
10680	3255.3	70.3	429	0.11	0.78	1.43	0.13	0.55	0.14	0.78	100	183	1.0	broad S2 with left shoulder
10710	3264.4	70.3	428	0.10	0.75	1.27	0.12	0.59	0.13	0.87	86	146	0.9	small left shoulder
10740	3273.6	70.2	431	0.09	0.75	0.93	0.11	0.81	0.12	0.85	88	109	0.8	**Peltex at 10720-10747 (250)**
10770	3282.7	70.8	422	0.40	2.30	2.16	0.15	1.06	0.33	1.90	121	114	1.1	broad S2 with left shoulder, **Peltex at 10747-10817 (250)**
10800	3291.8	70.4	428	0.17	1.53	1.86	0.10	0.82	0.24	1.53	100	122	1.0	small left shoulder, **Peltex at 10747-10817 (250)**
10830	3301.0	70.2	425	0.11	1.25	1.50	0.08	0.83	0.19	1.35	93	111	1.4	broad asymmetric S2
10860	3310.1	70.4	430	0.08	0.87	1.53	0.09	0.57	0.16	1.11	78	138	1.0	**Peltex at 10846-10938 (450)**
10890	3319.3	70.8	428	0.11	1.02	1.56	0.10	0.65	0.18	1.11	92	141	1.2	small left shoulder, **Peltex at 10846-10938 (450)**
10920	3328.4	70.6	429	0.10	0.98	1.58	0.09	0.62	0.15	1.10	89	144	0.8	**Peltex at 10846-10938 (450)**
10950	3337.6	70.4	431	0.09	0.92	1.57	0.09	0.59	0.15	1.07	86	147	0.9	**Peltex at 10938-10965 (200)**
10980	3346.7	70.3	429	0.12	1.12	1.73	0.10	0.65	0.18	1.27	88	136	0.8	
11010	3355.8	70.8	425	0.11	1.01	1.46	0.10	0.69	0.17	0.95	106	154	1.0	**Peltex at 10994-11037 (400)**
11040	3365.0	70.1	419	0.31	1.75	2.54	0.15	0.69	0.29	1.40	125	181	1.0	odd shaped angular S2
11070	3374.1	70.8	413	0.51	11.86	16.01	0.04	0.74	1.69	11.69	101	137	1.3	broad symmetric S2
11100	3383.3	70.2	417	0.17	4.36	5.94	0.04	0.73	0.64	4.55	96	131	1.4	broad symmetric S2, **Peltex at 11084-11219 (400)**
11130	3392.4	70.6	424	0.09	1.10	1.26	0.08	0.87	0.18	1.18	93	107	1.1	broad symmetric S2, **Peltex at 11084-11219 (400)**
11160	3401.6	70.2	422	0.11	2.55	5.25	0.04	0.49	0.44	3.41	75	154	1.3	broad symmetric S2, **Peltex at 11084-11219 (400)**
11190	3410.7	70.7	423	0.20	1.91	3.39	0.09	0.56	0.32	2.16	88	157	1.1	left shoulder, broad symmetric S2, **Peltex at 11084-11219 (400)**
11250	3429.0	70.0	429	0.08	0.82	0.93	0.09	0.88	0.13	0.94	87	99	0.8	
11280	3438.1	70.3	430	0.08	0.87	1.12	0.09	0.78	0.15	1.05	83	107	0.9	**Peltex at 11265-11345 (200)**
11310	3447.3	70.4	430	0.07	0.78	1.19	0.08	0.66	0.13	0.99	79	120	0.9	**Peltex at 11265-11345 (200)**
11340	3456.4	70.4	430	0.09	0.79	0.95	0.10	0.83	0.13	0.94	84	101	0.9	**Peltex at 11265-11345 (200)**
11370	3465.6	70.1	431	0.07	0.72	0.84	0.09	0.86	0.12	0.83	87	101	0.9	**Peltex at 11345-11481 (300)**
11400	3474.7	70.3	421	0.10	1.57	2.04	0.06	0.77	0.24	1.89	83	108	0.9	broad symmetric S2, **Peltex at 11345-11481 (300)**
11430	3483.9	71.0	428	0.10	1.12	1.76	0.09	0.64	0.19	1.37	82	128	0.8	**Peltex at 11345-11481 (300)**
11460	3493.0	70.0	429	0.12	1.01	1.62	0.11	0.62	0.17	1.31	77	124	0.9	**Peltex at 11345-11481 (300)**
11490	3502.2	70.9	422	0.14	1.72	2.39	0.07	0.72	0.26	1.99	86	120	0.9	broad symmetric S2
11520	3511.3	70.9	429	0.08	0.68	0.74	0.10	0.92	0.11	0.85	80	87	0.9	
11550	3520.4	70.2	419	0.17	1.26	1.35	0.12	0.93	0.19	1.27	99	106	0.8	broad S2 with left shoulder, **Peltex at 11524-11562 (1150)**
11580	3529.6	70.6	428	0.13	1.13	1.46	0.10	0.77	0.17	1.24	91	118	0.8	small left shoulder, **Peltex at 11607-11706 (650)**
11610	3538.7	70.5	431	0.12	0.92	1.34	0.11	0.69	0.15	0.99	93	135	0.9	small left shoulder, **Peltex at 11607-11706 (650)**
11640	3547.9	70.9	428	0.12	1.03	1.84	0.10	0.56	0.18	1.25	82	147	0.9	small left shoulder, **Peltex at 11607-11706 (650)**
11670	3557.0	70.6	428	0.17	1.06	1.42	0.14	0.75	0.16	1.15	92	123	0.7	left shoulder, **Peltex at 11607-11706 (650)**
11700	3566.2	70.0	414	0.33	1.95	1.04	0.14	1.88	0.24	1.22	160	85	0.7	large left shoulder on S2, **Peltex at 11607-11706 (650)**

Depth ft	m	Qty	Tmax	S1	S2	S3	PI	S2/S3	PC(%)	TOC(%)	HI	OI	MINC	Comments
11730	3575.3	70.8	413	0.11	1.07	0.94	0.09	1.14	0.14	1.06	101	89	0.9	broad asymmetric S2, **Peltex at 11706-11770 (650)**
11760	3584.4	70.4	433	0.12	1.00	1.17	0.11	0.85	0.15	1.12	89	104	0.8	left shoulder on S2, **Peltex at 11706-11770 (650)**
11790	3593.6	70.4	432	0.25	1.10	2.81	0.18	0.39	0.23	0.98	112	287	2.0	large left shoulder on S2
11810	3599.7	70.5	433	0.12	1.16	0.48	0.10	2.42	0.13	1.13	103	42	0.45	**core**
11830	3605.8	70.5	409	3.01	8.69	5.40	0.26	1.61	1.17	1.99	437	271	3.0	trimodal S2; **oil stain**
11835	3607.3	70.0	435	0.17	1.66	0.28	0.09	5.93	0.17	1.22	136	23	0.29	**core**
11860	3614.9	70.5	402	3.30	7.97	3.82	0.29	2.09	1.10	2.20	362	174	2.1	broad asymm. S2, left/right shoulders, **Peltex at 11855-11907 (150)**
11880	3621.0	70.9	404	4.58	9.98	5.24	0.31	1.90	1.42	2.65	377	198	2.3	broad asymm. bimodal S2, **Peltex at 11855-11907 (150)**
11920	3633.2	70.2	398	1.07	3.37	7.40	0.24	0.46	0.63	1.79	188	413	1.8	trimodal S2
11970	3648.5	70.1	337	0.79	2.51	7.22	0.24	0.35	0.51	1.62	155	446	1.1	asymmetric multi-modal S1 & S2
12010	3660.6	70.8	301	0.46	1.63	8.50	0.22	0.19	0.45	1.46	112	582	0.9	trimodal S2
12060	3675.9	70.8	332	0.69	1.93	4.57	0.26	0.42	0.37	1.51	128	303	0.8	broad asymmetric bimodal S2
12120	3694.2	70.3	426	0.39	1.70	3.79	0.19	0.45	0.31	1.50	113	253	0.7	broad asymmetric bimodal S2
12150	3703.3	70.9	422	0.76	1.87	2.68	0.29	0.70	0.32	1.41	133	190	0.6	broad asymmetric bimodal S2
12180	3712.5	70.9	426	0.34	0.97	2.36	0.26	0.41	0.19	1.33	73	177	0.5	large left shoulder on asymmetric S2
12210	3721.6	70.1	429	0.22	0.59	1.43	0.27	0.41	0.13	1.18	50	121	0.5	large left shoulder, asymm. S2, **Peltex at 12186-12232 (250)**
12240	3730.8	70.0	434	0.36	0.81	1.28	0.31	0.63	0.16	1.21	67	106	0.4	large left shoulder, asymm. S2, **Peltex at 12232-12281 (50)**
12270	3739.9	70.9	433	0.10	0.33	1.26	0.24	0.26	0.09	0.97	34	130	0.4	small left shoulder on S2, **Peltex at 12232-12281 (50)**
12300	3749.0	70.3	434	0.15	0.53	1.53	0.22	0.35	0.11	0.96	55	159	0.6	small left shoulder on S2
12330	3758.2	70.2	421	0.09	0.38	1.21	0.20	0.31	0.09	0.84	45	144	0.5	asymmetric S2, **Peltex at 12317-12366 (250)**
12360	3767.3	70.7	443	0.17	0.53	1.39	0.25	0.38	0.11	0.90	59	154	0.5	left shoulder on S2, **Peltex at 12317-12366 (250)**
12390	3776.5	70.2	319	0.42	1.65	2.44	0.20	0.68	0.26	1.28	129	191	0.5	broad asymm. bimodal S2, **Peltex at 12366-12415 (350)**
12420	3785.6	70.7	424	0.23	0.82	1.83	0.22	0.45	0.15	1.03	80	178	0.5	broad asymmetric bimodal S2
12450	3794.8	70.8	450	0.26	1.22	2.09	0.18	0.58	0.21	1.34	91	156	0.5	left shoulder on S2
12480	3803.9	70.8	426	0.09	0.28	1.48	0.25	0.19	0.09	1.04	27	142	0.5	broad S2 with left shoulder
12540	3822.2	70.8	429	0.12	0.44	1.01	0.21	0.44	0.09	1.09	40	93	0.4	small left shoulder on S2
12570	3831.3	70.5	433	0.07	0.35	0.94	0.16	0.37	0.08	0.91	38	103	0.4	**Peltex at 12570-12575 (800)**
12600	3840.5	70.4	427	0.19	0.48	0.61	0.28	0.79	0.09	1.01	48	60	0.4	left shoulder, **Peltex at 12593-12610 (500)**
12630	3849.6	70.9	431	0.09	0.36	1.00	0.19	0.36	0.08	0.75	48	133	0.5	**Peltex at 12610-12640 (200)**
12660	3858.8	70.4	424	0.14	0.56	0.73	0.20	0.77	0.09	1.11	50	66	0.5	**Peltex at 12656-12685 (150)**
12690	3867.9	70.7	427	0.14	0.53	0.64	0.21	0.83	0.09	1.09	49	59	0.5	small left shoulder, **Peltex at 12685-12739 (750)**
12720	3877.1	70.6	432	0.13	0.39	1.09	0.24	0.36	0.09	0.92	42	118	0.5	**Peltex at 12685-12739 (750)**
12750	3886.2	70.2	425	0.11	0.48	1.31	0.18	0.37	0.10	0.92	52	142	0.5	asymmetric S2, **Peltex at 12739-12792 (300)**
12790	3898.4	70.0	432	0.17	0.63	1.69	0.21	0.37	0.13	1.03	61	164	0.6	left shoulder, **Peltex at 12739-12792 (300)**
12810	3904.5	70.6	435	0.10	0.55	1.79	0.16	0.31	0.12	0.99	56	181	0.6	**Peltex at 12792-12846 (450)**
12840	3913.6	70.4	423	0.11	0.61	1.83	0.16	0.33	0.13	0.97	63	189	0.6	asymm. S2, **Peltex at 12792-12846 (450)**
12870	3922.8	70.4	433	0.13	0.53	1.63	0.19	0.33	0.12	0.92	58	177	0.5	broad left skewed S2, **Peltex at 12846-12889 (200)**
12900	3931.9	70.9	422	0.29	5.35	9.72	0.05	0.55	0.85	6.83	78	142	0.8	broad left skewed S2, **Peltex at 12889-12923 (200)**
12930	3941.1	70.9	423	0.30	5.32	12.20	0.05	0.44	0.94	7.58	70	161	0.9	**Peltex at 12923-12970 (200); oil stain**
12960	3950.2	70.7	432	0.16	0.64	1.66	0.20	0.39	0.13	1.23	52	135	0.5	**Peltex at 12923-12970 (200)**

Depth ft	m	Qty	Tmax	S1	S2	S3	PI	S2/S3	PC(%)	TOC(%)	HI	OI	MINC	Comments
12990	3959.4	70.1	429	0.18	0.80	1.86	0.19	0.43	0.16	1.32	61	141	0.6	**Peltex at 12980-13010 (150)**
13020	3968.5	70.4	432	0.10	0.44	0.74	0.19	0.59	0.08	0.98	45	76	0.6	**Peltex at 13010-13059 (550)**
13050	3977.6	70.5	432	0.09	0.40	0.94	0.18	0.43	0.08	0.94	43	100	0.6	**Peltex at 13010-13059 (550)**
13080	3986.8	70.9	435	0.09	0.38	1.28	0.19	0.30	0.09	0.96	40	133	0.5	small left peak on S2, **Peltex at 13059-13111 (350)**
13110	3995.9	71.3	437	0.07	0.37	0.88	0.15	0.42	0.07	0.89	42	99	0.5	**Peltex at 13059-13111 (350)**
13140	4005.1	70.2	429	0.25	0.98	1.76	0.20	0.56	0.17	0.99	99	178	0.5	large left shoulder, asymm. S2, **Peltex at 13111-13153 (500)**
13200	4023.4	71.0	432	0.08	0.41	1.48	0.16	0.28	0.11	1.00	41	148	0.5	small left S2 peak, **Peltex at 13185-13218 (950), 13218-224(2800)**
13230	4032.5	70.4	410	3.49	9.57	3.39	0.27	2.82	1.26	2.25	425	151	1.9	highly asymm., odd shaped bimodal S2, **Peltex at 13227-13257 (50)**
13260	4041.6	70.3	414	0.73	2.45	3.68	0.23	0.67	0.42	1.41	174	261	1.4	broad asymmetric bimodal S2
13290	4050.8	71.0	417	0.27	1.74	2.42	0.13	0.72	0.27	1.27	137	191	0.9	large left shoulder, asymm. S2, **Peltex at 13289-13319 (200)**
13320	4059.9	70.3	432	0.24	0.86	2.14	0.22	0.40	0.18	1.09	79	196	0.8	left shoulder on S2
13350	4069.1	70.6	438	0.12	0.60	2.59	0.17	0.23	0.15	0.95	63	273	0.7	left shoulder on S2, **Peltex at 13347-13375 (50)**
13380	4078.2	70.0	442	0.11	0.62	2.13	0.15	0.29	0.14	1.00	62	213	0.7	
13440	4096.5	70.9	421	0.34	0.86	3.04	0.28	0.28	0.20	0.94	91	323	0.6	broad asymm. bimodal S2, **Peltex at 13436-13468 (100)**
13470	4105.7	70.4	391	2.62	5.46	2.37	0.32	2.30	0.76	1.84	297	129	0.8	large left shoulder, asymm. S2, **Peltex at 13468-13491 (300)**
13500	4114.8	70.7	439	0.13	0.56	1.66	0.19	0.34	0.12	0.98	57	169	0.6	
13530	4123.9	70.3	440	0.12	0.58	1.55	0.17	0.37	0.12	0.92	63	168	0.6	**Peltex at 13520-13552 (100)**
13560	4133.1	70.5	426	0.34	1.54	1.39	0.18	1.11	0.21	1.11	139	125	0.6	broad S2, left shoulder, **Peltex at 13552-13572 (100)**
Ave			422.5											all values (107)
SD			21.9											
Ave			**431.0**											selected values (49 points)
SD			**3.7**											

Table 2. Parsons N-10 Rock-Eval 6 data (Rock-Eval 2 format).

- acceptable pyrogram
- dominated by recycled organic matter
- anomalous pyrogram
- %Ro analysis

Depth ft	m	Qty	Tmax	S1	S2	S3	PI	S2/S3	PC(%)	TOC(%)	HI	OI	MINC	Comments
									Iperk Sequence					
100	30.5	70.7	437	0.16	1.87	3.84	0.08	0.49	0.32	1.34	140	287	2.1	left shoulder on S2, recycled dominant
130	39.6	70.1	436	0.16	2.30	4.11	0.06	0.56	0.38	2.54	91	162	1.1	symmetric, recyled
160	48.8	70.7	433	0.19	2.33	3.80	0.07	0.61	0.39	1.85	126	205	2.3	left shoulder on S2, recycled dominant
190	57.9	70.2	428	0.52	5.33	8.04	0.09	0.66	0.82	5.30	101	152	2.0	large left shoulder, recycled dominant
220	67.1	70.0	426	1.39	10.14	11.21	0.12	0.90	1.45	7.13	142	157	2.0	bimodal S2, recycled dominant
250	76.2	70.2	308	1.52	10.12	16.19	0.13	0.63	1.65	7.86	129	206	2.5	bimodal S2, low T peak dominant
280	85.3	70.2	421	2.24	18.78	14.82	0.11	1.27	2.43	9.11	206	163	2.4	bimodal S2, high T peak dominant
310	94.5	69.8	323	4.06	27.69	35.51	0.13	0.78	4.17	17.87	155	199	2.2	asymmetric S2, right shoulder
340	103.6	50.3	325	5.50	30.18	34.66	0.15	0.87	4.52	17.78	170	195	2.1	asymmetric S2, right shoulder
370	112.8	50.3	324	5.35	31.36	34.87	0.15	0.90	4.60	18.06	174	193	2.2	asymmetric S2, right shoulder
400	121.9	70.8	423	0.21	2.79	3.08	0.07	0.91	0.38	2.03	137	152	0.5	bimodal S2, high T peak dominant
430	131.1	70.9	319	0.30	2.64	3.74	0.10	0.71	0.42	2.05	129	182	1.1	bimodal S2, low T peak dominant
460	140.2	70.4	419	0.04	0.19	0.75	0.19	0.25	0.05	0.28	68	268	0.3	asymmetric S2, left shoulder
490	149.4	70.7	425	0.06	0.12	0.30	0.34	0.40	0.03	0.19	63	158	0.2	low S2 peak, small left shoulder
520	158.5	70.2	408	0.45	6.68	7.63	0.06	0.88	0.95	5.97	112	128	0.8	asymmetric S2, left shoulder
550	167.6	70.6	393	1.12	13.35	13.91	0.08	0.96	1.90	11.78	113	118	1.2	broad asymmetric S2
580	176.8	70.2	417	0.29	5.07	7.41	0.05	0.68	0.78	5.50	92	135	1.5	asymmetric broad S2
610	185.9	70.5	425	0.11	1.46	4.22	0.07	0.35	0.32	2.62	56	161	1.0	asymmetric S2
640	195.1	70.5	414	0.09	2.83	5.78	0.03	0.49	0.51	4.20	67	138	1.1	asymmetric broad S2
670	204.2	70.3	402	0.81	15.88	16.13	0.05	0.98	2.22	15.49	103	104	0.9	broad asymmetric S2
Ave			395.3											all values (20)
SD			46.1											
Ave			**418.7**											selected values (3)
SD			**5.7**											
									Aklak Sequence					
700	213.4	70.4	418	1.11	21.65	19.49	0.05	1.11	2.80	17.14	126	114	1.2	asymmetric broad S2
800	243.8	70.5	426	0.27	7.15	6.78	0.04	1.05	0.92	5.66	126	120	0.8	
830	253.0	70.4	425	0.07	1.65	4.12	0.04	0.40	0.38	2.01	82	205	2.1	
870	265.2	70.5	434	0.09	1.96	4.29	0.05	0.46	0.33	2.32	84	185	0.6	symmetric S2, recycled
900	274.3	70.6	437	0.19	1.63	5.56	0.11	0.29	0.37	2.24	73	248	1.5	asymmetric S2, large left shoulder
930	283.5	70.5	429	0.20	1.98	3.32	0.09	0.60	0.33	2.16	92	154	0.2	
960	292.6	50.0	369	0.73	12.97	29.58	0.05	0.44	2.52	23.10	56	128	1.1	asymmetric S2, right skewed
990	301.8	70.2	425	0.29	4.48	9.04	0.06	0.50	0.78	6.60	68	137	0.5	asymmetric S2
1020	310.9	70.2	429	0.19	1.45	4.25	0.11	0.34	0.31	2.47	59	172	0.3	asymmetric S2, left shoulder
1050	320.0	70.0	427	0.27	2.11	7.30	0.11	0.29	0.50	4.46	47	164	0.6	asymmetric S2, left shoulder
1080	329.2	70.3	429	0.14	1.17	5.51	0.11	0.21	0.31	2.26	52	244	0.6	asymmetric S2, left shoulder
1110	338.3	50.4	394	3.29	57.96	58.19	0.05	1.00	7.55	44.76	129	130	2.0	broad asymmetric S2
1110	338.3	20.7	396	4.18	56.78	56.80	0.07	1.00	7.53	44.25	128	128	2.2	broad asymmetric S2
1140	347.5	70.3	421	0.34	5.39	8.60	0.06	0.63	0.82	5.92	91	145	0.5	
1170	356.6	70.0	428	0.18	3.78	8.89	0.05	0.43	0.69	5.88	64	151	0.6	
1200	365.8	70.7	416	0.36	4.17	7.85	0.08	0.53	0.73	5.35	78	147	0.5	bimodal S2, high T peak dominant
1230	374.9	70.2	427	0.23	3.82	8.24	0.06	0.46	0.68	5.40	71	153	1.0	
1260	384.0	70.4	435	0.12	1.09	4.17	0.10	0.26	0.25	2.07	53	201	0.6	asymmetric S2, left shoulder
1290	393.2	70.7	431	0.14	0.75	3.23	0.15	0.23	0.19	1.48	51	218	0.4	asymmetric S2, large left shoulder
1320	402.3	70.8	426	0.65	2.82	3.62	0.19	0.78	0.44	2.58	109	140	0.3	asymmetric S2, large left shoulder
1350	411.5	70.6	429	0.59	2.11	3.27	0.22	0.65	0.34	1.76	120	186	0.2	bimodal S2, high T peak dominant
1380	420.6	70.6	431	0.16	1.42	6.07	0.10	0.23	0.36	2.88	49	211	1.3	asymmetric S2, left shoulder
1410	429.8	70.2	432	0.22	1.39	4.27	0.13	0.33	0.29	2.05	68	208	0.5	asymmetric S2, large left shoulder
1440	438.9	70.6	430	0.18	1.84	3.93	0.09	0.47	0.32	2.34	79	168	0.7	asymmetric S2, left shoulder
1470	448.1	70.5	431	0.21	1.31	3.06	0.14	0.43	0.25	1.76	74	174	0.3	asymmetric S2, large left shoulder
1500	457.2	70.5	433	0.15	0.98	1.34	0.13	0.73	0.16	1.63	60	82	0.3	asymmetric S2, left shoulder
1530	466.3	70.0	429	0.65	4.66	5.37	0.12	0.87	0.65	3.47	134	155	0.4	asymmetric S2
1560	475.5	70.5	424	0.30	6.76	10.17	0.04	0.66	1.00	7.25	93	140	0.6	
1590	484.6	70.4	427	0.19	5.95	12.25	0.03	0.49	1.03	9.05	66	135	0.8	
1620	493.8	70.3	428	0.10	1.04	4.31	0.09	0.24	0.26	2.02	51	213	0.3	asymmetric S2
1650	502.9	70.9	403	0.17	1.30	4.72	0.12	0.28	0.36	3.10	42	152	0.4	broad asymmetric S2
1680	512.1	70.2	432	0.08	0.87	2.98	0.09	0.29	0.19	1.55	56	192	1.6	asymmetric S2, left shoulder
1710	521.2	70.6	427	0.25	4.23	6.59	0.06	0.64	0.65	4.86	87	136	0.7	
1740	530.4	70.6	430	0.18	2.18	4.69	0.08	0.46	0.38	3.05	71	154	0.4	
1770	539.5	70.9	431	0.06	0.43	2.20	0.13	0.20	0.12	0.97	44	227	0.3	asymmetric S2, large left shoulder
1800	548.6	70.2	431	0.33	2.24	4.07	0.13	0.55	0.36	2.44	92	167	0.4	asymmetric S2, left shoulder

ft	m	Qty	Tmax	S1	S2	S3	PI	S2/S3	PC(%)	TOC(%)	HI	OI	MINC	Comments
1830	557.8	70.6	432	0.31	2.51	6.11	0.11	0.41	0.45	2.57	98	238	0.8	asymmetric S2, left shoulder
1860	566.9	70.8	427	0.17	1.19	4.01	0.13	0.30	0.26	1.67	71	240	1.9	broad asymmetric S2
1890	576.1	70.1	423	0.68	9.57	15.97	0.07	0.60	1.51	11.94	80	134	0.9	
1920	585.2	70.9	427	0.24	1.95	5.91	0.11	0.33	0.41	2.80	70	211	0.6	asymmetric S2, large left shoulder
1950	594.4	71.0	436	0.09	0.53	2.10	0.15	0.25	0.13	1.01	52	208	0.6	bimodal S2, high T peak dominant
1980	603.5	70.6	428	0.28	1.73	5.93	0.14	0.29	0.40	3.58	48	166	0.7	asymmetric S2, large left shoulder
2010	612.6	70.4	428	2.09	3.74	2.33	0.36	1.61	0.59	2.13	176	109	0.3	bimodal S2, high T peak dominant
2040	621.8	70.0	428	0.33	1.16	3.41	0.22	0.34	0.24	1.24	94	275	0.4	bimodal S2, high T peak dominant
2070	630.9	70.9	430	0.97	4.05	4.57	0.19	0.89	0.59	2.75	147	166	0.4	bimodal S2, high T peak dominant
2100	640.1	70.5	423	0.39	9.64	11.14	0.04	0.87	1.32	9.44	102	118	0.5	
2130	649.2	70.3	427	0.39	2.99	5.27	0.12	0.57	0.48	2.99	100	176	0.4	asymmetric S2, left shoulder
2180	664.5	70.5	420	0.48	2.00	4.23	0.19	0.47	0.36	2.11	95	200	0.3	asymmetric S2, left shoulder
2210	673.6	70.3	430	0.21	0.68	2.77	0.23	0.25	0.16	1.12	61	247	0.2	bimodal S2, high T peak dominant
2270	691.9	70.2	434	0.34	1.45	3.40	0.19	0.43	0.26	1.65	88	206	0.3	bimodal S2, high T peak dominant
2300	701.0	70.8	427	0.99	2.92	3.31	0.25	0.88	0.45	2.56	114	129	0.3	bimodal S2, high T peak dominant
2330	710.2	70.3	315	0.47	1.02	1.55	0.32	0.66	0.19	1.09	94	142	0.2	bimodal S2, low T peak dominant
2360	719.3	70.3	308	0.61	1.09	1.60	0.36	0.68	0.21	1.13	96	142	0.3	bimodal S2, low T peak dominant
2390	728.5	70.4	430	1.03	1.62	1.78	0.39	0.91	0.28	1.38	117	129	0.3	bimodal S2, high T peak dominant
2430	740.7	70.4	428	0.85	1.67	1.98	0.34	0.84	0.29	1.53	109	129	0.3	bimodal S2, high T peak dominant
2460	749.8	70.4	430	0.71	1.75	2.58	0.29	0.68	0.29	1.64	107	157	0.5	bimodal S2, high T peak dominant
2490	759.0	70.3	431	0.14	0.40	1.42	0.25	0.28	0.09	0.96	42	148	0.4	bimodal S2, high T peak dominant
2540	774.2	70.1	425	1.19	7.27	9.67	0.14	0.75	1.12	8.30	88	117	0.7	
2570	783.3	70.7	426	0.41	2.90	5.91	0.12	0.49	0.53	4.91	59	120	0.5	
2600	792.5	70.5	427	0.74	2.50	2.87	0.23	0.87	0.39	2.62	95	110	0.4	asymmetric S2, large left shoulder
2640	804.7	70.7	427	0.20	1.42	2.75	0.12	0.52	0.25	2.05	69	134	0.4	asymmetric S2, small left shoulder
2670	813.8	70.2	424	0.40	1.99	3.82	0.17	0.52	0.37	3.35	59	114	0.3	asymmetric S2, small left shoulder
2700	823.0	70.7	426	1.48	3.54	3.42	0.30	1.04	0.57	3.28	108	104	0.3	bimodal S2, high T peak dominant
2740	835.2	70.2	428	2.12	2.18	1.82	0.49	1.20	0.43	1.64	133	111	0.3	bimodal S2, high T peak dominant
2770	844.3	70.3	429	0.45	1.46	3.04	0.23	0.48	0.28	2.08	70	146	0.6	bimodal S2, high T peak dominant
2800	853.4	70.5	429	0.80	3.65	5.37	0.18	0.68	0.60	4.38	83	123	0.3	asymmetric S2, large left shoulder
2840	865.6	70.4	429	0.78	3.19	4.29	0.20	0.74	0.49	2.92	109	147	0.3	asymmetric S2, large left shoulder
2870	874.8	70.7	426	1.09	3.55	4.26	0.24	0.83	0.57	3.10	115	137	0.3	asymmetric S2, large left shoulder
2900	883.9	70.4	430	0.10	1.07	7.26	0.08	0.15	0.33	2.20	49	330	0.6	asymmetric irregular S2
2930	893.1	70.4	436	0.46	1.77	3.04	0.21	0.58	0.31	2.24	79	136	0.6	bimodal S2, high T peak dominant
2960	902.2	70.5	434	0.14	1.48	2.95	0.09	0.50	0.26	2.21	67	133	0.6	asymmetric S2, small left shoulder
2990	911.4	70.7	431	0.14	2.40	6.38	0.06	0.38	0.48	4.66	52	137	0.6	
3020	920.5	70.8	426	0.55	2.47	4.83	0.18	0.51	0.45	3.91	63	124	0.4	asymmetric S2, large left shoulder
3050	929.6	70.8	422	1.59	3.96	4.67	0.29	0.85	0.67	4.35	91	107	0.4	bimodal S2, high T peak dominant
3080	938.8	70.9	431	1.00	2.12	2.97	0.32	0.71	0.38	2.67	79	111	0.4	bimodal S2, high T peak dominant
3110	947.9	70.0	423	1.32	6.35	6.44	0.17	0.99	0.93	6.75	94	95	0.5	asymmetric S2, small left shoulder
3140	957.1	70.4	417	1.29	17.68	15.24	0.07	1.16	2.32	16.54	107	92	1.1	
3170	966.2	70.1	431	0.21	2.23	3.80	0.09	0.59	0.36	3.08	72	123	2.1	asymmetric S2, small left shoulder
3200	975.4	70.3	431	0.19	0.82	1.61	0.18	0.51	0.15	1.30	63	124	0.3	bimodal S2, high T peak dominant
3230	984.5	70.9	319	3.81	4.14	1.75	0.48	2.37	0.73	1.93	215	91	0.5	bimodal S2, low T peak dominant
3260	993.6	70.7	296	1.55	1.60	2.65	0.49	0.60	0.36	1.58	101	168	0.4	bimodal S2, low T peak dominant
3290	1002.8	70.1	297	1.95	1.85	3.32	0.51	0.56	0.42	1.39	133	239	0.4	bimodal S2, low T peak dominant
3320	1011.9	70.7	300	3.15	2.88	1.69	0.52	1.70	0.56	1.75	165	97	0.4	bimodal S2, low T peak dominant
3350	1021.1	70.7	427	0.83	1.26	3.27	0.40	0.39	0.29	1.38	91	237	0.5	bimodal S2, high T peak dominant
3380	1030.2	70.5	296	0.85	0.97	1.29	0.47	0.75	0.20	1.06	92	122	0.4	bimodal S2, low T peak dominant
3440	1048.5	70.9	426	1.64	2.15	3.61	0.43	0.60	0.44	1.51	142	239	1.2	bimodal S2, high T peak dominant
3470	1057.7	70.7	298	0.32	0.63	1.63	0.34	0.39	0.15	0.90	70	181	1.6	bimodal S2, low T peak dominant
3500	1066.8	70.4	431	0.10	0.57	2.63	0.14	0.22	0.14	0.94	61	280	0.8	asymmetric S2, large left shoulder
3530	1075.9	70.5	428	0.17	0.60	0.00	0.22	0.00	0.07	0.82	73	0	1.6	bimodal S2, high T peak dominant
3560	1085.1	70.4	432	0.07	0.42	1.59	0.14	0.26	0.10	0.75	56	212	0.5	asymmetric S2, large left shoulder
3590	1094.2	70.7	428	0.17	0.93	2.01	0.16	0.46	0.17	1.44	65	140	0.5	asymmetric S2, large left shoulder
3620	1103.4	70.2	417	1.03	29.82	24.55	0.03	1.21	3.70	25.21	118	97	2.5	
3620	1103.4	20.2	417	1.07	30.49	30.94	0.03	0.99	4.04	26.47	115	117	1.4	
3650	1112.5	70.4	426	0.20	6.36	6.65	0.03	0.96	0.85	6.97	91	95	0.6	
3680	1121.7	70.1	432	0.18	2.14	3.65	0.08	0.59	0.34	2.77	77	132	1.1	asymmetric S2, small left shoulder
3710	1130.8	70.7	297	0.55	1.20	2.67	0.31	0.45	0.25	1.62	74	165	1.1	bimodal S2, low T peak dominant
3740	1140.0	70.2	424	0.95	17.80	16.07	0.05	1.11	2.30	17.29	103	93	0.8	
3740	1140.0	20.4	423	1.00	19.05	23.02	0.05	0.83	2.68	18.88	101	122	1.0	
3770	1149.1	70.3	398	0.44	2.01	2.43	0.18	0.83	0.30	1.89	106	129	0.5	irregular asymmetric S2, large left shoulder
3800	1158.2	70.5	430	0.16	0.95	2.00	0.15	0.48	0.17	1.30	73	154	0.9	asymmetric S2, large left shoulder
3830	1167.4	70.7	425	0.67	1.35	2.15	0.33	0.63	0.26	1.77	76	121	0.5	bimodal S2, high T peak dominant
3860	1176.5	70.5	428	1.52	2.41	2.46	0.39	0.98	0.42	1.73	139	142	0.6	bimodal irregular S2, high T peak dominant
3890	1185.7	71.0	408	0.78	1.33	1.94	0.37	0.69	0.26	1.49	89	130	1.4	broad irregular S2, large left shoulder
3930	1197.9	70.4	435	0.57	1.87	4.75	0.23	0.39	0.37	0.85	220	559	2.7	broad irregular S2, large left shoulder
3960	1207.0	70.5	423	0.70	3.35	6.15	0.17	0.54	0.58	1.95	172	315	3.3	asymmetric S2, large left shoulder
3990	1216.2	70.4	419	0.83	2.65	4.36	0.24	0.61	0.47	1.63	163	267	2.5	broad irregular S2, large left shoulder
4020	1225.3	70.1	389	0.90	1.80	4.66	0.33	0.39	0.39	0.90	200	518	3.1	broad mesa-shaped S2

ft	m	Qty	Tmax	S1	S2	S3	PI	S2/S3	PC(%)	TOC(%)	HI	OI	MINC	Comments
4050	1234.4	70.6	408	1.64	3.33	3.27	0.33	1.02	0.53	1.72	194	190	1.3	asymmetric S2, large left shoulder
4080	1243.6	70.0	377	0.47	1.77	3.34	0.21	0.53	0.30	1.01	175	331	1.6	broad mesa-shaped S2
4110	1252.7	70.3	419	0.44	1.71	2.66	0.21	0.64	0.28	1.49	115	179	1.3	broad asymmetric S2, large left shoulder
4140	1261.9	70.8	403	0.40	1.80	2.94	0.18	0.61	0.29	1.50	120	196	0.9	broad mesa-shaped S2
4200	1280.2	70.5	402	0.49	1.00	3.56	0.33	0.28	0.24	0.82	122	434	3.2	broad mesa-shaped S2
4230	1289.3	70.3	424	1.93	4.08	4.71	0.32	0.87	0.69	3.92	104	120	1.0	broad asymmetric S2, large left shoulder
4260	1298.4	70.5	425	0.93	2.03	4.60	0.31	0.44	0.42	1.94	105	237	1.6	broad asymmetric S2, large left shoulder
4290	1307.6	70.5	317	2.46	2.89	4.85	0.46	0.60	0.61	1.59	182	305	3.1	broad mesa-shaped S2
4320	1316.7	70.3	414	3.08	4.06	2.64	0.43	1.54	0.70	2.46	165	107	0.7	broad asymmetric S2, large left shoulder
4350	1325.9	70.2	427	2.10	3.50	4.91	0.38	0.71	0.68	4.14	85	119	0.9	broad asymmetric S2, large left shoulder
4380	1335.0	70.1	423	0.60	1.24	2.05	0.33	0.60	0.24	1.62	77	127	1.0	broad asymmetric S2, large left shoulder
4410	1344.2	70.5	423	0.43	1.07	2.59	0.28	0.41	0.22	1.59	67	163	1.1	broad asymmetric S2, large left shoulder
4440	1353.3	70.3	416	0.81	2.12	3.68	0.28	0.58	0.38	2.10	101	175	1.0	broad asymmetric S2, large left shoulder
4470	1362.5	70.1	420	0.60	1.67	3.04	0.26	0.55	0.30	2.09	80	145	1.0	broad asymmetric S2, large left shoulder
4500	1371.6	70.5	417	0.82	2.05	3.09	0.29	0.66	0.37	2.34	88	132	1.1	broad asymmetric S2, large left shoulder
4530	1380.7	70.3	434	0.44	1.31	3.30	0.25	0.40	0.28	2.51	52	131	0.7	asymmetric S2, small left shoulder
4560	1389.9	70.3	421	2.40	2.75	3.52	0.47	0.78	0.57	2.92	94	121	0.7	bimodal S2, low T peak dominant
4590	1399.0	70.0	431	0.72	1.54	3.63	0.32	0.42	0.34	2.69	57	135	1.0	bimodal S2, high T peak dominant
4620	1408.2	70.2	426	1.76	2.81	4.35	0.38	0.65	0.57	3.70	76	118	0.7	bimodal S2, high T peak dominant
4650	1417.3	70.2	415	4.24	4.52	3.53	0.48	1.28	0.87	3.23	140	109	0.7	bimodal S2, high T peak dominant
4680	1426.5	70.8	423	1.96	2.46	3.28	0.44	0.75	0.50	2.79	88	118	0.7	bimodal S2, high T peak dominant
4710	1435.6	70.5	403	4.86	4.84	5.32	0.50	0.91	1.01	3.55	136	150	0.9	broad mesa-shaped S2
Ave			425.2											selected values (28)
SD			4.0											
Ave			414.6											all values (129)
SD			33.9											
									Mason River					
5190	1581.9	70.5	386	2.03	4.42	2.56	0.31	1.73	0.67	3.46	128	74	0.5	irregular asymmetric S2, left shoulder
5220	1591.1	70.1	418	2.84	3.72	2.53	0.43	1.47	0.67	3.16	118	80	0.4	broad asymmetric S2, large flat left shoulder
5250	1600.2	70.3	417	1.65	5.06	3.74	0.25	1.35	0.73	4.33	117	86	0.5	asymmetric S2, large left shoulder
5280	1609.3	70.3	427	0.62	2.13	2.27	0.23	0.94	0.34	2.71	79	84	0.4	bimodal S2, high T peak dominant
5310	1618.5	70.3	428	0.73	1.97	2.51	0.27	0.78	0.35	2.72	72	92	0.4	broad asymmetric S2, left shoulder
5340	1627.6	70.3	434	0.25	0.70	1.47	0.26	0.48	0.15	1.46	48	101	0.4	asymmetric S2, small left shoulder
5370	1636.8	70.8	429	0.77	2.40	2.54	0.24	0.94	0.38	2.89	83	88	0.4	asymmetric S2, left shoulder
5430	1655.1	70.4	423	1.08	1.80	1.63	0.38	1.10	0.33	2.05	88	80	0.4	broad asymmetric S2, large flat left shoulder
5460	1664.2	70.5	423	0.61	2.11	2.08	0.22	1.01	0.34	2.48	85	84	0.3	broad asymmetric S2, large left shoulder
5490	1673.4	70.2	425	0.29	0.83	1.51	0.26	0.55	0.16	1.37	61	110	0.4	broad asymmetric S2, large flat left shoulder
5520	1682.5	70.6	410	0.21	0.87	1.20	0.19	0.73	0.17	1.37	64	88	0.4	irregular asymmetric S2, left shoulder
5550	1691.6	70.2	429	0.39	0.91	1.54	0.30	0.59	0.19	1.65	55	93	0.3	broad asymmetric S2, large left shoulder
5580	1700.8	70.8	423	0.90	1.78	2.31	0.34	0.77	0.34	2.46	72	94	0.4	broad asymmetric S2, large flat left shoulder
5610	1709.9	70.5	426	0.50	1.13	1.79	0.31	0.63	0.24	2.06	55	87	0.3	broad asymmetric S2, large left shoulder
5640	1719.1	70.6	417	2.61	2.19	1.51	0.54	1.45	0.47	1.84	119	82	0.5	bimodal S2
5670	1728.2	70.9	427	0.98	1.16	1.24	0.46	0.94	0.24	1.52	76	82	0.4	broad asymmetric S2, large flat left shoulder
5700	1737.4	70.2	416	2.41	2.05	0.69	0.54	2.97	0.41	1.77	116	39	0.4	broad mesa-shaped S2, bimodal
5730	1746.5	70.3	416	2.80	2.42	1.00	0.54	2.42	0.48	1.45	167	69	0.3	broad mesa-shaped S2, bimodal
5910	1801.4	70.4	419	3.58	3.78	1.96	0.49	1.93	0.72	2.99	126	66	0.5	broad asymmetric S2, large flat left shoulder
5940	1810.5	70.7	415	3.64	3.23	1.40	0.53	2.31	0.64	2.31	140	61	0.4	broad mesa-shaped S2, bimodal
6030	1837.9	70.5	411	3.34	3.34	0.81	0.50	4.12	0.61	1.61	207	50	0.3	broad asymmetric S2, mesa-shaped
6060	1847.1	70.8	425	1.02	0.88	0.62	0.54	1.42	0.20	0.94	94	66	0.2	broad asymmetric S2, large flat left shoulder
6090	1856.2	70.3	424	1.24	0.93	0.94	0.57	0.99	0.24	1.01	92	93	0.5	broad asymmetric S2, large flat left shoulder
6120	1865.4	70.1	414	2.20	2.34	0.74	0.48	3.16	0.42	1.37	171	54	0.3	broad asymmetric S2, mesa-shaped
6150	1874.5	70.7	303	12.66	16.19	3.28	0.44	4.94	2.55	3.67	441	89	0.6	multi-modal, broad mesa-shaped S2
Ave			415.4											all values (25)
SD			25.2											
									Smoking Hills Sequence					
6180	1883.7	70.5	422	1.21	1.11	0.75	0.52	1.48	0.23	1.03	108	73	0.4	broad asymmetric S2, large flat left shoulder
6210	1892.8	70.2	419	1.67	1.71	0.67	0.49	2.55	0.32	1.30	132	52	0.4	broad asymmetric S2, large flat left shoulder
6240	1902.0	70.4	428	0.32	0.68	0.64	0.32	1.06	0.12	1.08	63	59	0.2	asymmetric S2, small left shoulder
6270	1911.1	70.1	427	0.58	0.83	0.58	0.41	1.43	0.15	1.02	81	57	0.3	asymmetric S2, small left shoulder
6300	1920.2	70.5	423	0.10	0.70	0.97	0.13	0.72	0.15	1.61	43	60	0.3	asymmetric S2, small left shoulder
6330	1929.4	70.4	418	0.63	1.13	1.02	0.36	1.11	0.22	1.86	61	55	0.3	broad asymmetric S2, flat left shoulder
6360	1938.5	70.5	410	0.85	1.43	1.10	0.37	1.30	0.29	2.16	66	51	0.3	irregular asymmetric S2, left shoulder
6390	1947.7	71.1	410	0.35	4.86	2.00	0.07	2.43	0.57	3.52	138	57	0.3	
6420	1956.8	70.3	406	0.98	10.96	2.35	0.08	4.66	1.14	4.72	232	50	0.4	
6450	1966.0	70.0	409	2.45	4.70	1.44	0.34	3.26	0.70	3.15	149	46	0.4	asymmetric S2, small left shoulder
6510	1984.2	70.2	408	2.69	8.35	1.72	0.24	4.85	1.06	4.39	190	39	0.4	asymmetric S2, small left shoulder
6540	1993.4	70.9	408	0.61	3.56	2.07	0.15	1.72	0.47	2.73	130	76	0.4	asymmetric S2, small left shoulder
6570	2002.5	70.2	409	1.01	3.70	1.27	0.22	2.91	0.49	2.66	139	48	0.3	asymmetric S2, small left shoulder
6600	2011.7	70.2	406	3.50	3.63	1.05	0.49	3.46	0.67	2.57	141	41	0.4	broad asymmetric S2, large flat left shoulder
Ave			414.5											all values (14)

ft	m	Qty	Tmax	S1	S2	S3	PI	S2/S3	PC(%)	TOC(%)	HI	OI	MINC	Comments
SD			8.0											
							Boundary Creek Sequence							
6630	2020.8	70.5	406	1.07	5.01	1.71	0.18	2.93	0.62	2.85	176	60	0.4	asymmetric S2 peak, small left shoulder
6660	2030.0	70.7	411	1.81	3.07	1.03	0.37	2.98	0.48	2.51	122	41	0.4	asymmetric S2, small left shoulder
6690	2039.1	70.5	414	0.68	2.42	1.29	0.22	1.88	0.35	2.37	102	54	0.3	asymmetric S2, small left shoulder
6720	2048.3	70.0	413	1.42	2.46	0.89	0.37	2.76	0.39	2.40	102	37	0.4	asymmetric S2, small left shoulder
6750	2057.4	70.5	412	2.35	3.61	1.40	0.39	2.58	0.59	2.80	129	50	0.4	asymmetric S2, flat left shoulder
6780	2066.5	70.3	413	0.77	1.76	1.13	0.31	1.56	0.29	2.33	76	48	0.3	asymmetric S2, small left shoulder
6810	2075.7	70.3	420	0.56	1.62	1.80	0.25	0.90	0.28	2.82	57	64	0.4	asymmetric S2, small left shoulder
Ave			412.7											all values (7)
SD			4.2											
							Arctic Red Formation							
6840	2084.8	70.2	416	0.54	1.46	0.95	0.27	1.54	0.24	2.16	68	44	0.4	asymmetric S2, two left shoulders
6870	2094.0	70.6	419	0.59	1.38	1.07	0.30	1.29	0.23	2.02	68	53	0.4	asymmetric S2, small left shoulder
6900	2103.1	70.3	422	0.45	0.67	0.87	0.40	0.77	0.15	1.46	46	60	0.4	asymmetric S2, small flat left shoulder
6930	2112.3	70.4	416	3.82	3.75	1.08	0.50	3.47	0.71	2.83	133	38	0.3	broad mesa-shaped S2, bimodal
6960	2121.4	70.3	415	1.38	2.12	0.99	0.40	2.14	0.36	2.16	98	46	0.3	broad asymmetric S2, flat left shoulder
6990	2130.6	70.4	421	2.94	3.15	1.23	0.48	2.56	0.59	2.89	109	43	0.4	broad asymmetric S2, flat left shoulder
7020	2139.7	70.7	418	1.92	2.07	0.87	0.48	2.38	0.41	2.48	83	35	0.3	broad asymmetric S2, flat left shoulder
7050	2148.8	70.6	423	0.86	1.42	0.96	0.38	1.48	0.27	2.14	66	45	0.4	asymmetric S2, small flat left shoulder
7090	2161.0	70.2	422	1.56	1.82	0.83	0.46	2.19	0.34	2.12	86	39	0.3	broad asymmetric S2, flat left shoulder
7120	2170.2	70.2	424	0.54	1.82	1.03	0.23	1.77	0.27	2.49	73	41	0.3	asymmetric S2, small left shoulder
7150	2179.3	70.2	420	2.87	7.40	2.03	0.28	3.65	0.95	2.92	253	70	0.8	asymmetric S2, large flat left shoulder
7180	2188.5	70.4	424	0.52	2.44	1.44	0.18	1.69	0.30	2.53	96	57	0.5	asymmetric S2, flat left shoulder
7210	2197.6	70.3	432	0.14	1.24	1.36	0.10	0.91	0.18	2.25	55	60	0.5	
7240	2206.8	70.7	432	0.09	1.18	1.28	0.07	0.92	0.17	2.00	59	64	0.5	
7270	2215.9	70.8	433	0.07	1.10	0.88	0.06	1.25	0.15	2.20	50	40	0.5	
7300	2225.0	70.3	435	0.09	1.12	1.36	0.07	0.82	0.16	2.21	51	62	0.5	
7330	2234.2	70.6	433	0.06	1.08	1.26	0.05	0.86	0.16	2.12	51	59	0.6	
7360	2243.3	70.1	431	0.06	1.06	1.42	0.05	0.75	0.16	2.23	48	64	0.6	
7390	2252.5	70.5	433	0.08	1.18	1.27	0.06	0.93	0.17	2.24	53	57	0.5	
7420	2261.6	70.6	432	0.09	1.14	1.30	0.07	0.88	0.17	2.06	55	63	0.6	
7450	2270.8	70.9	433	0.10	1.20	1.31	0.08	0.92	0.17	2.04	59	64	0.6	
7480	2279.9	70.8	433	0.17	1.26	1.16	0.12	1.09	0.18	1.92	66	60	0.5	asymmetric S2, small left peak
7510	2289.0	70.3	433	0.08	1.06	1.26	0.07	0.84	0.15	1.97	54	64	0.6	
7540	2298.2	70.8	428	0.08	1.10	1.11	0.07	0.99	0.15	1.85	59	60	0.5	asymmetric S2, small left peak
7570	2307.3	70.5	435	0.07	1.06	1.18	0.06	0.90	0.15	1.93	55	61	0.7	
7600	2316.5	70.6	430	0.07	1.11	1.21	0.06	0.92	0.16	2.05	54	59	0.6	
Ave			426.7											all values (26)
SD			6.8											
Ave			**432.4**											selected values (> 7180 ft) (14)
SD			**1.8**											
							Mount Goodenough Formation							
7630	2325.6	70.2	434	0.07	1.14	1.25	0.06	0.91	0.16	2.18	52	57	0.6	
7660	2334.8	70.5	434	0.08	1.11	1.23	0.07	0.90	0.16	2.03	55	61	0.6	
7690	2343.9	70.1	431	0.09	1.09	1.05	0.07	1.04	0.15	1.88	58	56	0.6	
7720	2353.1	70.4	431	0.09	1.27	0.94	0.07	1.35	0.17	2.13	60	44	0.5	
7750	2362.2	71.0	429	0.08	1.23	1.00	0.06	1.23	0.17	2.14	57	47	0.5	
7780	2371.3	70.3	434	0.08	1.10	1.07	0.07	1.03	0.16	2.06	53	52	1.1	
7810	2380.5	69.8	432	0.09	0.77	1.22	0.10	0.63	0.13	1.43	54	85	0.8	
7840	2389.6	70.1	434	0.06	0.81	1.26	0.07	0.64	0.13	1.77	46	71	0.7	
7870	2398.8	69.9	429	0.08	0.87	0.96	0.08	0.91	0.13	1.70	51	56	0.7	
7900	2407.9	71.2	434	0.09	1.21	1.03	0.07	1.17	0.16	2.02	60	51	0.7	
7930	2417.1	70.6	432	0.10	1.26	1.13	0.07	1.12	0.17	2.11	60	54	0.7	
7960	2426.2	70.4	436	0.07	0.90	0.89	0.07	1.01	0.12	1.58	57	56	3.2	
7990	2435.4	70.3	429	0.08	1.02	1.08	0.07	0.94	0.15	1.69	60	64	1.4	
8020	2444.5	70.7	423	0.10	1.47	1.10	0.06	1.34	0.19	2.27	65	48	0.6	
8050	2453.6	70.7	430	0.08	1.22	1.06	0.06	1.15	0.17	2.04	60	52	0.9	
8080	2462.8	70.4	434	0.11	1.28	0.92	0.08	1.39	0.16	1.96	65	47	0.6	
8110	2471.9	71.0	435	0.08	0.99	0.78	0.07	1.27	0.13	1.63	61	48	0.9	
8140	2481.1	70.5	434	0.10	1.08	0.85	0.08	1.27	0.15	1.83	59	46	0.5	
8170	2490.2	70.8	432	0.10	1.11	0.92	0.09	1.21	0.15	1.75	63	53	1.4	
8200	2499.4	70.1	432	0.11	1.01	0.80	0.10	1.26	0.14	1.87	54	43	0.6	
8230	2508.5	70.9	434	0.10	0.87	0.76	0.10	1.14	0.12	1.48	59	51	0.5	
8260	2517.6	70.3	425	0.10	1.47	0.83	0.07	1.77	0.17	1.81	81	46	0.8	
8290	2526.8	70.9	433	0.08	0.89	0.73	0.09	1.22	0.12	1.68	53	43	0.4	
Ave			**431.8**											normal pyrograms (23)
SD			**3.2**											
							Siku Member							
8320	2535.9	70.6	434	0.10	1.02	0.79	0.09	1.29	0.14	1.77	58	45	0.7	

ft	m	Qty	Tmax	S1	S2	S3	PI	S2/S3	PC(%)	TOC(%)	HI	OI	MINC	Comments
8350	2545.1	70.3	434	0.12	1.09	0.96	0.10	1.14	0.15	1.78	61	54	0.6	
8380	2554.2	70.1	435	0.11	1.04	0.91	0.09	1.14	0.14	1.89	55	48	0.5	
8410	2563.4	70.6	434	0.13	1.14	1.00	0.10	1.14	0.16	2.00	57	50	0.6	
8440	2572.5	71.0	432	0.09	0.92	0.80	0.09	1.15	0.12	1.71	54	47	0.7	
8470	2581.7	70.4	434	0.09	0.88	0.90	0.09	0.98	0.12	1.66	53	54	1.0	
8500	2590.8	70.1	435	0.09	0.84	0.83	0.10	1.01	0.12	1.72	49	48	1.0	
8530	2599.9	70.5	434	0.12	0.80	0.75	0.13	1.07	0.12	1.54	52	49	1.6	
8560	2609.1	70.5	434	0.11	0.72	0.72	0.13	1.00	0.11	1.50	48	48	0.7	
Ave			**434.0**											normal pyrograms (9)
SD			**0.9**											
								Kamik Formation						
8590	2618.2	70.6	433	0.12	0.86	0.73	0.12	1.18	0.12	1.49	58	49	1.0	
8620	2627.4	70.8	426	0.14	1.09	0.54	0.12	2.02	0.14	1.53	71	35	0.5	slightly irregular
8650	2636.5	70.2	433	0.08	0.66	0.58	0.11	1.14	0.09	1.31	50	44	0.6	
8680	2645.7	70.7	436	0.07	0.62	0.67	0.10	0.93	0.10	1.21	51	55	0.7	right skewed
8710	2654.8	70.3	436	0.07	0.66	0.59	0.10	1.12	0.09	1.29	51	46	0.5	right skewed
8740	2664.0	70.4	419	0.13	3.05	0.51	0.04	5.98	0.30	1.49	205	34	0.5	narrow peak
8770	2673.1	70.6	434	0.09	0.86	0.62	0.09	1.39	0.12	1.52	57	41	0.6	right skewed
8800	2682.2	70.7	436	0.09	0.82	0.60	0.10	1.37	0.11	1.46	56	41	0.4	right skewed
8830	2691.4	70.2	436	0.11	0.70	0.58	0.14	1.21	0.10	1.45	48	40	1.4	right skewed
8870	2703.6	70.4	436	0.08	0.58	0.37	0.13	1.57	0.08	1.06	55	35	0.3	right skewed
8900	2712.7	70.5	444	0.11	0.93	0.35	0.11	2.66	0.11	1.48	63	24	0.3	
8930	2721.9	70.7	434	0.10	0.91	0.67	0.10	1.36	0.12	1.57	58	43	1.1	
8960	2731.0	70.7	434	0.13	1.01	0.73	0.11	1.38	0.13	1.55	65	47	0.6	asymmetric S2, small left shoulder
8990	2740.2	70.7	436	0.13	1.34	0.66	0.09	2.03	0.16	1.90	71	35	0.5	
9020	2749.3	70.6	439	0.12	1.54	0.43	0.07	3.58	0.18	1.91	81	23	0.6	
9080	2767.6	70.9	431	0.12	1.30	0.97	0.08	1.34	0.17	1.75	74	55	0.6	
9110	2776.7	70.3	435	0.10	0.86	0.51	0.10	1.69	0.11	1.51	57	34	0.6	
9140	2785.9	71.0	436	0.13	1.11	0.49	0.11	2.27	0.14	1.67	66	29	0.4	
9170	2795.0	70.6	434	0.30	1.53	0.51	0.17	3.00	0.19	1.76	87	29	0.6	asymmetric S2, small left shoulder
9210	2807.2	70.7	433	0.29	1.06	0.55	0.22	1.93	0.14	1.61	66	34	0.5	asymmetric S2, small left peak
9240	2816.4	70.2	433	0.22	3.80	1.09	0.05	3.49	0.40	3.32	114	33	0.7	
9270	2825.5	70.9	425	1.02	17.67	0.67	0.05	26.37	1.65	7.48	236	9	0.2	
Ave			**433.6**											normal pyrograms (22)
SD			**5.0**											
								McGuire Formation						
9300	2834.6	70.7	427	0.46	2.16	0.75	0.18	2.88	0.27	1.70	127	44	0.7	bimodal irregular S2, high T peak dominant
9329	2843.5	70.4	439	0.16	2.70	0.75	0.06	3.60	0.29	1.89	143	40	0.5	**core**
9520	2901.7	70.4	435	0.30	1.64	0.60	0.16	2.73	0.20	1.63	101	37	0.4	
Ave			**437.0**											selected values (2)
SD			**2.8**											
								Husky Formation						
9550	2910.8	70.7	436	0.22	1.52	0.46	0.12	3.30	0.18	1.48	103	31	0.6	
9580	2920.0	70.9	439	0.23	1.72	0.54	0.12	3.19	0.20	1.63	106	33	0.6	
9610	2929.1	70.7	438	0.31	2.02	0.62	0.13	3.26	0.24	2.14	94	29	0.6	
9640	2938.3	70.2	429	3.42	6.21	1.11	0.36	5.59	0.86	2.98	208	37	0.5	asymmetric S2, flat left shoulder
9670	2947.4	70.8	437	0.51	2.07	0.85	0.20	2.44	0.27	2.14	97	40	0.5	asymmetric S2, small flat left shoulder
9700	2956.6	70.4	438	0.10	1.11	0.49	0.08	2.27	0.13	1.41	79	35	0.7	
9730	2965.7	70.2	436	0.14	0.89	0.54	0.13	1.65	0.12	1.18	75	46	0.6	
9760	2974.8	70.7	439	0.10	0.92	0.51	0.10	1.80	0.11	1.15	80	44	0.8	
9790	2984.0	70.4	439	0.08	0.69	0.52	0.10	1.33	0.09	1.03	67	50	0.7	
9820	2993.1	70.2	438	0.10	0.70	0.46	0.13	1.52	0.09	1.02	69	45	0.5	
9850	3002.3	70.7	438	0.13	1.02	0.47	0.11	2.17	0.13	1.36	75	35	0.5	
9880	3011.4	70.5	437	0.10	0.85	0.42	0.11	2.02	0.10	1.13	75	37	0.6	
9910	3020.6	70.3	439	0.11	0.92		0.11			1.26	73		0.5	
9940	3029.7	70.3	439	0.09	0.93	0.38	0.09	2.45	0.11	1.10	85	35	0.6	
9970	3038.9	70.3	439	0.13	1.59	0.44	0.08	3.61	0.17	1.84	86	24	0.5	
10000	3048.0	70.4	441	0.17	1.61	0.64	0.09	2.52	0.18	2.04	79	31	0.6	
10030	3057.1	70.5	440	0.18	1.66	0.68	0.10	2.44	0.19	2.05	81	33	0.5	
10060	3066.3	71.0	441	0.21	2.09	0.53	0.09	3.94	0.23	2.51	83	21	0.4	
10090	3075.4	70.8	439	0.22	2.75	0.55	0.07	5.00	0.29	2.83	97	19	0.4	
Ave			**438.5**											selected values (18)
SD			**1.4**											
Ave			**438.0**											all values (19)
SD			**2.6**											
								Middle Ordovician (Franklin Mountain Fm.)						
10120	3084.6	70.1	440	0.10	0.86	0.32	0.11	2.69	0.10	1.16	74	28	5.1	
10150	3093.7	70.9	438	0.06	0.23	0.19	0.20	1.21	0.03	0.51	45	37	10.1	
10180	3102.9	70.5	437	0.10	0.44	0.42	0.18	1.05	0.06	0.77	57	55	7.9	asymmetric S2, small flat left shoulder
10210	3112.0	70.4	436	0.28	0.75	0.38	0.27	1.97	0.11	1.09	69	35	3.1	asymmetric S2, small flat left shoulder

ft	m	Qty	Tmax	S1	S2	S3	PI	S2/S3	PC(%)	TOC(%)	HI	OI	MINC	Comments
10240	3121.2	70.7	437	0.30	0.44	0.42	0.41	1.05	0.08	0.63	70	67	7.5	asymmetric S2, flat left shoulder
10270	3130.3	70.1	433	0.21	0.33	0.47	0.39	0.70	0.07	0.54	61	87	8.3	asymmetric S2, flat left shoulder
10300	3139.4	70.5	436	0.33	0.69	0.55	0.32	1.25	0.12	0.89	78	62	6.8	asymmetric S2, small flat left shoulder
10330	3148.6	70.5	434	0.20	0.23	0.37	0.46	0.62	0.05	0.31	74	119	10.5	multi-modal, broad S2
10360	3157.7	70.3	441	0.14	0.23	0.25	0.38	0.92	0.04	0.30	77	83	9.3	asymmetric S2, small flat left shoulder
10390	3166.9	70.7	437	0.13	0.14	0.20	0.49	0.70	0.03	0.26	54	77	8.3	asymmetric S2, small flat left shoulder
10420	3176.0	70.2	436	0.11	0.14	0.23	0.44	0.61	0.03	0.24	58	96	9.5	irregular, two left shoulders on S2
10450	3185.2	70.6	439	0.20	0.28	0.33	0.42	0.85	0.06	0.63	44	52	8.2	asymmetric S2, small flat left shoulder
10490	3197.4	70.0	311	5.59	14.94	10.68	0.27	1.40	2.33	6.82	219	157	4.0	irregular, right shoulder, walnut shells
Ave			**439.0**											selected values (2)
SD			**1.4**											
Ave			**427.3**											all values (13)
SD			**35.0**											

Table 3. Kugaluk N-02 Rock-Eval 6 data (Rock-Eval 2 format).

Invert mud - 149-3855 ft; Invermul mud - 3855-4360 ft; Polymer mud - 4360-8045 ft

green	true Tmax?
purple	anomalous pyrogram (Tmax < 400°C); anomalous PI (> 0.2)
orange	anomalous pyrogram (Tmax > 400°C)
yellow	%Ro analysis (vitrinite, bitumen)

Depth ft	Depth m	Qty	Tmax	S1	S2	S3	PI	S2/S3	PC(%)	TOC(%)	HI	OI	MINC	Comment
								Imperial Formation						
818	249.3	70.5	336	0.24	0.61	0.17	0.28	3.59	0.08	0.94	65	18	0.1	bimodal S2, low T peak dominant, 2nd peak ~ 500
851	259.4	70.5	321	0.41	0.88	0.19	0.32	4.63	0.12	0.86	102	22	0.1	bimodal S2, low T peak dominant, 2nd peak ~ 500
884.5	269.6	70.5	315	0.18	0.41	0.23	0.30	1.78	0.06	0.92	45	25	0.1	bimodal S2, low T peak dominant, 2nd peak ~ 500
917	279.5	70.0	301	0.54	0.80	0.20	0.40	4.00	0.12	1.16	69	17	0.1	bimodal S2, low T peak dominant, 2nd peak ~ 500
950	289.6	70.5	330	0.33	0.66	0.20	0.33	3.30	0.09	0.79	84	25	0.1	bimodal S2, low T peak dominant, 2nd peak ~ 500
983	299.6	70.4	327	0.49	0.96	0.12	0.34	8.00	0.13	0.97	99	12	0.2	bimodal S2, low T peak dominant, 2nd peak ~ 500
1016.5	309.8	70.4	329	0.26	0.55	0.30	0.32	1.83	0.08	0.89	62	34	0.1	bimodal S2, low T peak dominant, 2nd peak ~ 500
1049	319.7	70.9	309	0.41	0.63	0.09	0.39	7.00	0.11	0.98	64	9	0.1	bimodal S2, low T peak dominant, 2nd peak ~ 500
1082	329.8	71.0	301	0.58	0.69	0.30	0.46	2.30	0.12	1.04	66	29	0.1	bimodal S2, low T peak dominant, 2nd peak ~ 500
1115.6	340.0	70.7	321	0.64	0.89	0.09	0.42	9.89	0.14	0.85	105	11	0.1	bimodal S2, low T peak dominant, 2nd peak ~ 500
1148	349.9	70.6	318	0.40	0.59	0.18	0.40	3.28	0.09	0.82	72	22	0.1	bimodal S2, low T peak dominant, 2nd peak ~ 500
1181	360.0	70.5	532	0.12	0.26	0.25	0.32	1.04	0.05	1.00	26	25	0.2	bimodal S2, high T peak dominant, 2nd peak ~ 500
1214	370.0	70.4	323	0.43	0.71	0.24	0.38	2.96	0.11	0.78	91	31	0.1	bimodal S2, low T peak dominant, 2nd peak ~ 500
1247	380.1	70.4	300	0.11	0.16	0.25	0.40	0.64	0.03	0.79	20	32	0.3	bimodal S2, low T peak dominant, 2nd peak ~ 500
1280	390.1	70.6	308	0.41	0.52	0.17	0.44	3.06	0.09	0.82	63	21	0.1	bimodal S2, low T peak dominant, 2nd peak ~ 500
1313	400.2	70.5	307	0.36	0.51	0.17	0.42	3.00	0.09	0.79	65	22	0.1	bimodal S2, low T peak dominant, 2nd peak ~ 500
1346	410.3	69.9	309	0.25	0.34	0.15	0.42	2.27	0.06	0.93	37	16	0.2	bimodal S2, low T peak dominant, 2nd peak ~ 500
1379	420.3	70.7	316	0.45	0.67	0.23	0.40	2.91	0.11	1.21	55	19	0.3	bimodal S2, low T peak dominant, 2nd peak ~ 500
1412	430.4	70.2	303	0.87	0.78	0.20	0.53	3.90	0.15	1.16	67	17	0.2	bimodal S2, low T peak dominant, 2nd peak ~ 500
1445	440.4	70.5	309	0.57	0.70	0.24	0.45	2.92	0.12	1.18	59	20	0.3	bimodal S2, low T peak dominant, 2nd peak ~ 500
1478	450.5	71.1	313	0.18	0.33	0.24	0.36	1.38	0.06	0.88	38	27	0.1	bimodal S2, low T peak dominant, 2nd peak ~ 500
1511	460.6	70.3	310	0.29	0.49	0.15	0.37	3.27	0.08	0.86	57	17	0.2	bimodal S2, low T peak dominant, 2nd peak ~ 500
1547	471.5	70.3	301	0.65	0.61	0.13	0.51	4.69	0.12	1.02	60	13	0.2	bimodal S2, low T peak dominant, 2nd peak ~ 500
1580	481.6	70.9	315	0.50	0.59	0.17	0.46	3.47	0.10	0.86	69	20	0.1	bimodal S2, low T peak dominant, 2nd peak ~ 500
1613	491.6	70.0	298	0.27	0.20	0.20	0.58	1.00	0.05	0.90	22	22	0.2	bimodal S2, low T peak dominant, 2nd peak ~ 500
1646	501.7	70.1	310	0.12	0.24	0.18	0.33	1.33	0.04	0.75	32	24	0.1	bimodal S2, low T peak dominant, 2nd peak ~ 500
1679	511.8	70.3	309	0.27	0.45	0.19	0.37	2.37	0.07	0.89	51	21	0.2	bimodal S2, low T peak dominant, 2nd peak ~ 500
1712	521.8	70.2	309	0.36	0.33	0.21	0.53	1.57	0.07	0.92	36	23	0.2	bimodal S2, low T peak dominant, 2nd peak ~ 500
1745	531.9	70.2	325	0.32	0.44	0.18	0.42	2.44	0.07	0.76	58	24	0.1	bimodal S2, low T peak dominant, 2nd peak ~ 500
1778.2	542.0	70.4	310	0.51	0.47	0.23	0.52	2.04	0.09	1.14	41	20	0.3	bimodal S2, low T peak dominant, 2nd peak ~ 500
1811	552.0	70.1	309	0.57	0.53	0.19	0.52	2.79	0.11	0.78	68	24	0.2	bimodal S2, low T peak dominant, 2nd peak ~ 500
1844	562.1	70.2	299	0.30	0.20	0.24	0.60	0.83	0.05	2.16	9	11	0.2	asymmetric S2, right skewed
1877	572.1	70.5	320	0.37	0.51	0.29	0.42	1.76	0.09	1.06	48	27	0.3	bimodal S2, low T peak dominant, 2nd peak ~ 500
1910.2	582.2	70.7	309	0.63	0.60	0.21	0.51	2.86	0.11	1.04	58	20	0.3	asymmetric S2, right skewed
1943	592.2	70.1	303	0.11	0.16	0.19	0.40	0.84	0.03	0.94	17	20	0.2	asymmetric S2, broad flat right shoulder
1976	602.3	70.1	313	0.41	0.41	0.14	0.50	2.93	0.07	0.87	47	16	0.1	bimodal S2, low T peak dominant, 2nd peak ~ 500
2009	612.3	70.5	315	0.45	0.56	0.21	0.44	2.67	0.09	0.86	65	24	0.5	asymmetric S2, broad flat right shoulder
2042	622.4	70.5	311	1.13	0.83	0.21	0.58	3.95	0.18	1.18	70	18	0.2	asymmetric S2, broad flat right shoulder
2075	632.5	70.2	307	0.18	0.29	0.20	0.38	1.45	0.05	0.87	33	23	0.2	bimodal S2, low T peak dominant, 2nd peak ~ 600
2108	642.5	70.7	320	0.80	0.77	0.19	0.51	4.05	0.15	1.09	71	17	0.2	asymmetric S2, broad flat right shoulder
2141	652.6	70.9	300	0.61	0.41	0.20	0.60	2.05	0.09	0.95	43	21	0.3	asymmetric S2, right skewed
2174	662.6	71.0	313	0.52	0.58	0.19	0.47	3.05	0.10	1.08	54	18	0.3	asymmetric S2, right skewed
2207	672.7	70.2	325	0.73	0.59	0.17	0.55	3.47	0.11	0.85	69	20	0.2	asymmetric S2, right skewed
2240	682.8	70.2	299	0.44	0.23	0.20	0.66	1.15	0.06	0.91	25	22	0.2	asymmetric S2, right skewed
2272.5	692.7	70.1	318	0.19	0.38	0.12	0.33	3.17	0.06	1.18	32	10	0.2	bimodal S2, low T peak dominant, 2nd peak ~ 600
2306.4	703.0	70.1	313	0.09	0.16	0.17	0.36	0.94	0.03	0.68	24	25	0.1	bimodal S2, low T peak dominant, 2nd peak ~ 600
2339.4	713.0	70.4	325	0.42	0.51	0.20	0.45	2.55	0.08	0.85	60	24	0.3	asymmetric S2, right skewed
2379	725.1	70.9	315	0.67	0.93	0.16	0.42	5.81	0.14	0.73	127	22	0.1	asymmetric S2, right skewed
2405	733.0	70.2	302	0.21	0.17	0.25	0.56	0.68	0.04	0.80	21	31	0.3	asymmetric S2, right skewed
2438.2	743.2	70.9	311	0.19	0.24	0.17	0.44	1.41	0.05	0.47	51	36	0.1	asymmetric S2, right skewed
2471.4	753.3	70.8	316	0.38	0.57	0.19	0.40	3.00	0.09	0.75	76	25	0.1	asymmetric S2, right skewed
2504.8	763.5	70.8	339	0.63	1.00	0.18	0.39	5.56	0.15	0.94	106	19	0.1	asymmetric S2, right skewed
2537	773.3	70.1	299	0.17	0.20	0.19	0.45	1.05	0.04	3.33	6	6	0.7	asymmetric S2, right skewed
2570.8	783.6	69.9	309	0.43	0.44	0.36	0.50	1.22	0.09	3.66	12	10	0.2	bimodal S2, low T peak dominant, 2nd peak ~ 600
2603	793.4	70.1	297	0.66	0.65	0.16	0.51	4.06	0.12	3.56	18	4	0.3	bimodal S2, low T peak dominant, 2nd peak ~ 600
2636.3	803.5	70.4	307	1.18	0.88	0.34	0.57	2.59	0.20	5.71	15	6	0.1	bimodal S2, low T peak dominant, 2nd peak ~ 600
Ave			**312.3**											anomalous pyrograms (55)
Std			**9.8**											
			532											true maturity? (1)
								Canol Formation						
2674.8	815.3	70.8	298	0.10	0.19	0.30	0.34	0.63	0.04	6.33	3	5	0.2	bimodal S2, low T peak dominant, 2nd peak ~ 600
2707	825.1	70.1	306	0.51	0.56	0.33	0.48	1.70	0.11	5.49	10	6	0.1	bimodal S2, low T peak dominant, 2nd peak ~ 600
2740	835.2	70.6	606	0.12	0.27	0.13	0.31	2.08	0.05	1.23	22	11	0.1	trimodal S2, high T peak dominant
2773	845.2	70.1	318	0.60	0.64	0.28	0.49	2.29	0.12	3.32	19	8	0.2	asymmetric S2, right skewed
2806	855.3	70.7	315	0.50	0.81	0.19	0.38	4.26	0.12	3.94	21	5	0.3	bimodal S2, low T peak dominant, 2nd peak ~ 600
2839	865.3	50.7	296	1.83	1.08	0.41	0.63	2.63	0.28	7.40	15	6	0.3	bimodal S2, low T peak dominant, 2nd peak ~ 600

ft	m	Qty	Tmax	S1	S2	S3	PI	S2/S3	PC(%)	TOC(%)	HI	OI	MINC	Comment
2871.8	875.3	70.2	607	0.21	0.41	0.28	0.34	1.46	0.07	3.20	13	9	0.6	bimodal S2, high T peak dominant
Ave			**306.6**											anomalous pyrograms (5)
Std			**9.8**											
Ave			**606.5**											
Std			**0.7**											true maturity? (2)
Bluefish Member														
2906	885.7	70.1	327	0.15	0.48	0.24	0.24	2.00	0.08	3.98	12	6	0.4	bimodal S2, low T peak dominant, 2nd peak ~ 600
2938.8	895.7	70.0	601	0.04	0.37	0.68	0.10	0.54	0.06	3.27	11	21	4.6	trimodal S2, high T peak dominant
Hume Formation														
2972	905.9	70.2	300	0.22	0.12	0.18	0.66	0.67	0.03	0.38	32	47	11.9	multi-modal, low signal
3005.6	916.1	70.0	334	0.23	0.45	0.35	0.33	1.29	0.07	1.20	38	29	7.2	bimodal S2, low T peak dominant, 2nd peak ~ 600
3038	926.0	70.3	440	0.22	0.65	0.34	0.25	1.91	0.09	0.25	260	136	12.0	unimodal asymmetric S2 with left shoulder
3071	936.0	70.2	313	0.43	0.47	0.42	0.48	1.12	0.10	0.15	313	280	3.3	broad asymmetric S2, right skewed
3104	946.1	70.5	350	0.17	0.27	0.59	0.39	0.46	0.05	0.17	159	347	3.0	broad asymmetric S2, right skewed
Ave			**324.3**											anomalous pyrograms - mode 1 (4)
Std			**22.2**											
Ave			**440**											anomalous pyrogram - mode 2 (1)
Landry Formation														
3137	956.2	70.2	348	0.07	0.25	0.60	0.23	0.42	0.05	1.19	21	50	8.7	bimodal S2, low T peak dominant, 2nd peak ~ 600
3170	966.2	71.1	433	0.18	0.19	0.29	0.49	0.66	0.04	0.52	37	56	12.0	broad asymmetric S2 with left shoulder
3203	976.3	71.1	431	0.12	0.14	0.25	0.47	0.56	0.03	0.13	108	192	11.8	broad asymmetric S2 with left shoulder
3236.7	986.5	70.3	428	0.03	0.04	0.23	0.40	0.17	0.01	0.11	36	209	11.7	broad asymmetric S2 with left shoulder
3269.9	996.7	70.5	430	0.06	0.06	0.32	0.50	0.19	0.02	0.11	55	291	12.1	broad asymmetric S2 with left shoulder
3302.8	1006.7	70.7	427	0.08	0.07	0.32	0.55	0.22	0.02	0.17	41	188	12.2	broad asymmetric S2 with left shoulder
3338	1017.4	70.6	435	0.03	0.08	0.24	0.27	0.33	0.02	0.09	89	267	11.6	unimodal asymmetric S2 with left shoulder
3371	1027.5	70.3	309	0.14	0.11	0.33	0.56	0.33	0.03	0.51	22	65	12.9	bimodal S2, low T peak dominant, 2nd peak ~ 600
3440	1048.5	70.7	349	0.04	0.11	0.43	0.28	0.26	0.03	0.24	46	179	11.4	multi-modal S2, low T peak dominant
3470.4	1057.8	70.7	431	0.01	0.03	0.32	0.27	0.09	0.03	0.07	43	457	12.3	broad asymmetric S2 with left shoulder
3502	1067.4	70.1	432	0.37	0.17	0.39	0.68	0.44	0.06	0.47	36	83	12.2	broad asymmetric S2 with left shoulder
3536.2	1077.8	70.5	429	0.30	0.16	0.36	0.66	0.44	0.07	0.37	43	97	12.0	broad asymmetric S2 with left shoulder
3569.4	1088.0	70.9	417	0.01	0.05	0.25	0.21	0.20	0.01	0.10	50	250	12.2	broad asymmetric S2 with left shoulder
3602	1097.9	70.1	434	0.02	0.06	0.32	0.20	0.19	0.02	0.07	86	457	12.4	broad asymmetric S2 with left shoulder
3635.6	1108.1	70.0	428	0.02	0.07	0.31	0.22	0.23	0.02	0.10	70	310	12.3	broad asymmetric S2 with left shoulder
3668	1118.0	70.1	436	0.01	0.08	0.38	0.15	0.21	0.03	0.09	89	422	12.3	broad asymmetric S2 with left shoulder
3700	1127.8	70.7	428	0.02	0.07	0.33	0.19	0.21	0.03	0.10	70	330	12.3	broad asymmetric S2 with left shoulder
3734.8	1138.4	70.7	435	0.01	0.05	0.30	0.18	0.17	0.02	0.10	50	300	12.3	broad asymmetric S2 with left shoulder
3767	1148.2	70.5	435	0.25	0.48	0.51	0.34	0.94	0.09	0.24	200	213	12.1	broad asymmetric S2 with left shoulder
3800	1158.2	70.2	425	0.01	0.03	0.33	0.30	0.09	0.01	0.08	38	413	11.8	broad asymmetric S2 with left shoulder
3833	1168.3	70.3	433	0.01	0.03	0.26	0.19	0.12	0.01	0.06	50	433	12.1	bimodal S2, high T peak dominant
3870	1179.6	20.5	342	0.61	1.13	1.31	0.35	0.86	0.20	14.38	8	9	1.3	bimodal S2, low T peak dominant, 2nd peak ~ 600
3901	1189.0	70.6	435	0.10	0.22	0.21	0.30	1.05	0.04	0.14	157	150	10.9	broad asymmetric S2 with left shoulder
3934	1199.1	70.3	436	0.14	0.28	0.27	0.34	1.04	0.06	0.34	82	79	13.1	broad asymmetric S2 with left shoulder
3967	1209.1	70.2	428	0.06	0.06	0.27	0.47	0.22	0.03	0.11	55	245	13.2	broad asymmetric S2 with left shoulder
4000.7	1219.4	70.5	434	0.24	0.28	0.27	0.46	1.04	0.06	0.20	140	135	13.2	broad asymmetric S2 with left shoulder
4030	1228.3	70.6	438	0.29	0.44	0.22	0.40	2.00	0.08	0.21	210	105	13.2	broad asymmetric S2 with left shoulder
4065.8	1239.3	50.0	309	2.67	1.97	0.62	0.58	3.18	0.42	11.25	18	6	5.8	bimodal S2, low T peak dominant, 2nd peak ~ 600
4099.5	1249.5	70.4	426	0.08	0.09	0.16	0.45	0.56	0.02	0.25	36	64	11.7	broad asymmetric S2 with left shoulder
4135	1260.3	70.5	433	0.06	0.12	0.22	0.32	0.55	0.02	0.12	100	183	12.0	broad asymmetric S2 with left shoulder
4165	1269.5	70.4	433	0.04	0.03	0.18	0.57	0.17	0.02	0.08	38	225	11.7	broad asymmetric S2 with left shoulder
4198	1279.6	70.5	428	0.42	0.33	0.32	0.56	1.03	0.08	0.99	33	32	11.5	broad asymmetric S2 with left shoulder
4230	1289.3	70.3	319	1.89	1.18	0.38	0.62	3.11	0.28	3.30	36	12	9.5	asymmetric S2, right skewed
4264.8	1299.9	70.9	424	0.05	0.07	0.22	0.40	0.32	0.02	0.13	54	169	13.0	broad asymmetric S2 with left shoulder
Ave			**329.3**											anomalous pyrograms - mode 1 (6)
Std			**19.1**											
Ave			**430.8**											anomalous pyrograms - mode 2 (28)
Std			**4.6**											
Arnica Formation														
4297	1309.7	70.5	429	0.10	0.08	0.27	0.56	0.30	0.02	0.19	42	142	13.3	broad asymmetric S2 with left shoulder
4329	1319.5	70.5	431	0.18	0.20	0.27	0.48	0.74	0.05	0.58	34	47	11.9	broad asymmetric S2 with left shoulder
4363	1329.8	70.7	429	0.35	0.37	0.29	0.49	1.28	0.08	0.24	154	121	13.2	broad asymmetric S2 with left shoulder
4396	1339.9	70.0	437	0.02	0.09	0.32	0.19	0.28	0.02	0.14	64	229	13.2	broad asymmetric S2 with left shoulder
4429	1350.0	70.9	433	0.01	0.03	0.29	0.20	0.10	0.02	0.16	19	181	13.2	broad asymmetric S2 with left shoulder
4461	1359.7	70.2	436	0.01	0.06	0.21	0.14	0.29	0.02	0.16	38	131	13.2	broad asymmetric S2 with left shoulder
4495	1370.1	70.4	430	0.34	0.26	0.34	0.57	0.76	0.07	0.24	108	142	13.0	broad asymmetric S2 with left shoulder
Ave			**432.1**											anomalous pyrograms - mode 2 (7)
Std			**3.3**											
Tatsieta Formation														
4528	1380.1	71.1	411	0.03	0.15	0.43	0.17	0.35	0.03	0.09	167	478	10.2	bimodal S2, high T peak dominant
4561	1390.2	70.2	343	0.04	0.10	0.25	0.28	0.40	0.02	0.06	167	417	10.8	multi-modal, low T peak dominant
4594	1400.3	70.3	433	0.01	0.05	0.30	0.17	0.17	0.02	0.08	62	375	10.5	broad asymmetric S2 with left shoulder
4627	1410.3	70.5	431	0.01	0.03	0.30	0.22	0.10	0.01	0.05	60	600	10.9	broad asymmetric S2 with left shoulder
4660	1420.4	70.3	339	0.03	0.11	0.61	0.23	0.18	0.04	0.09	122	678	3.6	asymmetric S2, right skewed
Ave			**341.0**											anomalous pyrograms - mode 1 (2)
Std			**2.8**											
Ave			**425.0**											anomalous pyrograms - mode 2 (3)
Std			**12.2**											

ft	m	Qty	Tmax	S1	S2	S3	PI	S2/S3	PC(%)	TOC(%)	HI	OI	MINC	Comment
								Peel Formation						
4693	1430.4	71.0	342	2.74	3.34	0.37	0.45	9.03	0.52	0.77	434	48	0.7	asymmetric S2, right skewed
4726	1440.5	70.0	436	0.18	0.18	0.35	0.49	0.51	0.04	0.12	150	292	12.7	bimodal S2, high T peak dominant
4759	1450.5	70.1	433	0.43	0.29	0.33	0.60	0.88	0.07	0.17	171	194	11.2	broad asymmetric S2 with left shoulder
4792	1460.6	70.3	442	2.98	1.17	0.37	0.72	3.16	0.36	0.66	177	56	10.8	broad asymmetric S2 with left shoulder
4825	1470.7	70.7	432	0.47	0.21	0.40	0.69	0.53	0.08	0.23	91	174	12.5	broad asymmetric S2 with left shoulder
4857	1480.4	70.9	407	0.02	0.05	0.30	0.27	0.17	0.02	0.07	71	429	12.5	broad asymmetric S2 with left shoulder
4891	1490.8	70.9	430	0.04	0.05	0.27	0.43	0.19	0.02	0.07	71	386	12.3	broad asymmetric S2 with left shoulder
4924	1500.8	70.4	412	0.03	0.04	0.38	0.43	0.11	0.02	0.10	40	380	11.7	broad asymmetric S2 with left shoulder
4957	1510.9	70.3	422	0.02	0.03	0.35	0.41	0.09	0.02	0.11	27	318	12.5	broad asymmetric S2 with left shoulder
4990	1521.0	70.4	427	0.24	0.24	0.32	0.50	0.75	0.05	0.23	104	139	12.0	broad asymmetric S2 with left shoulder
5023	1531.0	70.6	342	0.12	0.09	0.23	0.57	0.39	0.03	0.12	75	192	11.5	multi-modal, low T peak dominant
5056	1541.1	70.1	407	0.04	0.05	0.30	0.44	0.17	0.02	0.10	50	300	12.1	broad asymmetric S2 with left shoulder
5089	1551.1	70.9	330	0.06	0.06	0.36	0.48	0.17	0.02	0.13	46	277	12.1	broad asymmetric S2
5122	1561.2	70.6	414	0.14	0.11	0.30	0.56	0.37	0.03	0.13	85	231	12.3	broad asymmetric S2 with left shoulder
5155.2	1571.3	70.2	323	0.05	0.10	0.37	0.36	0.27	0.03	0.17	59	218	10.3	asymmetric S2, right skewed
5188	1581.3	70.3	404	0.05	0.07	0.48	0.42	0.15	0.03	0.16	44	300	11.7	broad asymmetric S2 with left shoulder
5223	1592.0	70.2	360	0.04	0.13	0.35	0.22	0.37	0.03	0.66	20	53	0.6	asymmetric S2, right skewed
5257	1602.3	70.8	360	0.03	0.12	0.40	0.21	0.30	0.03	1.10	11	36	6.2	bimodal S2, low T peak dominant, 2nd peak ~ 600
5287	1611.5	70.7	366	0.02	0.09	0.27	0.15	0.33	0.03	0.12	75	225	0.5	broad asymmetric S2, right skewed
5318	1620.9	70.4	382	0.03	0.08	0.14	0.23	0.57	0.02	1.05	8	13	1.1	broad asymmetric S2, right skewed
5353	1631.6	70.3	411	0.00	0.02	0.32	0.16	0.06	0.02	0.09	22	356	11.8	broad asymmetric S2 with left shoulder
5384	1641.0	70.8	369	0.03	0.18	0.43	0.13	0.42	0.03	0.70	26	61	6.5	broad asymmetric S2, right skewed
5417	1651.1	70.5	370	0.05	0.14	0.34	0.25	0.41	0.03	0.20	70	170	12.0	broad asymmetric S2, right skewed
5450	1661.2	70.5	412	0.05	0.08	0.29	0.37	0.28	0.02	0.11	73	264	12.7	broad asymmetric S2 with left shoulder
5483	1671.2	70.6	403	0.04	0.05	0.25	0.44	0.20	0.02	0.09	56	278	12.7	broad asymmetric S2 with left shoulder
5516	1681.3	70.4	406	0.01	0.04	0.34	0.18	0.12	0.02	0.10	40	340	12.1	bimodal S2, high T peak dominant
Ave			**354.4**											anomalous pyrograms - mode 1 (10)
Std			**19.2**											
Ave			**418.6**											anomalous pyrograms - mode 2 (16)
Std			**12.9**											
								Mount Kindle Formation						
5549	1691.3	70.4	358	0.06	0.21	0.31	0.22	0.68	0.04	0.17	124	182	9.9	broad asymmetric S2, right skewed
5582	1701.4	71.0	338	0.04	0.07	0.34	0.36	0.21	0.02	0.09	78	378	11.9	broad asymmetric S2, right skewed
5615	1711.5	70.5	420	0.01	0.03	0.37	0.24	0.08	0.02	0.13	23	285	12.9	broad asymmetric S2 with left shoulder
5648	1721.5	70.1	415	0.01	0.04	0.38	0.18	0.11	0.02	0.09	44	422	12.7	broad asymmetric S2 with left shoulder
5681	1731.6	70.6	343	0.13	0.22	0.37	0.36	0.59	0.04	0.15	147	247	11.2	broad asymmetric S2, right skewed
5714	1741.6	70.5	420	0.01	0.06	0.29	0.12	0.21	0.02	0.09	67	322	13.1	broad asymmetric S2 with left shoulder
5747	1751.7	70.3	427	0.01	0.06	0.35	0.17	0.17	0.02	0.08	75	438	13.1	broad asymmetric S2 with left shoulder
5780	1761.7	70.6	423	0.03	0.06	0.27	0.36	0.22	0.02	0.09	67	300	12.7	bimodal S2, high T peak dominant
5813	1771.8	70.1	424	0.02	0.05	0.28	0.28	0.18	0.01	0.05	100	560	12.9	broad asymmetric S2 with left shoulder
5846	1781.9	70.3	423	0.03	0.07	0.31	0.32	0.23	0.02	0.10	70	310	12.8	broad asymmetric S2 with left shoulder
5879	1791.9	70.4	423	0.01	0.04	0.31	0.16	0.13	0.01	0.09	44	344	12.9	broad asymmetric S2 with left shoulder
5912	1802.0	70.5	420	0.01	0.06	0.33	0.20	0.18	0.02	0.08	75	413	13.0	broad asymmetric S2 with left shoulder
5945	1812.0	70.5	421	0.01	0.05	0.22	0.13	0.23	0.02	0.12	42	183	12.8	broad asymmetric S2 with left shoulder
5978	1822.1	70.1	427	0.23	0.16	0.34	0.59	0.47	0.06	0.14	114	243	12.7	broad asymmetric S2 with left shoulder
6011	1832.2	70.0	422	0.01	0.04	0.33	0.17	0.12	0.01	0.09	44	367	13.0	bimodal S2, high T peak dominant
6044	1842.2	70.4	400	0.12	0.07	0.24	0.62	0.29	0.02	0.23	30	104	12.4	broad asymmetric S2 with left shoulder
6077.5	1852.4	70.6	408	0.02	0.03	0.36	0.33	0.08	0.02	0.28	11	129	12.7	broad asymmetric S2 with left shoulder
6110	1862.3	70.7	422	0.00	0.02	0.34	0.13	0.06	0.02	0.08	25	425	13.0	broad asymmetric S2 with left shoulder
6143	1872.4	70.2	399	0.02	0.05	0.27	0.30	0.19	0.02	0.26	19	104	12.5	broad asymmetric S2 with left shoulder
6176	1882.4	70.1	414	0.01	0.04	0.29	0.19	0.14	0.01	0.08	50	363	12.9	broad asymmetric S2 with left shoulder
6209.8	1892.7	70.7	431	0.02	0.08	0.30	0.21	0.27	0.03	0.12	67	250	13.1	broad asymmetric S2 with left shoulder
6242	1902.6	70.3	417	0.00	0.03	0.34	0.12	0.09	0.01	0.07	43	486	12.9	broad asymmetric S2 with left shoulder
6275	1912.6	70.6	422	0.02	0.04	0.33	0.30	0.12	0.01	0.11	36	300	13.1	broad asymmetric S2 with left shoulder
6308	1922.7	70.5	421	0.01	0.03	0.51	0.15	0.06	0.03	0.12	25	425	13.1	broad asymmetric S2 with left shoulder
6341.4	1932.9	70.7	417	0.03	0.03	0.35	0.45	0.09	0.02	0.08	38	438	12.8	broad asymmetric S2 with left shoulder
6372	1942.2	70.6	416	0.00	0.02	0.31	0.17	0.06	0.01	0.09	22	344	13.1	broad asymmetric S2 with left shoulder
6407	1952.9	71.0	426	0.00	0.02	0.00	0.20	0.00	0.00	0.06	33	0	12.8	broad asymmetric S2 with left shoulder
6440	1962.9	70.0	426	0.00	0.02	0.31	0.14	0.06	0.02	0.09	22	344	13.1	broad asymmetric S2 with left shoulder
6473	1973.0	70.5	429	0.01	0.04	0.27	0.17	0.15	0.02	0.07	57	386	12.9	broad asymmetric S2 with left shoulder
6506	1983.0	70.2	425	0.02	0.05	0.33	0.32	0.15	0.02	0.07	71	471	13.2	broad asymmetric S2 with left shoulder
6539	1993.1	70.5	429	0.01	0.05	0.23	0.18	0.22	0.01	0.08	62	288	12.8	broad asymmetric S2 with left shoulder
6572	2003.1	70.7	423	0.01	0.03	0.21	0.20	0.14	0.01	0.08	38	263	12.8	broad asymmetric S2 with left shoulder
6605	2013.2	71.1	429	0.01	0.02	0.23	0.19	0.09	0.01	0.07	29	329	12.7	broad asymmetric S2 with left shoulder
6638	2023.3	70.6	430	0.00	0.02	0.23	0.15	0.09	0.01	0.10	20	230	13.3	broad asymmetric S2 with left shoulder
6671	2033.3	70.5	420	0.01	0.04	0.24	0.20	0.17	0.01	0.07	57	343	12.9	broad asymmetric S2 with left shoulder
6704	2043.4	70.2	368	0.11	0.10	0.33	0.53	0.30	0.03	0.14	71	236	12.7	broad bimodal S2, low T peak dominant
6737	2053.4	70.8	433	0.03	0.07	0.34	0.29	0.21	0.03	0.09	78	378	12.9	broad asymmetric S2 with left shoulder
Ave			**351.8**											anomalous pyrograms - mode 1 (4)
Std			**13.8**											
Ave			**421.3**											anomalous pyrograms - mode 2 (33)
Std			**7.7**											
								Franklin Mountain Formation						
6770	2063.5	70.4	419	0.01	0.04	0.25	0.22	0.16	0.02	0.08	50	313	12.5	broad asymmetric S2 with left shoulder
6803	2073.6	70.5	425	0.00	0.02	0.43	0.15	0.05	0.02	0.09	22	478	12.8	broad asymmetric S2 with left shoulder
6835	2083.3	70.3	440	0.01	0.03	0.28	0.16	0.11	0.01	0.08	38	350	12.8	broad asymmetric S2 with left shoulder

ft	m	Qty	Tmax	S1	S2	S3	PI	S2/S3	PC(%)	TOC(%)	HI	OI	MINC	Comment
6869	2093.7	70.9	423	0.00	0.02	0.28	0.17	0.07	0.01	0.09	22	311	12.7	broad asymmetric S2 with left shoulder
6902	2103.7	70.5	430	0.00	0.02	0.26	0.11	0.08	0.02	0.12	17	217	13.2	broad asymmetric S2 with left shoulder
6935	2113.8	70.5	422	0.00	0.01	0.31	0.17	0.03	0.01	0.06	17	517	10.9	broad asymmetric S2 with left shoulder
6968	2123.8	70.1	427	0.02	0.04	0.22	0.30	0.18	0.03	0.10	40	220	12.9	broad asymmetric S2 with left shoulder
7001	2133.9	71.0	430	0.04	0.08	0.31	0.33	0.26	0.02	0.08	100	388	12.8	broad asymmetric S2 with left shoulder
7034	2144.0	70.6	417	0.01	0.02	0.24	0.19	0.08	0.01	0.07	29	343	12.6	broad asymmetric S2 with left shoulder
7067	2154.0	70.5	422	0.00	0.02	0.24	0.17	0.08	0.01	0.10	20	240	12.8	broad asymmetric S2 with left shoulder
7100	2164.1	70.0	370	0.08	0.10	0.28	0.47	0.36	0.03	0.11	91	255	12.1	broad asymmetric flat-topped S2
7133	2174.1	70.3	417	0.01	0.02	0.24	0.19	0.08	0.01	0.06	33	400	12.6	broad asymmetric S2 with left shoulder
7166	2184.2	70.4	426	0.01	0.03	0.26	0.19	0.12	0.01	0.08	38	325	13.0	broad asymmetric S2 with left shoulder
7199	2194.3	70.7	413	0.01	0.03	0.27	0.23	0.11	0.01	0.06	50	450	10.1	broad asymmetric S2 with left shoulder
7231	2204.0	70.6	426	0.01	0.04	0.26	0.17	0.15	0.02	0.05	80	520	1.0	broad asymmetric S2 with left shoulder
7265	2214.4	71.0	382	2.22	0.70	0.27	0.76	2.59	0.27	0.37	189	73	7.9	broad asymmetric flat-topped S2
7299	2224.7	70.0	429	0.01	0.04	0.23	0.22	0.17	0.01	0.07	57	329	12.6	broad asymmetric S2 with left shoulder
7331	2234.5	70.6	436	0.01	0.05	0.26	0.19	0.19	0.01	0.09	56	289	13.0	broad asymmetric S2 with left shoulder
7363	2244.2	71.0	427	0.03	0.07	0.31	0.31	0.23	0.02	0.11	64	282	11.7	broad asymmetric S2 with left shoulder
7397	2254.6	70.7	424	0.02	0.07	0.32	0.18	0.22	0.02	0.08	88	400	12.7	broad asymmetric S2 with left shoulder
7430	2264.7	70.7	431	0.01	0.04	0.27	0.16	0.15	0.02	0.08	50	338	12.6	broad asymmetric S2 with left shoulder
7463	2274.7	70.2	429	0.01	0.04	0.33	0.22	0.12	0.02	0.06	67	550	12.8	broad asymmetric S2 with left shoulder
7496	2284.8	70.6	423	0.00	0.02	0.27	0.19	0.07	0.01	0.08	25	338	12.7	broad asymmetric S2 with left shoulder
7529	2294.8	70.3	429	0.01	0.03	0.39	0.18	0.08	0.02	0.08	38	488	12.7	broad asymmetric S2 with left shoulder
7562	2304.9	70.3	426	0.06	0.10	0.35	0.37	0.29	0.03	0.10	100	350	11.4	broad asymmetric S2 with left shoulder
7595	2315.0	70.8	426	0.00	0.03	0.82	0.15	0.04	0.03	0.12	25	683	12.9	broad asymmetric S2 with left shoulder
7628	2325.0	70.5	431	0.01	0.06	0.12	0.15	0.50	0.01	0.07	86	171	8.0	broad asymmetric S2 with left shoulder
7661	2335.1	70.0	437	0.01	0.04	0.27	0.13	0.15	0.01	0.13	31	208	13.0	broad asymmetric S2 with left shoulder
7694	2345.1	70.4	433	0.01	0.04	0.35	0.13	0.11	0.02	0.07	57	500	13.1	broad asymmetric S2 with left shoulder
7727	2355.2	70.2	427	0.00	0.02	0.25	0.14	0.08	0.01	0.06	33	417	12.6	broad asymmetric S2 with left shoulder
7760	2365.2	70.8	421	0.01	0.03	0.33	0.19	0.09	0.02	0.06	50	550	12.2	broad asymmetric S2 with left shoulder
7793	2375.3	70.7	417	0.02	0.04	0.35	0.29	0.11	0.02	0.05	80	700	12.4	broad asymmetric S2 with left shoulder
7827	2385.7	71.0	420	0.00	0.02	0.30	0.17	0.07	0.01	0.13	15	231	12.1	broad asymmetric S2 with left shoulder
7859	2395.4	70.9	427	0.01	0.03	0.25	0.17	0.12	0.02	0.06	50	417	7.4	broad asymmetric S2 with left shoulder
7892	2405.5	70.7	425	0.01	0.05	0.26	0.12	0.19	0.01	0.07	71	371	11.5	broad asymmetric S2 with left shoulder
7925	2415.5	70.5	422	0.01	0.07	0.33	0.14	0.21	0.02	0.04	175	825	12.2	broad asymmetric S2 with left shoulder
7958	2425.6	70.4	419	0.01	0.04	0.32	0.21	0.13	0.02	0.10	40	320	12.1	broad asymmetric S2 with left shoulder
7991	2435.7	70.6	432	0.11	0.09	0.41	0.56	0.22	0.04	0.12	75	342	12.4	broad asymmetric S2 with left shoulder
8024	2445.7	70.4	417	0.07	0.09	0.41	0.45	0.22	0.03	0.10	90	410	12.7	broad asymmetric S2 with left shoulder
8044	2451.8	70.0	429	0.01	0.02	0.36	0.19	0.06	0.01	0.09	22	400	12.8	broad asymmetric S2 with left shoulder
Ave			**376.0**											anomalous pyrograms - mode 1 (2)
Std			**8.5**											
Ave			**425.6**											anomalous pyrograms - mode 2 (38)
Std			**6.0**											

Table 4. Rock-Eval samples selected for extraction and geochemical analysis.

Depth (ft)	(m)	Tmax	S1	S2	PI	TOC (wt%)	HI	OI	Comments
Mallik A-06									
Iperk Sequence									
730	222.5	299	1.53	7.40	0.17	5.53	134	155	bimodal S1, 1/3 recovery to baseline, bimodal S2 peak, reduced Tmax
840	256.0	298	0.70	3.18	0.18	2.08	153	191	bimodal S1, 1/3 recovery to baseline, bimodal S2 peak, reduced Tmax
Mackenzie Bay Sequence									
1740	530.4	403	0.16	0.66	0.19	1.29	51	198	S1 80% recovery, large left shoulder on S2, reduced Tmax
Kugmallit Sequence									
3060	932.7	405	0.05	0.84	0.06	0.93	90	309	S1 70% recovery, broad unimodal S2, reduced Tmax
4180	1274.1	379	0.15	1.12	0.12	0.87	129	307	S1 60% recovery, right shoulder on S2, reduced Tmax
Richards Sequence									
4420	1347.2	419	0.25	1.24	0.17	1.20	103	289	S1 70% recovery, left shoulder on S2, reduced Tmax
5990	1825.8	421	0.12	1.39	0.08	1.43	97	182	S1 70% recovery, left shoulder on S2, reduced Tmax
8010	2441.4	416	0.44	1.89	0.19	1.87	101	68	S1 80% recovery, two left shoulders on S2 peak, reduced Tmax, oil stain
8340	2542.0	303	1.23	2.97	0.29	1.52	195	138	S1 peak ht > S2, 45% recovery, bimodal S2, reduced Tmax, oil stain
9480	2889.5	297	7.99	11.98	0.40	3.13	383	116	large S1, bimodal S2, reduced Tmax, oil stain
Taglu Sequence									
10500	3200.4	424	0.32	0.93	0.26	0.69	135	122	bimodal S2, reduced Tmax
11830	3605.8	409	3.01	8.69	0.26	1.99	437	271	trimodal S2; core %Ro at 11835 ft, oil stain, reduced Tmax
12930	3941.1	423	0.30	5.32	0.05	7.58	70	161	unimodal S2, suppressed %Ro due to oil staining, reduced Tmax
13440	4096.5	421	0.34	0.86	0.28	0.94	91	323	broad asymmetric bimodal S2, reduced Tmax
Parsons N-10									
Iperk Sequence									
370	112.8	324	5.35	31.36	0.15	18.06	174	193	asymmetric S2, right shoulder, reduced Tmax
Aklak Sequence									
1110	338.3	394	3.29	57.96	0.05	44.76	129	130	broad asymmetric S2, reduced Tmax
3320	1011.9	300	3.15	2.88	0.52	1.75	165	97	S1 > S2, bimodal S2, low T peak dominant, reduced Tmax
Mason River Formation									
5340	1627.6	434	0.25	0.70	0.26	1.46	48	101	S1 peak ht > S2, asymmetric S2, small left shoulder
5670	1728.2	427	0.98	1.16	0.46	1.52	76	82	S1 peak ht > S2, broad asymmetric S2, large flat left shoulder
6330	1929.4	418	0.63	1.13	0.36	1.86	61	55	S1 peak ht > S2, broad asymmetric S2, flat left shoulder
Smoking Hills Sequence									
6600	2011.7	406	3.50	3.63	0.49	2.57	141	41	S1 peak ht > S2, broad asymmetric S2, large flat left shoulder
Boundary Creek Sequence									
6660	2030.0	411	1.81	3.07	0.37	2.51	122	41	S1 peak ht > S2, asymmetric S2, small left shoulder
6810	2075.7	420	0.56	1.62	0.25	2.82	57	64	S1 peak ht > S2, asymmetric S2, small left shoulder
Arctic Red Formation									
6840	2084.8	416	0.54	1.46	0.27	2.16	68	44	S1 peak ht > S2, asymmetric S2, two left shoulders
7120	2170.2	424	0.54	1.82	0.23	2.49	73	41	S1 peak ht > S2, asymmetric S2, small left shoulder
Kamik Formation									
9270	2825.5	425	1.02	17.67	0.05	7.48	236	9	unimodal S2, Tmax low
McGuire Formation									
9329	2843.5	439	0.16	2.70	0.06	1.89	143	40	unimodal S2, coal sample from core

Table 5. Key for maceral and organic type reference for Tables 6 to 8.

CODE	ORGANIC TYPE (Org Type)
2	Huminite/Vitrinite
2.1	Huminite/Vitrinite; caved
2.2	Huminite/Vitrinite; 2.2, 2.3 etc. refers to reworked populations
4	Bitumen
21	Pyrobitumen (PB) Isotropic
22	Pyrobitumen (PB) Anisotropic

Table 6. Vitrinite (organic type 2) reflectance (%Ro_R) for various Mallik A-06 samples. Location: 69° 25' 01" N, 134° 30' 16" W. See Table 5 for organic type definitions-code for macerals. Plotted %Ro_R values for primary vitrinite (Fig. 22a,b) highlighted in yellow (cuttings), green (core) and purple (suppressed).

C #	Cuttings Interval (ftKB)	Pellet #	Depth (mKB)	TVD (mKB)	TVD (mGL)	Organic Type	%Ro_R	S.D.	N	Stratigraphic Unit	Comments
C-531003	800-810	**194/09**	245.4	245.4	237.2	2	0.23	0.03	9	Iperk	
						4	0.15	0.02	6		
						2.2	0.35	0.05	8		
						2.3	0.58	0.02	3		
C-531032	1670-1680	**195/09**	510.5	510.5	502.3	2	0.26	0.05	18	Mackenzie Bay	
						2.2	0.45	0.06	16		
						2.3	0.77		1		
C-531050	2210-2220	**196/09**	675.1	675.1	666.9	2	0.24	0.03	27	Kugmallit	
						2.2	0.51	0.03	2		
C-531068	2750-2760	**197/09**	839.7	839.7	831.5	2	0.28	0.05	45	Kugmallit	
						2.2	0.51	0.01	5		
C-531075	2960-2970	**198/09**	903.7	903.7	895.5	2	0.27	0.04	48	Kugmallit	
						2.2	0.46	0.08	2		
C-531420	3125 core	**303/08**	952.5	952.5	944.3	2	0.43	0.04	38	Kugmallit	recycled
						2.2	0.67	0.03	2		
C-531106	3900-3910	**199/09**	1190.2	1190.2	1182.0	2	0.31	0.04	48	Kugmallit	
						2.2	0.46	0.08	2		
C-531120	4410-4420	**200/09**	1345.7	1345.6	1337.4	2	0.33	0.04	44	Richards	
C-531421	4470 core	**304/08**	1362.5	1362.4	1354.2	2	0.48	0.05	17	Richards	recycled
						2.2	0.64	0.04	2		
						2.3	0.89	0.03	2		
						2.4	1.07	0.02	3		
C-531136	4890-4900	**201/09**	1492	1491.9	1483.7	2	0.34	0.05	48	Richards	
						2.2	0.49	0.05	2		
C-531156	5500-5510	**202/09**	1677.9	1677.7	1669.5	2	0.38	0.05	51	Richards	
C-531172	5980-5990	**203/09**	1824.2	1823.8	1815.6	2	0.42	0.05	46	Richards	
						2.2	0.56	0.01	8		
C-531185	6370-6380	**204/09**	1943.1	1942.5	1934.3	2	0.40	0.07	16	Richards	
						2.2	0.61	0.01	2		
						2.1	0.25				
C-531214	7240-7250	**205/09**	2208.3	2206.2	2198.0	2	0.44	0.04	60	Richards	
C-531234	7910-7920	**206/09**	2412.5	2407.9	2399.7	2	0.46	0.03	62	Richards	
C-531253	8480-8490	**207/09**	2586.2	2576.9	2568.7	2	0.49	0.04	60	Richards	some oil stain
C-531258	8630-8640	**208/09**	2631.9	2621.2	2613.0	2	0.49	0.05	60	Richards	
C-531422	8671 core	**305/08**	2642.9	2631.8	2623.6	2	0.51	0.04	51	Richards	
C-531273	9110-9120	**209/09**	2778.3	2761.7	2753.5	2	0.51	0.05	60	Richards	
C-531423	9276 core	**306/08**	2827.3	2808.6	2800.4	2	0.48	0.03	27	Richards	
						2.2	0.63	0.02	2		
C-531286	9500-9510	**210/09**	2897.1	2875.3	2867.1	2	0.48	0.05	56	Richards	suppressed
C-531424	9661 core	**307/08**	2944.7	2920.5	2912.3	2	0.56	0.04	11	Richards	
						2.2	0.67	0.02	3		
C-531302	9980-9990	**211/09**	3043.4	3013.7	3005.5	2	0.52	0.03	60	Richards	
C-531310	10220-10230	**212/09**	3116.6	3082.6	3074.4	2	0.54	0.04	55	Richards	
C-531320	10520-10530	**213/09**	3208	3168.9	3160.7	2	0.55	0.04	47	Taglu	
						2.2	0.67	0.01	3		

C #	Cuttings Interval (ftKB)	Pellet #	Depth (mKB)	TVD (mKB)	TVD (mGL)	Organic Type	%Ro$_R$	S.D.	N	Stratigraphic Unit	Comments
C-531425	10540 core	**308/08**	3212.6	3173.3	3165.1	2	0.57	0.05	13	Taglu	
C-531330	10820-10830	**214/09**	3299.5	3256	3247.8	2	0.56	0.04	49	Taglu	
						2.2	0.67	0.01	11		
C-531338	11060-11070	**215/09**	3372.6	3325.6	3317.4	2	0.56	0.04	10	Taglu	
						2.1	0.34	0.05	54		
C-531352	11480-11490	**216/09**	3500.6	3446.3	3438.1	2	0.55	0.05	61	Taglu	
						2.2	0.72	0.01	3		
C-531426	11810 core	**309/08**	3599.7	3538.3	3530.1	2	0.56	0.01	51	Taglu	
C-531427	11835 core	**310/08**	3607.3	3545.3	3537.1	2	0.59	0.05	56	Taglu	
C-531382	12440-12450	**217/09**	3793.2	3708	3699.8	2	0.57	0.06	54	Taglu	suppressed?
						2.1	0.43	0.01	9		
						2.2	0.72		1		
C-531398	12920-12930	**218/09**	3939.5	3820	3811.8	2	0.59	0.04	45	Taglu	suppressed
						2.1	0.42	0.06	20		
C-531416	13460-13470	**219/09**	4104.1	3937.7	3929.5	2	0.65	0.04	31	Taglu	suppressed?
						2.2	0.52	0.03	7		
						2.3	0.82	0.05	3		

Table 7. Vitrinite (organic type 2) reflectance (%Ro_R) for various Parsons N-10 samples. Location: 68° 59' 49" N, 133° 31' 50" W. See Table 5 for organic type definitions-code for macerals. Plotted %Ro_R values (Fig. 23) highlighted in yellow (cuttings) and green (core).

C #	Cuttings Interval (ftKB)	Pellet #	Depth (mKB)	Depth (mGL)	Organic Type	%Ro_R	S.D.	N	Stratigraphic Unit	Comments
C-531864	540-550	**220/09**	166.1	160	2	0.25	0.03	30	Iperk	coal
					2.2	0.38	0.03	21		
					2.3	0.49	0.01	3		
C-531880	1100-1110	**221/09**	336.8	330.7	2	0.30	0.03	39	Aklak	coal
					2.1	0.20	0.02	21		
C-531890	1400-1410	**222/09**	428.2	422.1	2	0.31	0.04	36	Aklak	
					2.1	0.22	0.02	14		
					2.2	0.44		1		
C-531905	1880-1890	**223/09**	574.5	568.4	2	0.32	0.04	50	Aklak	coal
C-531917	2290-2300	**224/09**	699.5	693.4	2	0.33	0.04	51	Aklak	
					2.2	0.52		1		
C-531934	2860-2870	**225/09**	873.3	867.2	2	0.33	0.04	34	Aklak	
					2.1	0.25	0.01	8		
					2.2	0.42	0.03	8		
C-531943	3130-3140	**226/09**	955.5	949.4	2	0.41	0.03	44	Aklak	coal
					2.1	0.34	0.01	5		
					2.2	0.49	0.01	2		
C-531958	3610-3620	**227/09**	1101.9	1095.8	2	0.40	0.03	52	Aklak	coal
C-531962	3730-3740	**228/09**	1138.4	1132.3	2	0.39	0.03	29	Aklak	coal
					2.2	0.47	0.02	18		
C-531977	4220-4230	**229/09**	1287.8	1281.7	2	0.37	0.06	51	Aklak	
C-531991	4640-4650	**230/09**	1415.8	1409.7	2	0.34	0.03	43	Aklak	
					2.2	0.52	0.03	6		
					2.1	0.22	0.01	2		
C-532002	5450-5460	**231/09**	1662.7	1656.6	2	0.43	0.03	17	Mason River	
					2.1	0.34	0.04	33		
					2.2	0.57		1		
C-532018	6140-6150	**232/09**	1873	1866.9	2?	0.34		1	Mason River	
					2.1	0.29		1		
					2.2	0.60	0.01	2		
					2.3	0.87	0.09	2		
C-531029	6500-6510	**233/09**	1982.7	1976.6	2	0.45	0.03	21	Smoking Hills	
					2.1	0.35	0.05	20		
					2.2	0.63	0.07	3		
C-532038	6770-6780	**234/09**	2065	2058.9	2	0.41	0.03	23	Boundary Creek	
					2.1	0.31	0.05	5		
					2.2	0.61	0.07	11		
C-532052	7200-7210	**235/09**	2196.1	2190	2	0.48	0.02	6	Arctic Red	
					2.1	0.39	0.03	2		
					2.2	0.61	0.05	10		
C-532069	7710-7720	**236/09**	2351.5	2345.4	2	0.52	0.04	19	Mount Goodenough	
					2.1	0.42	0.03	18		
					2.2	0.74	0.02	3		
					2.3	0.90		1		

C #	Cuttings Interval (ftKB)	Pellet #	Depth (mKB)	Depth (mGL)	Organic Type	$\%Ro_R$	S.D.	N	Stratigraphic Unit	Comments
C-532087	8250-8260	**237/09**	2516.1	2510	2	0.53	0.05	22	Mount Goodenough	
					2.1	0.42	0.00	2		
					2.2	0.74	0.08	8		
C-532103	8730-8740	**238/09**	2662.4	2656.3	2	0.58	0.03	9	Kamik	
					2.1	0.44	0.06	11		
					2.2	0.70	0.04	6		
C-420034	9030' core	**538/01**	2752.3	2746.2	2	0.57	0.02	50	Kamik	
	9030' core		2752.3	2746.2	2	0.60	0.03	20	Kamik	Gunther (1974)
	9059' core		2761.2	2755.1	2	0.57	0.03	21	Kamik	Gunther (1974)
	9184' core		2799.3	2793.2	2	0.61	0.03	21	Kamik	Gunther (1974)
C-420035	9185' core	**539/01**	2799.6	2793.5	2	0.61	0.05	50	Kamik	coal
	9193' core		2802	2795.9	2	0.59	0.03	21	Kamik	Gunther (1974)
C-532118	9230-9240	**239/09**	2814.8	2808.7	2	0.58	0.02	19	Kamik	
					2.1	0.51	0.03	42		
					2.2	0.67		1		
C-532154	9329' core	**344-08**	2843.5	2837.4	2	0.63	0.04	55	McGuire	
C-532125	9630-9640	**240/09**	2936.7	2930.6	2	0.65	0.03	11	Husky	
					2.1	0.53	0.06	39		
C-532140	10080-10090	**241/09**	3073.9	3067.8	2	0.66	0.03	13	Husky	
					2.1	0.55	0.04	34		
					2.2	0.74	0.02	5		
C-532153	10480-10490	**242/09**	3195.8	3189.7	2.1	0.69	0.04	7	Franklin Mountain	caved
					2.1	0.57	0.02	19		
					2.1	0.34	0.11	17		

Table 8. Vitrinite (organic type 2) reflectance (%Ro_R) for various Kugaluk N-02 samples. Location: 68° 31' 55" N, 131° 31' 19" W. See Table 5 for organic type definitions-code for macerals. Plotted %Ro_R values (Fig. 24) highlighted in yellow (vitrinite) and green (pyrobitumen %Ro equivalent).

C #	Core Depth (ftKB)	Pellet #	Depth (mKB)	Depth (mGL)	Organic Type	%Ro_R	S.D.	N	Stratigraphic Unit	Comments
C-408216	917	**251/09**	279.5	277.1	2	1.62	0.08	33	Imperial	
					2.1	1.34	0.05	9		
					2.2	1.89	0.10	28		
C-408230	1379	**252/09**	420.3	417.9	2	1.62	0.10	36	Imperial	
					2.1	1.28	0.12	15		
					4	1.97	0.13	12		%Roeq = 1.62
					4	2.25	0.02	3		%Roeq = 1.79
C-408244	1844	**253/09**	562.1	559.7	2	1.71	0.08	13	Imperial	
					21	2.33	0.08	18		%Roeq = 1.84
					4	2.00	0.08	5		%Roeq = 1.64
					2.1	1.46	0.07	7		
C-408268	2636.3	**254/09**	803.5	801.1	2	1.75	0.13	21	Imperial	
					4	2.11	0.07	20		%Roeq = 1.70
					21	2.40	0.09	20		%Roeq = 1.88
					2.1	1.39	0.10	3		
C-408274	2839	**255/09**	865.3	862.9	2	1.82	0.08	18	Canol	
					21	2.20	0.10	27		%Roeq = 1.76
					21	2.59	0.08	2		%Roeq = 2.0
					2.1	1.52	0.06	10		
					2.1	1.23	0.07			
C-408283	3137	**256/09**	956.2	953.8	21	2.46	0.08	14	Landry	%Roeq = 1.92
					22	2.17	0.10	11		
					21	2.69	0.07	16		%Roeq = 2.06
					21	2.91	0.05	8		%Roeq = 2.20
					21	3.10	0.09	7		%Roeq = 2.32
C-408302	3767	**257/09**	1148.2	1145.8	21	2.51	0.03	4	Landry	%Roeq = 1.95
					21	2.71		2		
					21	3.53	0.55	2		
C-408311	4065.8	**258/09**	1239.3	1236.9	2	2.05	0.09	12	Landry	
					22	2.55	0.16	38		
					22	3.07	0.15	10		
					2.1	1.48	0.37	9		
C-408316	4230	**259/09**	1289.3	1286.9	21	2.44	0.08	8	Landry	%Roeq = 1.91
					22	3.01	0.19	47		
					22	3.80	0.12	4		
C-408330	4693	**260/09**	1430.4	1428					Peel	no measurements
C-408347	5257	**261/09**	1602.3	1599.9	21	2.22	0.07	9	Peel	%Roeq = 1.77
					22	2.74	0.14	23		
					22	3.17	0.04	3		
					21	4.47	0.36	2		%Roeq = 3.16
					2.1	1.89	0.06	7		
C-408360	5681	**262/09**	1731.6	1729.2					Mount Kindle	no measurements
C-408369	5978	**263/09**	1822.1	1819.7					Mount Kindle	no measurements
C-408392	6737	**264/09**	2053.4	2051					Mount Kindle	no measurements

C #	Core Depth (ftKB)	Pellet #	Depth (mKB)	Depth (mGL)	Organic Type	$\%Ro_R$	S.D.	N	Stratigraphic Unit	Comments
C-408408	7265	**265/09**	2214.4	2212	21	2.25	0.14	9	Franklin Mountain	%Roeq = 1.79
					22	2.81	0.14	10		
					22	3.53	0.18	14		
					22	4.32	0.02	2		
C-408428	7925	**266/09**	2415.5	2413.1					Franklin Mountain	no measurements